EXPERIMENTAL INVESTIGATION OF TWO STOREY BALLOON FRAMED COUPLED CLT SHEAR WALLS

by

Abdul Basit

B.Sc., University of Engineering & Technology Peshawar, 2017

THESIS SUBMITTED IN PARTIAL FULFILLMENT OF
THE REQUIREMENTS FOR THE DEGREE OF
MASTER OF APPLIED SCIENCE
IN
ENGINEERING

UNIVERSITY OF NORTHERN BRITISH COLUMBIA

June 2025

Abstract

The growing demand for sustainable urban development has accelerated the adoption of mass timber systems, with cross-laminated timber (CLT) emerging as a promising solution due to its structural efficiency. While platform-type CLT shear walls are currently included in design standards such as the NBCC and CSA-O86, balloon-type configurations provide various advantages such as reduced cumulative shrinkage and fewer floor-level connections.

In this thesis, the seismic performance of two-storey balloon-type coupled-panel CLT shear walls was evaluated through full-scale experimental testing. Different connection configurations: i) screw orientation in hold-downs (HD); ii) stiffness of vertical joints (VJ); and iii) addition of tension straps (TS) and horizontal splices were evaluated to study their impact on lateral load resistance, stiffness, cyclic strength degradation, and energy dissipation.

Across all tests, walls with mixed-angle HD demonstrated higher initial strength than shear-only configurations at lower drift levels but experienced more strength degradation at larger drifts. Increasing VJ stiffness enhanced performance. At the maximum drift of 5.7%, all balloon-type CLT wall configurations maintained global stability despite significant inelastic deformation and localized connection damage.

Compared to platform-type systems, balloon-framed walls achieved improved lateral resistance and more uniform inter-storey drift distribution. The findings provide valuable insight into the seismic behavior of balloon-type CLT shear walls and emphasize the critical role of connection detailing in achieving resilient structural performance.

Table of contents

List of tables

List of figures

Acknowledgements

I would like to express my deepest and most sincere gratitude to Professor Thomas Tannert for his support and invaluable guidance throughout this journey. His generosity in sharing knowledge, his patience, and his encouragement have been central in shaping both this research and my growth as a scholar. I am truly fortunate to have had the opportunity to work under his supervision—this achievement would not have been possible without him.

The project was funded by the government of British Columbia through a Forest Innovation Investment (FII) grant (24/25-UNBC-BFC-W25-045) and the BC Leadership Chair in Hybrid Wood Structures Engineering. The support received from: Kalesnikoff Lumber Co. Ltd. And MTC Solutions Inc (in-kind contribution in form of CLT panels and STS supplied at discounted prices); Aspect Structural Engineers, Fast+Epp TIMBER Engineering Inc. and FPInnovations (in form of supporting the FII application), as well as the UNBC technicians James Andal, Nathan and Ryan Stern are greatly appreciated.

I would also like to thank my friends and colleagues, Orhan Sahutoglu and Houman Ganjali, whose constant support during testing and throughout the thesis process was truly invaluable.

I would like to dedicate this work to my parents and siblings, especially my sister Uzma Ali Khan, and express my deepest gratitude for their unconditional love, encouragement, and constant belief in me throughout this journey. Their support has been the foundation of my strength and perseverance.

Chapter 1 Introduction

1.1 Background

The global population reached 8 billion in 2022, and the United Nations anticipates it to grow up to 9.8 billion by 2050, prompting a need to accommodate approximately 2 billion more people in urban areas over the next three decades [1]. Concrete was the most frequently used construction material during the 20th century due to its structural properties and ability to be cast into almost any shape [2]. Due to such construction practices, the building sector is responsible for 39% of global carbon emissions, with construction materials alone contributing around 11% [3], [4]. To reduce carbon footprints, it is essential to use more sustainable and renewable construction materials like wood [5]. Timber structures are regarded as a sustainable solution since the quantity of carbon retained in them surpasses the carbon produced during the harvesting and installation process [6]. Timber construction is also less harmful to the environment in terms of air and water pollution and global warming than steel or concrete structures [7]. Furthermore, due to prefabrication and lower on-site labor costs, timber construction can also be cost-effective [8]. Over the past 20 years, the use of mass timber in residential and non-residential structures has increased due to the emphasis on sustainable construction [9].

1.2 Mass-timber shear walls

In parallel to the rising demand for wooden buildings due to increased urbanization and the need for sustainable building practices, there have been significant technological and regulatory advances in wood products and construction. Mass timber panels, compared to conventional lumber, offer superior fire and load resistance, homogeneity, and dimensional

stability [10]. Cross-laminated timber (CLT), a mass timber product made of gluing lumber elements in alternating directions, offers high in-plane strength and stiffness [2], making it suitable for resisting earthquake loads through diaphragms and shear walls in a seismic-force-resisting system (SFRS) [11]. However, CLT panels are considered to behave as rigid bodies; therefore, the strength, stiffness, and ductility of CLT shear wall are determined by the vertical joints (VJ) between the CLT panels, the hold downs (HD) and shear brackets (SB) connecting the panels to their base, and horizontal tension straps (TS) between panels [12].

Design provisions for encapsulated mass timber construction have been included in the 2020 National Building Code of Canada (NBCC) [4], and the 2021 International Building Code [13]. The NBCC defines ductility-related (R_d) and overstrength-related (R_o) force modification factors to reduce seismic design forces and refers to the Standard for Engineering Design in Wood CSA-O86 [14] for design provisions for CLT shear walls. These guidelines aim to ensure that CLT shear walls exhibit coupled wall rocking as the kinematic behavior for dissipating energy during seismic events. These provisions are based on extensive research carried out on CLT connections [15], [16], [17], [18] and shear walls. However, they apply exclusively to platform type construction, where the floors serve as a platform for the storeys above [19].

In balloon-type construction, CLT wall panels span multiple stories continuously, where floors are attached to the sides of the wall panels at each storey [20]. This approach eliminates compression stress perpendicular to the grain in CLT floor panels, eliminates cumulative perpendicular-to-grain shrinkage over the building height, requires fewer panels to achieve slender panel aspect-ratios and eliminates the need for HD and SB connections at typical floors except at the wall base [21].

1.3 Research need and objective

NBCC and CSA-O86 [22] provisions are restricted to platform-type construction and balloon-style construction has not been adequately explored [23]; various aspects like HD and panel-to-panel connections require further research to establish standardized design provisions for this construction configuration to be used as SFRS [20].

The objective of this research is to experimentally investigate the performance of balloon-framed coupled CLT shear walls. The specific objectives are to evaluate the impact of:

1) different HD configuration in balloon framing.
2) different VJ stiffness/strength.
3) horizontally spliced panels with TS.

1.5 Scope and limitations

This study is centered on a full-scale experimental investigation of two-storey balloon-type CLT shear wall system as SLRS, with particular emphasis on quantifying the influence of HDs configurations, VJ stiffness, and TS inclusion on lateral load resistance, strength degradation, energy dissipation, deformation characteristics, and the distribution of kinematic contributions under both monotonic and reversed cyclic loading protocols.

This study is limited to strength evaluation; however, the comprehensive experimental data generated through this research can support future assessments of stiffness and ductility. Factors such as compression zones, frictional effects, biaxial behavior of fasteners, and wall openings were also not considered. Additionally, aspects related to building physics, cost analyses, and constructability fall outside the scope of this work.

Chapter 2 Literature review

2.1 Cross-laminated timber

2.1.1 Overview

Throughout history, wood has been an essential building material, and the use of wood has been increasing recently as part of the transition towards more sustainable building methods. To provide better, more consistent, and more predictable mechanical and physical properties, mass timber products were created [24]. In contrast to conventional dimensional lumber, mass timber products are made by gluing together smaller pieces, like boards, veneers, or strands, to form more robust structural components. Due to the larger sections and better dimensional stability, they are considered an alternative to concrete and steel in the construction industry [10]. There are various mass timber products, the notable ones being glue-laminated timber (glulam), nail-laminated timber (NLT), dowel-laminated timber (DLT), and cross-laminated timber (CLT).

CLT was first developed in the early 1990s in Europe [2]. After initial experiments in Switzerland and Austria, CLT was first used in buildings in the mid-1990s and increasingly in the past two decades due to establishment of standards. CLT comprises of at least 3 orthogonal layers of lumber as shown in Figure 1 [25]; this arrangement provides two-directional strength and dimensional stability. These properties make CLT suitable for various construction elements such as roofs, floors, and shear walls [26] and offer rapid construction [27]. Further, due to the massiveness, CLT also exhibits favorable thermal, acoustic, and fire-resistant properties [28].

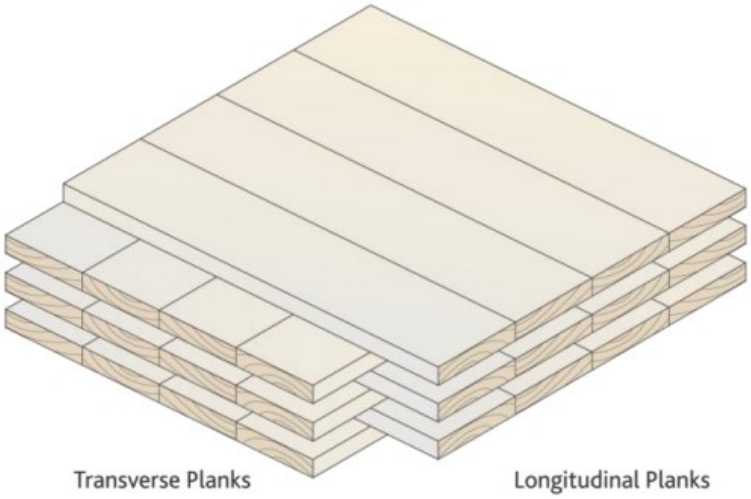

Figure 1 CLT panel configuration [29]

2.1.3 Connections in CLT

CLT because of its in-plane strength, stiffness and dimensional stability, is widely used for the construction of diaphragms and shear walls [26]. But CLT panels lack ductility —the capacity of a material to experience plastic deformation prior to failure— and display rigid body behavior. As a result, the connections in CLT shear walls are required to dissipate energy under seismic loading and provide the required ductility [30], [31], [32], [33].

In CLT shear walls, the primary connection types comprise of panel-to-panel, wall-to-wall, wall-to-floor, and wall-to-foundation connections. Mechanical fasteners like bolts, dowels, and nails were the norm; however, there has been a recent trend toward more innovative solutions, especially self-tapping screws (STS). Just as CLT has revolutionized the timber construction industry, STS has become a significant advancement at the connection level and is considered as state-of-the-art in wood connector technology. STS often do not require predrilling, and their performance in withdrawal and lateral shear has been thoroughly tested and confirmed through extensive research [26], [34], [35].

Panel-to-panel connections along the edges of walls or floors need to be built to resist both out-of-plane bending and in-plane shear. Amongst spline joints, butt joints, and half-lap joints, shown in Figure 2, spline joints where plywood or laminated veneer lumber (LVL) sheets are nailed or screwed into the CLT panels' surface, are the most commonly used type [26]. To connect the CLT shear walls to the foundation or the CLT floor below, HD and SB are employed [19]. The vertical legs of HD are attached to the walls with nails or STS, while bolts are used to anchor the horizontal leg to the foundation. SB are used to connect the walls and floors using screws, nails or bolts, primarily designed to handle shear forces, although SB can also support vertical loads [36].

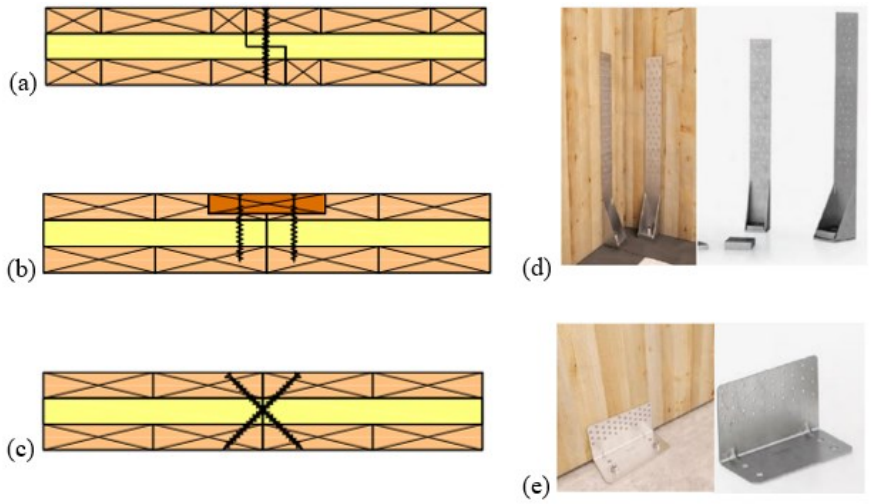

Figure 2 Connections; (a) Half-lap; (b) Surface spline; (c) Butt joint; (d) HD; (e) SB [37]

2.2 CLT shear walls

2.2.1 Overview

For tall timber structures to withstand earthquake loads, SLRS is necessary. Numerous options are available like braced frames, moment frames, shear walls (light wood frame and CLT) and various hybrid systems [33]. Among these, CLT shear walls have become a focal

point of research due to their high in-plane stiffness and strength [18]. Compared to conventional light-frame construction, CLT exhibits a higher strength-to-weight ratio, contributing to consistent and predictable behavior under seismic loading [38]. Moreover, CLT panels are prefabricated, allowing for rapid on-site installation and reduced construction time while maintaining quality [39]. These combined features make CLT shear walls a compelling solution for resilient and sustainable seismic design in modern timber construction.

The two available construction configurations for CLT structures are platform-type and balloon-type. Conventionally, low and mid-rise timber structures are constructed with platform-type configuration in which each floor added to the structure acts as a platform for the storey above it [40], while in balloon-type, the CLT panels are extended through multiple stories, and at times span through the entire structure's height. In contrast to platform-type, balloon-type structures do not transfer gravity loads through the CLT floors [41] and compression perpendicular to grain is avoided [42]. As shown in Figure 3, fewer floor-to-panel and panel-to panel connections make balloon-type construction more efficient [32].

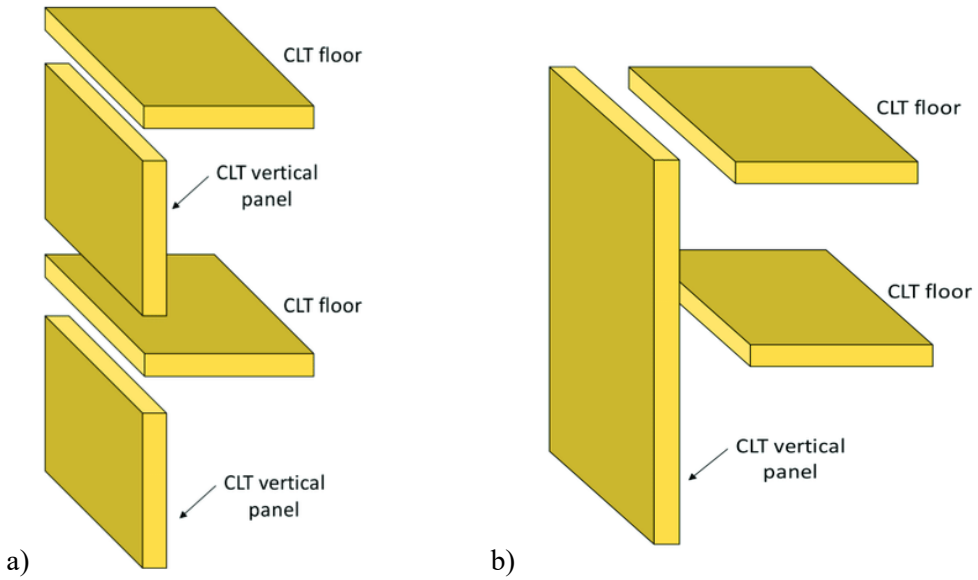

Figure 3 CLT construction: (a) platform-type; (b) balloon-type [32]

2.2.2 Research on platform-type CLT shear walls

In 2004, Dujic et al. examined the boundary conditions of CLT shear walls subjected to seismic forces [43] and concluded that the panels exhibit rigid behavior, with the key to an effective design lying in optimization of ductile connections. The research conducted through the project "SOFIE", which began in 2006, stands as one of the most comprehensive studies. The project aimed to evaluate durability, seismic performance, and fire resistance of CLT buildings through various tests on shear walls and connections. In 2013, Ceccotti et al. [12] concluded the project with three full-scale shake table tests (Figure 4b). The findings demonstrated that CLT multi-storey structures are suitable for seismic regions, displaying high stiffness and appropriate ductility. Additionally, ductile joints were shown to contribute to energy dissipation while ensuring that brittle components remain capacity protected.

In 2010, CLT research began in Canada. Popovski et al. [44] tested a two-storey CLT house under both cyclic and monotonic loading (Figure 4a). Despite variations in parameters such as the number of fasteners and loading direction, all tests revealed a consistent failure pattern, primarily due to the nails failing in the first-floor brackets from the sliding and rocking.

a)  b) 

Figure 4 CLT structure tests (a) FP-Innovation [45]; (b) SOFIE project [12]

Most research on CLT shear walls as LLRS focused on evaluating the performance of connections, which are vital for dissipating energy during seismic events in timber structures. Research conducted at the UNBC Wood Innovation and Research Laboratory has contributed to this field. One study by Pan et al. [35] evaluated the performance of single-storey CLT shear walls with STS connections. 48 component-level tests and 26 single-storey shear walls tests with varying panels (single, double, and triple panels) were conducted. Shear wall tests demonstrated that an increasing number of STS in HD and VJ increased, both stiffness and load-carrying capacity. The number of connected panels had a direct relationship with the strength and associated displacement of the shear walls, while the aspect ratio exhibited an inverse relationship.

a)  b) 

Figure 5 UNBC testing (a) single storey structure [35]; (b) two storey structure [36]

Another study conducted at UNBC by Masroor and Gheisari et al. [36], focused on two-storey coupled platform-type CLT shear walls with STS connections. The structures were tested under reversed cyclic loadings by varying several parameters, such as the presence of

floor mass and acoustic layers, as well as the variation in inter-storey SB and TS. While the addition of acoustic layers had negligible impact on the performance of the structure, the presence of dead load increased the resistance. Furthermore, it was evident that TS were crucial in influencing rocking behavior and maintaining consistent storey drifts.

While the global response of CLT shear walls is largely influenced by geometry, loading, and coupling, the role of connections remains equally vital in defining energy dissipation and ductility under seismic loading. Popovski et al. [46] conducted tests on CLT panels, altering their aspect ratio and connection type. Through a series of quasi-static tests, they concluded that using nails and screws as fasteners resulted in satisfactory seismic performance. Popovski and Karacabeyli [47] demonstrated that using nails as fasteners in HD, along with the addition of vertical load, improves the structure's seismic resilience and ductility. Gavric et al. [48] evaluated the performance of coupled CLT shear walls with various anchoring systems. Increasing the aspect ratio and the number of panels enhanced strength with most deformation occurring in the connections while the CLT panels exhibited minimal deformation. Coupled walls exhibited lower strength and stiffness compared to single walls. However, coupled walls demonstrated greater displacement capacity and ductility.

While extensive research has been conducted on platform-type CLT shear walls, particularly focusing on the performance of different connections and panel aspect ratios [36], [46] several limitations remain unaddressed. Chief among these is the discontinuity at each floor level in platform construction, which introduces vertical joints and potential weak points that may compromise load transfer. Although coupling elements such as TS and AB have been studied, their effectiveness in maintaining continuity and controlling inter-storey drift depends

on the complexity of inter-floor connections [36]. These configurations also increase construction time and detailing demands.

Balloon-framed CLT systems, by contrast, eliminate intermediate floor discontinuities and offer enhanced stiffness, reduced inter-storey slip, and more predictable seismic performance [35], [36]. This research therefore aims to address the knowledge gap by experimentally evaluating the lateral performance of balloon-framed CLT shear walls, investigating how vertical continuity and connection detailing influence global system behavior, energy dissipation, and structural resilience under seismic loading.

2.2.3 Connections in CLT shear walls

In CLT shear walls, the connections are critical in providing ductility since the panels themselves lack this property. It is important that during an earthquake the vertical wall to wall joint connection should be ductile to dissipate energy and undergo inelastic deformations to ensure structural stability. Tannert and Loss [49] discussed different HD solutions. While nailed steel brackets are adequate for low-rise structures, commercially available HD may result in brittle wood failure under higher demand [50]. Doweled slotted-in steel plates also resulted in wood failure. The ductility of such HD may increase by increasing the row spacing and end distance of the fasteners, but it may not always be possible due to dimension constraints [51]. Pinching free connectors were introduced, and instead of using slender fasteners, stocky fasteners with steel side plates (held down with a spring system) were used [52]. Slip friction devices comprise side steel plates that are held together with bolts and disc springs. They exhibit the ability to dissipate more energy without pinching but have a limiting self-centering capability. An advanced version known as resilient slip friction (RSF) connectors was developed to overcome this shortcoming [53].

STS connections have become a state-of-the-art approach. Gavric et al.[18] the behavior of half-lap and spline joints with STS and revealed that half-lap joints offered higher initial stiffness, while spline joints provided greater resistance and displacement capacity. Tomasi et al. [54] were among the first to explore the benefits of mixed-angle screws in timber connections, using screws placed both perpendicular (90°) and inclined (30°-60°) to the grain. They found that inclined screws offered high strength and stiffness but lacked ductility, while perpendicular screws had greater ductility but lower stiffness. Combining both orientations provided a balanced connection with high strength, stiffness, and ductility. This approach was later extended to CLT wall systems, enhancing performance in both in-plane and orthogonal joints [55], [56]. Hossain et al. [16] also examined the performance of half-lap joints, spline joints, and butt joints using inclined STS fasteners under monotonic and cyclic loading. The results indicated that butt joints with doubly inclined STS exhibited greater load-bearing capacity and energy dissipation, offering a cost-effective alternative by eliminating the need for panel machining.

Further investigations by Hossain et al. [57] tested half-lap connections by varying the STS angles for shear and withdrawal loads, concluding that a combination of both provided optimal ductility and stiffness. Joyce et al. [58] also tested double spline and butt joints with angled STS, showing that fully threaded STS inclined at 45 degrees delivered higher stiffness in cases where elastic stiffness was critical. Collectively, these experimental studies highlight the importance of optimizing STS placement and connection types to improve the ductility, stiffness, and seismic resilience of CLT shear walls.

Wright et al. [59] evaluated the seismic performance of STS HD, combining 45° and 90° screws, through monotonic and cyclic tests. They found that these connections could

achieve improved stiffness and displacement capacity over dowel-type connections as shown by Ottenhaus et al. [51]. In a follow-up study, Wright et al. [60] tested CLT specimens with screw angles in HD ranging from 30° to 60°. HD with mixed angled screws demonstrated high strength, stiffness, and ductility. Optimal seismic performance was achieved with 2:1 or 1.5:1 ratio of inclined to perpendicular screws, depending on screw dimensions. Wright et al. [61] expanded the work to evaluate overstrength factors and design approaches. Design strengths based on NZS AS 1720.1 [62] were found conservative, with average overstrength factors of on average 2.0. Moerman et al. [63] tested six CLT shear walls under cyclic loading using mixed-angle HD with a consistent 3:2 ratio of 45° to 90° screws. Strength, stiffness, and panel utilization improved over conventional connectors, though longer walls required out-of-plane restraints to prevent buckling. With proper detailing, HD achieved high ductility without brittle failure. System overstrength factors ranged from 1.7 to 2.0, influenced by frictional uplift resistance, supporting improved seismic design of CLT walls.

2.2.3 Research on balloon-type CLT shear walls

Balloon-framing, introduced by George Snow in 1832, was a groundbreaking construction method that emerged out of necessity due to rapid urban growth, limited access to large timbers, and a shortage of skilled labor [64]. By utilizing standardized, lightweight lumber and machine-cut nails, Snow created a more efficient way to build, which revolutionized construction in the expanding American Midwest. This technique enabled settlers to quickly construct sturdy buildings in areas lacking timber, driving the settlement of resource-scarce regions. Its simplicity and adaptability marked a significant shift from traditional construction methods, laying the foundation for modern light-frame buildings and emphasizing speed, efficiency, and accessibility[65]. Despite advantages such as eliminating

perpendicular-to-grain bearing and shrinkage, requiring fewer panels and connections, and reducing flexural deformation due to minimized cumulative deformation understanding of the design of balloon-type CLT shear walls remains limited [23], [66] highlighting the need for further studies on balloon-frame construction.

Li and Wang et al. [67] compared balloon-type and platform-type CLT shear walls through quasi-static tests on four two-storey walls (S1–S4), varying between monolithic and segmented configurations. Balloon walls demonstrated higher initial stiffness and energy dissipation but experienced joint and HD failures. Wang and He et al. [21] extended this work by testing four reduced-scale (1:3) two-storey specimens, incorporating energy dissipators: O-shaped Flexural Plates (OFP) and Plates with Openings (PO). Balloon-type walls with OFP dissipated 59% more energy than their platform counterparts but experienced greater stiffness degradation and early uplift. Wang and He et al. [68] validated a modified dowel-type model using previous experimental data [69] and revealed that balloon-type walls generally had initial stiffness and ductility. Higher aspect ratios reduced stiffness more than capacity, and vertical loads improved ductility across both configurations. While stiffer HD increased stiffness, they slightly compromised ductility.

To evaluate the effect of connection stiffness on the seismic performance of balloon-type CLT shear walls, Zhang et al. [70] designed two prototype structures: a 12-storey and an 18-storey building. The study demonstrated the pivotal role of STS connections in enhancing structural stiffness and seismic performance. Specifically, STS connections acting in withdrawal provided superior stiffness, reaching up to 12 kN/mm per screw, while combining shear and withdrawal actions further optimized both stiffness and ductility. Horizontal connections had the greatest impact, with reduced stiffness leading to increases in inter-storey

drifts of up to 47%. In contrast, vertical connections had minimal influence, contributing to less than a 1% change in overall stiffness. These findings emphasize the critical importance of STS connections in achieving effective lateral load resistance in balloon-type CLT shear walls.

Krauss et al. [71] studied balloon-type CLT shear walls with high-capacity HD using mixed-angle STS (12 at 90° and 8 at 45°) through cyclic testing of three full-scale, two-storey coupled walls. The specimens featured half-lap wall-to-wall joints, and variations in screws spacing and angles were tested to assess their influence. Results proved previous findings [34] and showed that angled STS in HD and wall joints improved panel utilization, strength, and stiffness. A supporting numerical study of 36 configurations revealed that increasing wall height, length, and base HD enhanced overall strength, stiffness, and energy dissipation. Stronger wall-to-wall joints also contributed to better system performance.

Xing et al. [72] investigated the lateral deformation behavior of balloon-type CLT shear walls, focusing on the influence of HD, VJ stiffness and wall aspect ratios. An analytical model, validated through finite element analysis, evaluated the effect of bending, shear, rocking, and sliding contribute to lateral stiffness. The results showed a nonlinear relationship between normalized lateral stiffness and VJ stiffness, with significant variation based on HD stiffness. Higher aspect ratios reduced overall stiffness, with rocking dominating at low stiffness and bending becoming more significant with high aspect ratios. The study emphasized that joint stiffness and aspect ratio are critical factors in deformation behavior.

A study conducted at UNBC investigated the influence of ledger beams on the performance of balloon-type CLT shear walls [73]. Twelve half-scale, two-storey balloon shear wall specimens with a 3:1 aspect ratio were tested using four different ledger types: Type A (steel with distributed screws), Type B (steel with concentrated screws), Type C (pin-

connected steel), and Type D (wood with distributed screws). Each configuration underwent two monotonic and one cyclic test to assess lateral performance. Dickof et al. [73] reported that ductility ratios ranged from 2.9 to 3.7, with Type B ledgers showing the highest ductility and Type C the lowest. Type A ledgers provided the greatest stiffness and energy dissipation, while Type C allowed unrestricted rocking but had reduced energy dissipation. Shahnewaz et al. [66] further evaluated the seismic performance of these configurations, confirming that all ledger types retained gravity load-carrying capacity after seismic loading, with minimal strength reduction. Type A again demonstrated the highest energy dissipation and stiffness. Both studies concluded that the ledger systems did not impede rocking behavior and validated the seismic suitability of balloon-type CLT walls for multi-storey applications.

Chen and Popovski developed predictive models to evaluate the seismic response of balloon-type CLT shear walls, focusing on the influence of HD, SB and VJ. The model was validated through experimental testing of four specimens—two single walls and two coupled walls—subjected to static and cyclic loading. Later, Chen and Popovski [74] enhanced these models to also account for panel resistance [75]. The updated models were used to analyze the effects of vertical load and aspect ratio on wall behavior. Results showed that increasing wall height and thickness improved stiffness and lateral resistance, while both properties declined with higher aspect ratios. Sliding had minimal influence on total deflection, but bending deflection became dominant reaching up to 80% as aspect ratio increased. Shear and rotational deflections contributed less, at 1% and 20% respectively. The models also revealed that vertical load effects varied with the ratio of compression zone length to wall height.

While most seismic research on CLT shear walls has focused on platform-type configurations, the understanding of balloon-type systems remains limited [23], [66]

highlighting the need for further investigation. To address this, the Canadian Construction Materials Centre (CCMC) developed a technical guide to help establish force modification factors (R_d and R_o) for engineers to design new lateral load resisting systems like balloon type CLT shear walls [76]. This guide outlines a performance-based framework involving archetype development, testing of energy-dissipative components, and nonlinear dynamic analyses to ensure compliance with life safety and seismic performance objectives.

Yang et al. [77] applied this guideline to assess the seismic behavior of two 12-storey balloon-type CLT structures designed per NBCC [4]. Each structure featured single and coupled rocking walls in both directions, with R_d/R_o values of 4/1.2 (east-west) and 2.0/1.5 (north-south). Non-linear history analyses confirmed that the collapse margin ratios met FEMA P695 [78] criteria. In a related study, Lepine-Lacroix and Yang [79] proposed a dual-pinned self-centering wall (DSCW) system for balloon-type CLT structures, using friction dampers to enhance seismic performance. Designed through the equivalent energy design procedure (EEDP), the 12-storey prototype met displacement targets and satisfied FEMA P695 [78] criteria under both time history and incremental dynamic analyses. These results highlight the potential of balloon-type coupled CLT walls with innovative dissipators as effective solutions for resilient tall timber buildings.

The above research highlights significant progress in understanding the seismic performance of balloon-type CLT shear walls, including insights into panel aspect ratios, connection detailing, and system-level deformation modes. However, most of these studies were limited to reduced-scale testing [68], focused on component-level behavior [71], or explored configurations using idealized or novel dissipative devices [79], which do not fully represent full-scale balloon-framed construction as it would be deployed in practice. Few

studies have addressed how the continuity of full-height CLT panels and vertical connection detailing affect overall lateral performance, including inter-storey drift, hold-down performance, and wall-to-wall interaction under realistic seismic demands. Additionally, while existing research often isolates the effect of connections (HD, SB, VJ), the combined influence of these parameters on system behavior remains insufficiently explored.

These limitations underscore the need for comprehensive investigation at the system level. Accordingly, this research examines the seismic performance of full-scale balloon-framed CLT shear wall systems with varying connection configurations subjected to reversed cyclic loading. By emphasizing realistic construction details, continuity across stories, and inter-panel coupling effects, this study addresses the disconnect between component-level test results and the global response of full structures. The findings aim to inform the development of rational design methodologies and contribute to establishing performance-based guidelines for balloon-type CLT systems under seismic demands.

2.2.4 Code implementations

Although CLT was developed in Europe over two decades ago, only the forthcoming Eurocode 8 [80] is expected to include guidelines CLT structures, categorizing multi-panel CLT walls separately from monolithic ones [81]. In the US, CLT was first included in the 2015 International Building Code (IBC) [82] and the National Design Specification for Wood Construction (NDS) [83], supported by ANSI/APA PRG320 [84]. The IBC-2021[13] provides guidelines for constructing mass timber buildings up to 18 stories. While ASCE 7-16 [85] allowed only timber plywood shear walls as LLRS, but the 2022 ASCE-7 [86] added seismic design guidelines for CLT shear walls. Furthermore, SDPWS (Special Design Provisions for

Wind and Seismic) were also included in NDS-2021 [83] provisions, addressing CLT as lateral load-resisting system.

In Canada, in 2014, Clause 8 of CSA O86 [87] introduced design specifications for CLT in compliance with the ANSI/APA PRG 320 [84]. In 2016, CSA O86 [88] was updated to include guidelines for CLT shear walls and diaphragms, targeting platform-type structures in seismic regions with height limits of 20 meters in high seismic areas and 30 meters in low seismic areas. Capacity-based design provisions were established, requiring energy-dissipative connections at specific locations while other connections must remain non-dissipative [9]. In the 2019 edition of CSA O86 [22], the provisions were revised significantly, eliminating combined rocking/sliding as an acceptable kinematic mode to achieve the response modification factors (R_o=1.5, R_d=2.0) specified in NBCC-2020 [4]. The provisions also required discrete HD to resist uplift and be designed as non-dissipative, ensuring brittle components remain protected while ductile components absorb seismic energy. The 2024 updates to CSA O86 introduced further refinements to CLT seismic design. A key addition was the explicit requirement to include connector deformation in lateral drift calculations, reflecting the connection-governed, rocking behavior that dominates CLT wall response.

2.3 Summary of literature review

As mass timber construction continues to gain prominence, the use of CLT shear walls has become increasingly viable, even in seismically active regions. The review highlights that CLT panels behave as rigid bodies, relying on connections such as VJs, HD, and TS to dissipate energy during seismic events. These connections are crucial to achieving the desired rocking and ductile behavior, with VJs playing a primary role in energy dissipation. Research also

shows that greater panel aspect ratios enhance deformation capacity but reduce stiffness, emphasizing the importance of optimizing design for specific applications.

While platform-type CLT structures dominate current design provisions, balloon-type systems present significant advantages, including minimized cumulative shrinkage, enhanced energy dissipation, and fewer inter-floor connections. While recent studies have demonstrated the potential of balloon-type CLT shear walls to meet seismic performance criteria, the performance of critical connections, including VJ, HD, and TS significantly influences system behavior, especially under lateral loads. Further research is needed to optimize these connections and understand their interaction with wall aspect ratios. Addressing these gaps is essential for developing comprehensive design guidelines and enabling the formal codification of balloon-type CLT shear walls in seismic design provisions, ultimately advancing their use in resilient and sustainable tall timber buildings.

The recent advancements in CSA O86 demonstrate growing confidence in CLT as a viable SFRS. The incorporation of capacity-based design, explicit recognition of connection ductility, and the requirement to account for connector deformation in lateral drift calculations reflect a shift toward performance-based engineering for mass timber. However, these provisions remain specific to platform-type CLT construction. This research addresses that gap by investigating the seismic performance of balloon-framed CLT shear walls—a system with the potential for improved continuity, reduced cumulative deformation, and enhanced seismic resilience, but currently not addressed by Canadian design standards.

Chapter 3 Materials and methods

3.1 Objective and overview

The objective of this experimental investigation was to evaluate the seismic performance of balloon-type CLT shear walls, specifically to evaluate the impact of:

1) Different HD configurations.
2) Different VJ stiffness/strength.
3) Horizontally spliced panels with TS.

To achieve these objectives, two-storey structures, each 2.64 m tall, 1 m × 2 m on plan, as shown in Figure 6, were constructed and tested. The program consisted of a total of eleven tests, each conducted with different fastening configurations, as shown in Table 1.

a) b) c)

Figure 6 Two-storey CLT structure: a) front view, b) side view, c) isometric view

Table 1 Test parameters

Test	Load	HD	1st storey spline	2nd storey spline
B1-S [1)]	Mon	21 - ø12×120 mm @90˚	16 - ø8×100 mm	10 - ø8×100 mm
B1-M	Mon	12 - ø12×120 mm @90˚ +8 - ø10×160 mm @45˚	16 - ø8×100 mm	10 - ø8×100 mm
B2-S	Cyclic	21 - ø12×120 mm @90˚	-	-
B2-Si	Cyclic	15 - ø12×120 mm @90˚	-	-
B2-M	Cyclic	9 - ø12×120 mm @90˚ +6 - ø12×200 mm @45˚	-	-
B2-Mi	Cyclic	9 - ø12×120 mm @90˚ +6 - ø10×160 mm @45˚	-	-
B3-S	Cyclic	15 - ø12×120 mm @90˚	12 - ø8×100 mm	8 - ø8×100 mm
B3-M	Cyclic	9 - ø12×120 mm @90˚ +6 - ø10×160 mm @45˚	12 - ø8×100 mm	8 - ø8×100 mm
B4-S	Cyclic	15 - ø12×120 mm @90˚	24 - ø8×100 mm	16 - ø8×100 mm
B4-M	Cyclic	9 - ø12×120 mm @90˚ +6 - ø10×160 mm @45˚	24 - ø8×100 mm	16 - ø8×100 mm
B5-S [2)]	Cyclic	15 - ø12×120 mm @90˚	12 - ø8×100 mm	8 - ø8×100 mm

Note 1: In all tests, the SBs were attached with 6 - ø12×120 mm screws, and the ledgers were attached with 8 - ø12×120 mm screws to each shear wall panel.

Note 2: In B5-S, the panels were spliced and connected with TS. The outer TS were attached with 8 - ø12×200 mm screws and the inner TS were attached with 8 - ø10×180 mm screws.

On **Structure B1**, two monotonic tests were conducted to verify the test set-up and obtain a monotonic push-over curve. B1-S used 21 - ø12×120 mm @90° screws in the HD (replicating the configuration used in previous platform-type tests), while B1-M used the mixed angle HD configuration: 12 - ø12×120 mm @90° and 8 - ø12×120 mm @45°.

On **Structure B2**, four reversed cyclic tests were conducted, all without VJ, to isolate the impact of HD configuration. In B2-S, the original HD was tested, because of floor fixture restraints, the number of screws in the HD was reduced to 15 in B2-Si. In structure B2-M, by accident fully threaded screws ø12×200 mm @45° were installed; however, this test provided some valuable insights, too. In B2-Mi, 9 - ø12×120 mm @90° fully threaded screws were combined with 6 - partially threaded screws ø10×160 mm @45˚.

On **Structures B3** and **B4**, two reversed cyclic tests were conducted each. B3-S and B4-S had HD configurations of 15 - ø12×120 mm @90°, while B3-M and B4-M used the mixed angle HD configuration of 9 - ø12×120 mm @90° and 6 - ø12×120 mm @45°. The difference between B3 and B4 was in the number of screws in VJ. B3 had VJ with 12 - ø8×100 mm on the first level and 8 - ø8×100 mm on the second, whereas B4 had stiffer VJ, using 24 - ø8×100 mm on the first level and 16 - ø8×100 mm on the second. These tests were conducted to evaluate the impact of VJ stiffness on shear wall performance.

On **Structure B5**, one reversed cyclic test conducted was conducted to evaluate the impact of horizontally spliced panels. B5-S had the same HD and VJ configuration as B3-S; the horizontal splices were connected with outer TS, fastened with 8 - ø12×200 mm screws, and inner TS, fastened with 8 - ø10×180 mm screws.

3.2 Materials and connections

3.2.1 CLT panels

The CLT panels were strength grade E1 with Douglas Fir-Larch MSR rated lumber. These panels were 5-ply and 139 mm thick (35+17+35+17+35 individual layers thicknesses). The panels were 6.0 m × 1.0 m and had an average moisture content of 10.6% and an apparent density of 547 kg/m³. The 2.0 m × 1.0 m floor and roof panels were constructed from strength grade V2 5-ply CLT, with thickness of 139 mm (35+17+35+17+35).

3.2.2 Screws

Various types of STS were used, all manufactured from hardened carbon steel with protective coatings for indoor use, and their strengths according to ETA-16/0906 [89]: fully threaded Kombi LT ø12×120 mm (11.2 kN withdrawal resistance and 10.4 kN shear resistance); partially threaded CSK ø10×160 mm (8.6 kN withdrawal, 6.3 kN shear); CSK ø10×180 mm (8.6 kN withdrawal, 6.3 kN shear); fully threaded CSK ø12×200 mm (11.2 kN withdrawal, 8.6 kN shear); and partially threaded Ecofast ø8×100 mm (5.2 kN withdrawal and 3.9 kN shear).

3.2.3 Hold-downs

The HD were custom-made steel plates of steel grade 44W/300W. Each HD measured 370 mm in width, 975 mm in height, and featured a 70 mm long horizontal leg. The vertical component was 12.7 mm thick, while the base plate was 28.2 mm thick. For screws installation, the vertical section had 13 mm circular holes for STS to be installed at 90° and elliptical holes for STS to be installed at 45° STS. The HD base plate had three ø19 mm holes for anchoring.

Two types of screw configuration in the HD were used to assess the performance of balloon-type CLT shear walls: Type S, which utilized only fully threaded STS (ø12×120 mm) installed at a 90°; and Type M, which maintained the same number of screws but featured a mixed configuration: fully threaded STS ø12×120 mm installed at 90° and partially threaded STS ø12×160 mm positioned at a 45° using special washers, as shown in Figure 7. The number of screws followed a 3:2 ratio of perpendicular to inclined screws, based on previous experimental studies on balloon-type systems [34]. The objective was to assess whether a mixed-angle configuration could achieve comparable strength while enhancing stiffness.

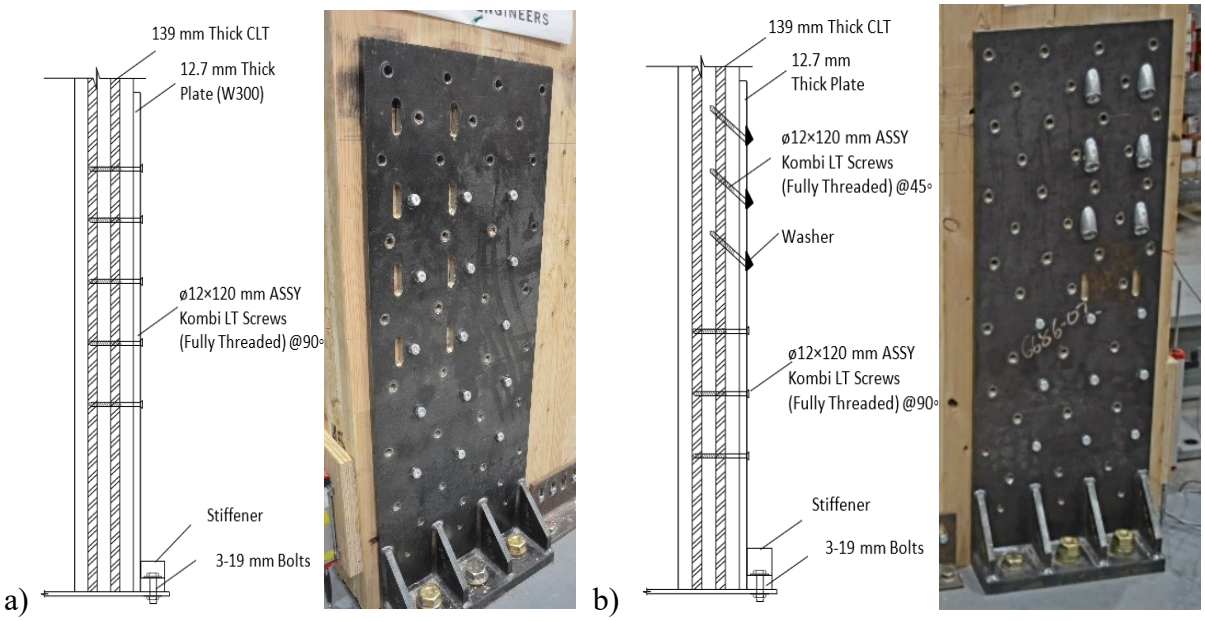

Figure 7 HD: a) type-S sketch and photo; b) type-M sketch and photo

3.2.4 Shear brackets

The SB, shown in Figure 8, were fabricated from custom steel plates of grade 44W/300W. Each bracket was 340 mm wide, with vertical and horizontal legs measuring 127 mm and 89 mm in length, respectively, and a thickness of 6.35 mm. The vertical leg

featured elliptical slots, each 11 mm wide, allowing for the installation of STS to eliminate uplift resistance and ensure that only shear forces are resisted. In tests B1-S and B1-M, the SB were attached with 8 - ø12×120 mm screws, in the remaining tests, the SB were attached with 6 - ø12×120 mm screws. In all tests, 3 bolts each 19 mm in diameter were installed on the horizontal leg to anchor the SB.

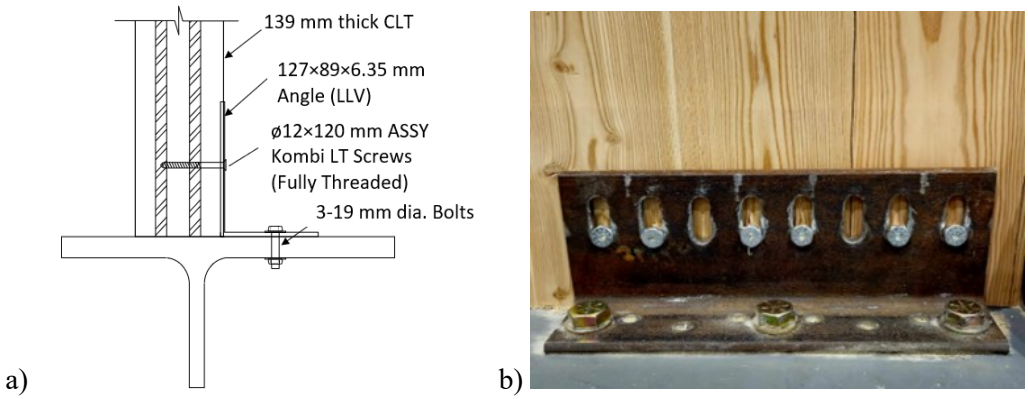

Figure 8 Custom shear bracket: a) schematic; b) SB attached by STS and bolts

3.2.5 Vertical joints

The VJ between panels utilized surface-mounted Douglas Fir plywood splines measuring 25 mm × 140 mm × 2440 mm at each storey. These splines were fastened to the panels using ø8×100 mm partially threaded STS, with an edge distance of 30 mm and screw spacing of 150 mm, as illustrated in Figure 9. Two VJ configurations with differing stiffness levels, by varying the number of screws, were employed to evaluate the influence on overall shear wall behavior. The objective was to investigate how increased joint stiffness affects lateral strength, energy dissipation capacity, and the global seismic response of the system. In most structures, splines were attached with 12 STS per panel edge at the first storey and 8 STS per panel edge at the second storey, resulting in a total of 24 and 16 screws per spline,

respectively. For structures B4-S and B4-M, the number of STS was increased to 24 and 16 per panel edge for the first and second storey, respectively.

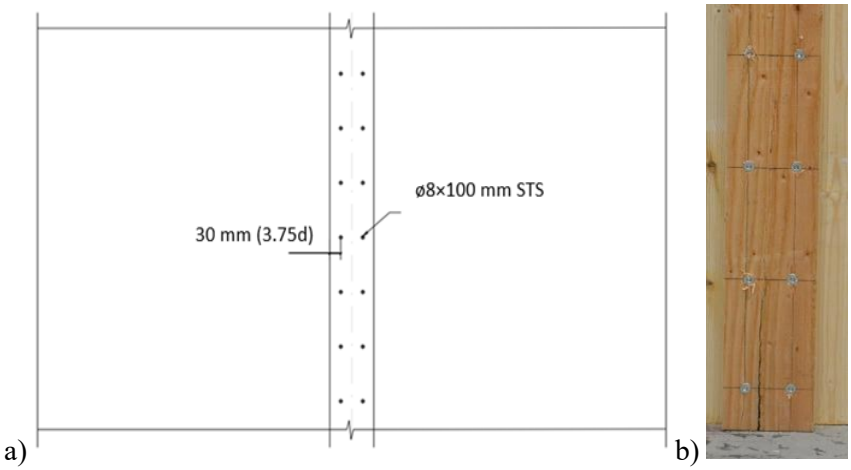

Figure 9 VJ: a) sketch, b) photo

3.2.6 Tension straps

In Structure B5, the panels were horizontally cut above the first storey level and then reconnected using TS. This configuration was motivated by the practical length limits of CLT panels, which require vertical splicing in buildings exceeding six stories. The joint was proportioned to rely solely on TS for vertical continuity, enabling an assessment of their impact on uplift resistance, ductility, and energy dissipation under seismic loading. These TS were made of custom steel plates of grade 44W/300W. The outer TS was 200 wide, 660 mm long, and 6.5 mm thick, while the TS, positioned next to the vertical wall-to-wall joint, were 186 mm wide, 929 mm long, and 4.8 mm thick. The TS, shown in Figure 10, featured ø13 mm elliptical holes. Fastening was achieved using 8 fully threaded STS ø12×200 mm at the top and bottom of the outer TS and 8 fully threaded STS ø10×180 mm at each end of the inner TS. All screws were installed at a 45° angle with 45° washers.

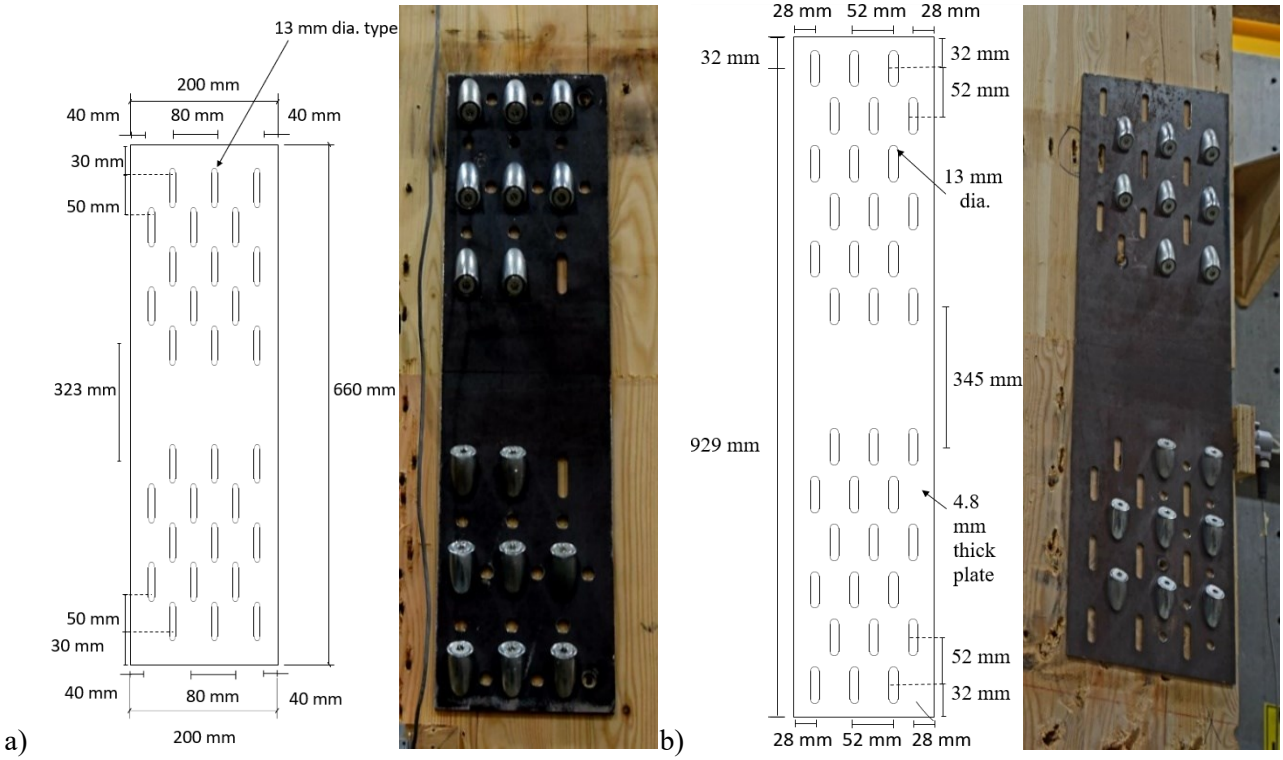

Figure 10 TS a) inner TS sketch, b) outer TS sketch, c) photo

3.2.7 Ledgers

To support the CLT panels of the first and second floors, and to transfer the lateral loads from these floors to the shear walls, ledgers were installed at both floor levels. L-shaped steel angles, with dimensions of 152 × 152 × 10 mm, were attached to the floor and wall panels using 16 fully threaded STS ø12×120 mm along its vertical leg and horizontal legs,, as shown in Figure 11. The ledgers were designed as capacity-protected elements to ensure that inelastic deformations would be concentrated in the intended energy-dissipating HD and VJ.

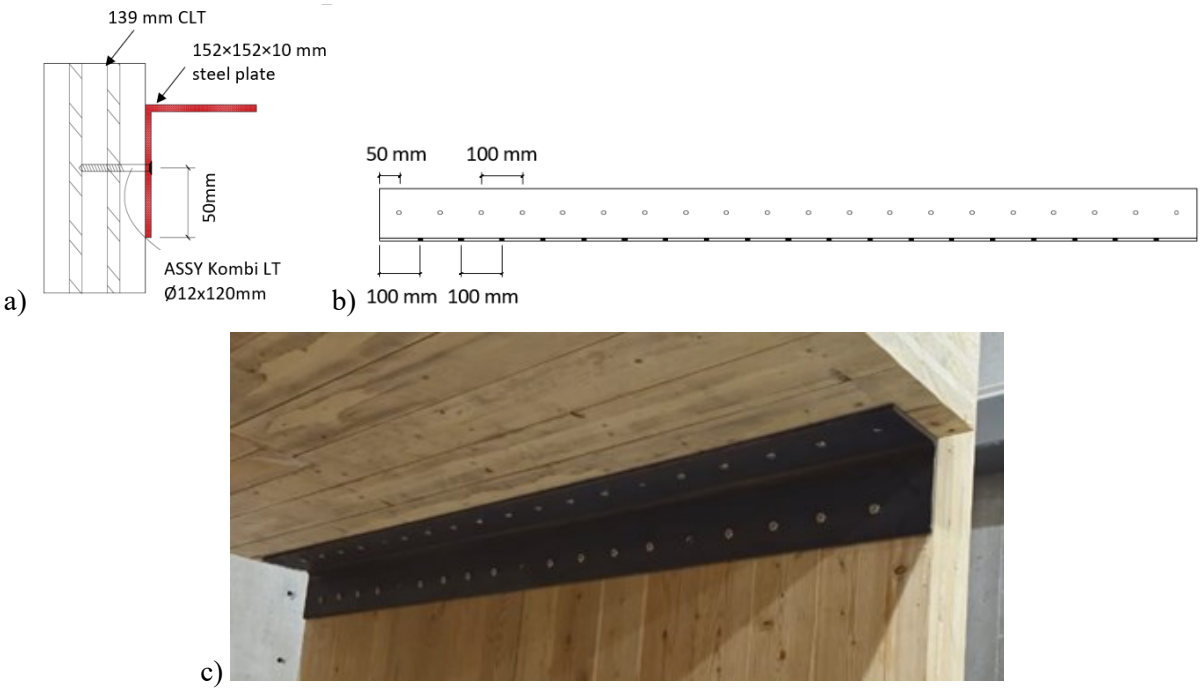

Figure 11 Custom ledger: a) side view; b) front view; c) photo

3.3 Methods

3.3.1 Assembly

The structures were built following a balloon-framing configuration, in which CLT panels run continuously. The panels were connected to the base steel fixture using HD at the exterior ends and SB at the center of the panel base on a steel base fixture that was bolted to the reaction floor (Figure 12a). After lifting the first two opposite panels (south-left and north-right) into place and securing them to the steel base fixture, the first-floor ledgers were attached at mid-height, and the corresponding floor panel was installed onto the ledgers and between the first two panels. Subsequently, the remaining two panels (south-right and north-left) were lifted into position (Figure 12b), connected to the base fixture, and anchored to the first-storey ledgers with screws. Finally, the second-storey ledgers were attached, and the second-level floor was installed. No additional dead loads were applied to the structures to isolate and

evaluate the behavior of the shear walls under lateral loading conditions without the influence of vertical compressive forces.

a)  b) 

Figure 12 Assembly of house: a) steel base fixture; b) installation of panels on base fixture

3.3.2 Instrumentation

A total of 32 sensors (Figure 14 and Figure 14) were installed to measure the following metrics:

- Load and stroke from the top and mid actuators (a1, a2)
- Uplift of shear walls at HD (#1, #4, #5 and #8)
- Uplift of inner corners at base level (#2, #3, #6 and #7)
- Sliding against steel base fixture at the base level (#9, #10, #11 and #12)
- Relative slip between wall panels at first storey (#13 and #14)
- Relative slip between wall panels at second storey (#25 and #26)
- Distortion of the CLT panels at first storey (#15, #16, #17, #18, #19, #20, #21 and #22)
- Ledger slips at first storey (#23 and #24)
- Ledger slips at second storey (#27 and #28)

- Horizontal displacement of the first and second storey slabs (#29 and #30)
- Wall lateral displacement at second floor level (#31 and #32)
- Uplift at outer and inner TS (#15', #16', #17', #18', #19', #20', #21', #22')

String pots and Linear Variable Differential Transducer (LVDT) were used. Half of the sensors were installed on the North side and half of them on the South side shear walls. The sensor locations are illustrated in Figure 14.

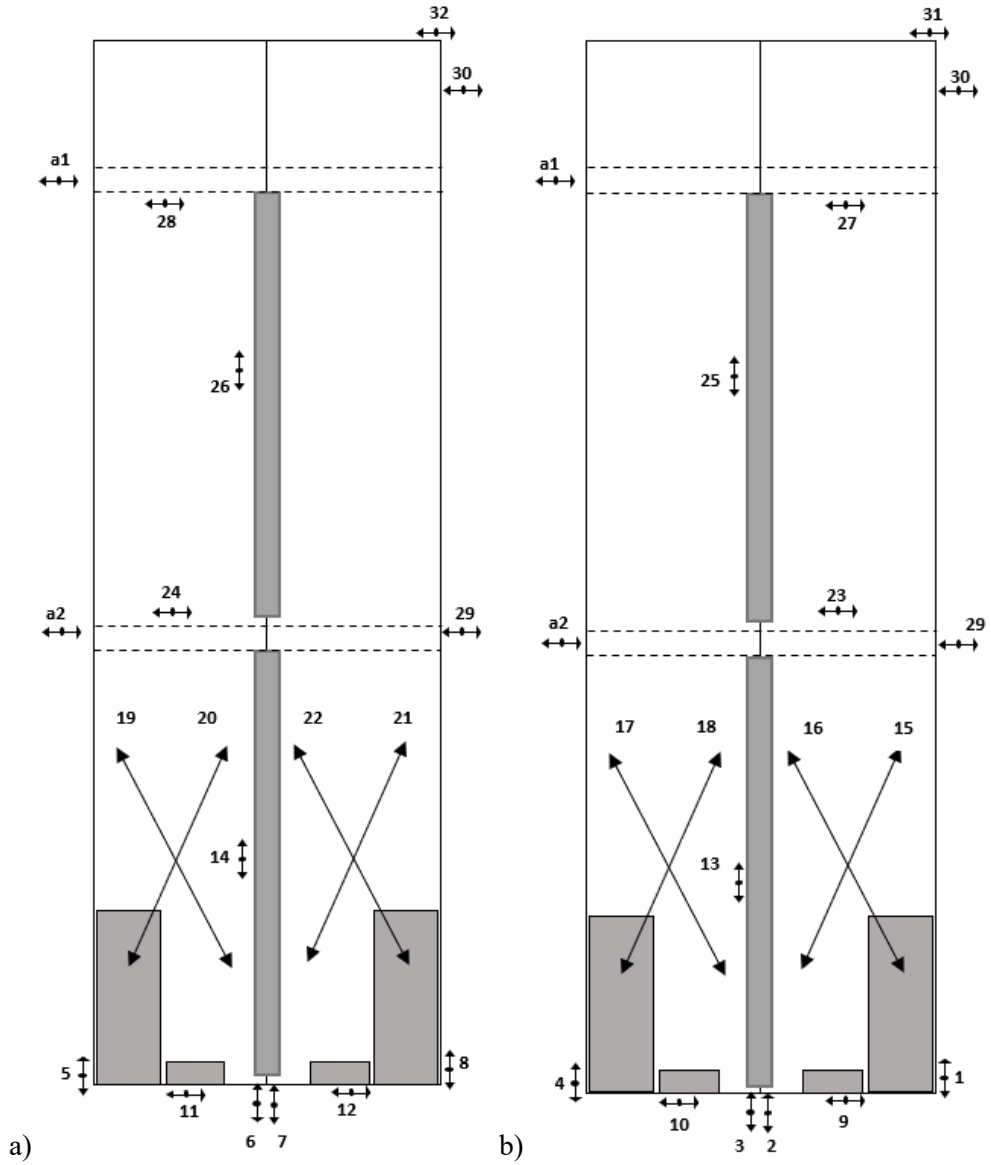

Figure 13 The location of sensors: a) north face; b) south face

Panel distortion was recorded to isolate the contribution of in-plane deformation of the CLT panels. For Structures 1 to 4, sensors #15 to #22 were dedicated to measuring panel distortion in monolithic walls. In structure 5, these sensors were reassigned to measure uplift at the TS. To differentiate, the sensors were labelled in #15' to #22', as shown in Figure 14.

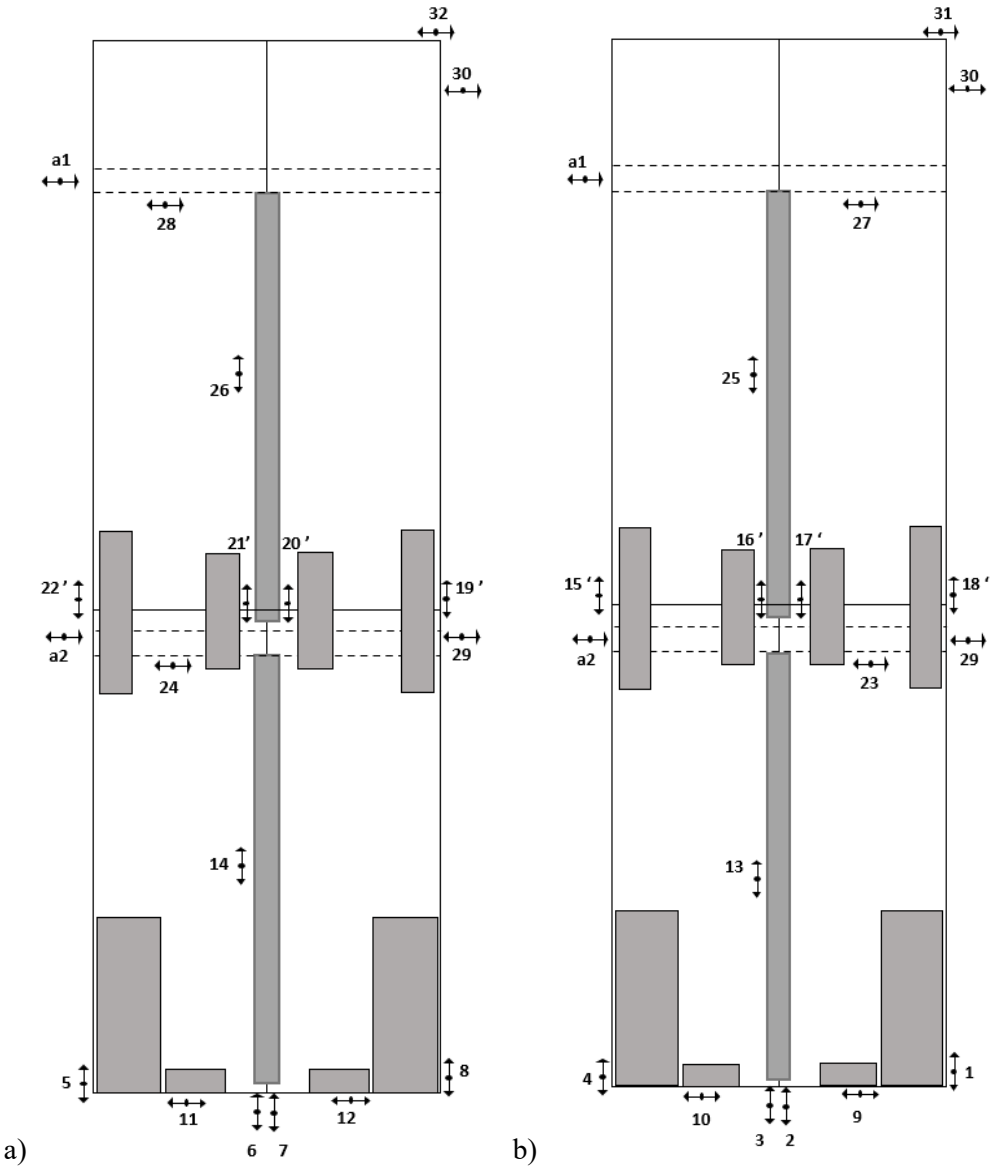

Figure 14 The location of sensors (B5-S): a) north face; b) south face

3.3.3 Loading protocol

The reversed cyclic tests adhered to the ISO-16670 protocol, as outlined in ASTM E2126-09 [90]. This protocol groups displacement cycle into phases with progressively increasing amplitudes as shown in Figure 15, with 300 mm lateral displacement chosen as the target displacement. This target displacement was selected to evaluate the displacement capacity and post-peak performance of the balloon-framed CLT shear walls beyond the code-prescribed limits. After initial cycles of smaller magnitudes, each phase includes three fully reversed cycles at displacement levels of increments of 60 mm (1.15% drift based on the centre line of top floor height of 5215 mm):

60 mm → 1.15% drift,

120 mm → 2.30% drift,

180 mm → 3.45% drift,

240 mm → 4.60% drift,

300 mm → 5.75% drift,

360 mm → 6.90% drift.

Two actuators were used, the one on the second floor (lead actuator) was displacement-controlled, and the one on the first floor (slave actuator) was forced-controlled. At each step of loading, the force F_{lead} was recorded at the second level actuator and half of that force was applied by the first storey actuator to follow an inverted triangular load distribution as shown in Figure 16a. These lateral loads were applied by means of two steel plates which were bolted to the first and second floor panels as shown in Figure 16b.

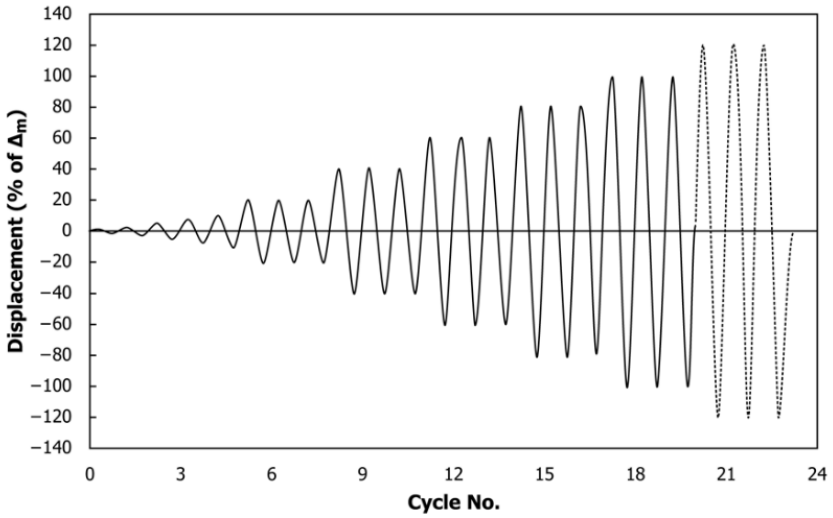

Figure 15 Loading protocol

a)

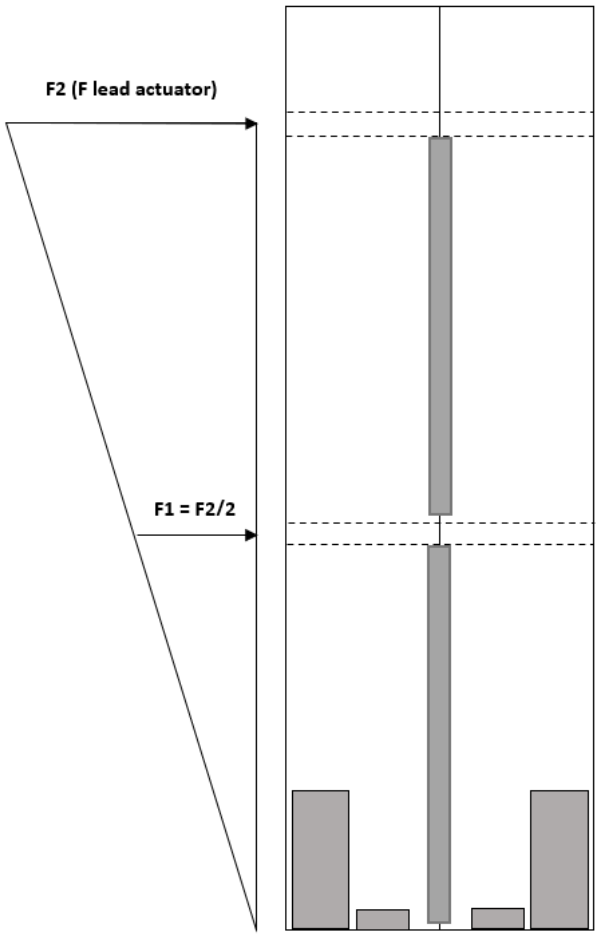

b)

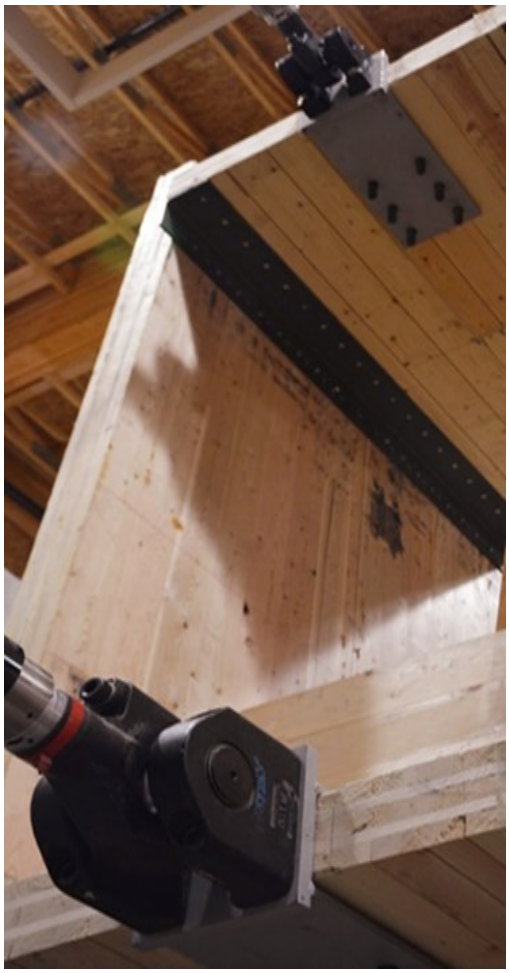

Figure 16 Load application; a) schematic, b) photo of fixture

Chapter 4 Results

The detailed results and failure modes for tests B3-S and B3-M are exemplary presented in Figure 17 to Figure 29. The results of the other tests are presented in Appendices 2-4. The primary difference between the B3-S and B3-M wall configurations lies in the HD detailing. B3-S employed a HD with all screws oriented in shear (90°), whereas B3-M utilized a mixed-angle screw configuration, combining screws at both 90° and 45°. All other connection details remained consistent between the two tests, as summarized in Table 1.

4.1 Horizontal displacements

The total horizontal storey displacements and drifts of the two floors for structures B3-S and B3-M are illustrated in Figure 17. B3-S, which comprises HD with screws installed in shear, exhibited linear and elastic behavior up to 3.4% drift. The lateral load at this drift ($F_{+3.4\%}$) reached 288 kN. Beyond this point, a reduction in load was observed, and at 5.7% drift, the load decreased to 274 kN. The positive and negative envelope curves were closely matched: the maximum negative lateral force at -3.4% drift ($F_{-3.4\%}$) was approximately 306 kN, while at -5.7% drift, it decreased to 290 kN. At 5.7% drift (300 mm second storey displacement), the first storey experienced displacements of 137 mm and -136 mm in positive and negative directions, respectively.

Structure B3-M, comprising of HD with mixed angled screws, followed a similar trend, but exhibited a linear behavior only up to 2.2% drift. The lateral load at 3.4% drift ($F_{+3.4\%}$) reached 262 kN, and at 5.7% drift, it dropped to 219 kN. At -3.4% drift, the lateral resistance was -254 kN, and at -5.7% drift, it dropped to -225 kN. The first storey displacements at 5.7% drift were 138 mm and -136 mm, identical to those observed at the B3-S structure.

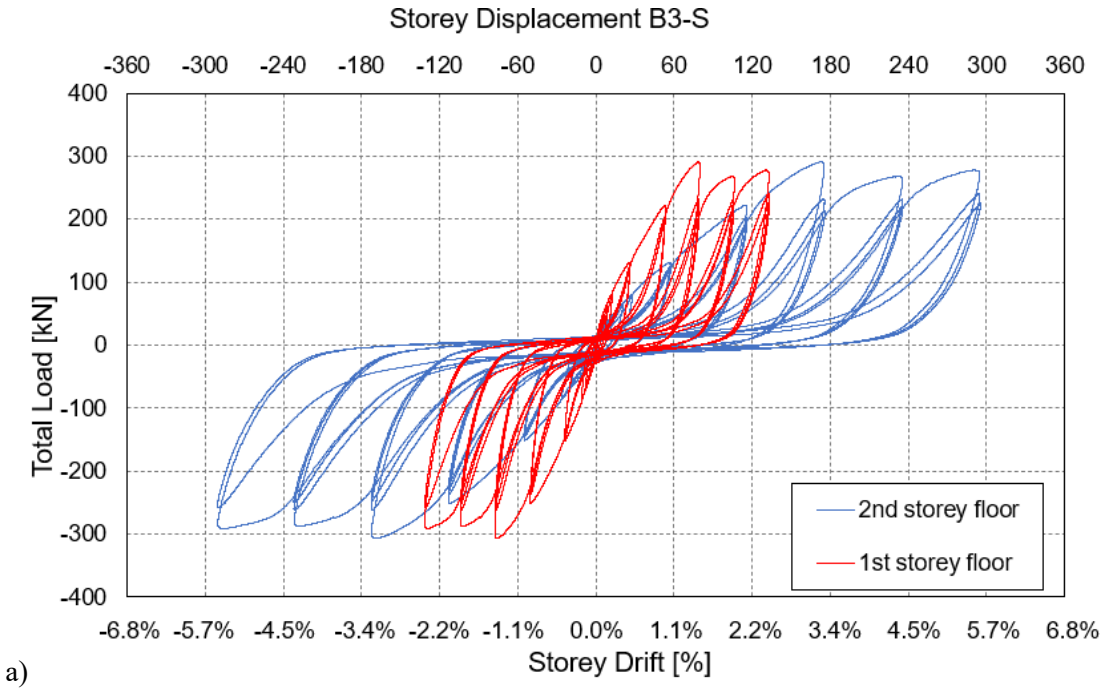

a)

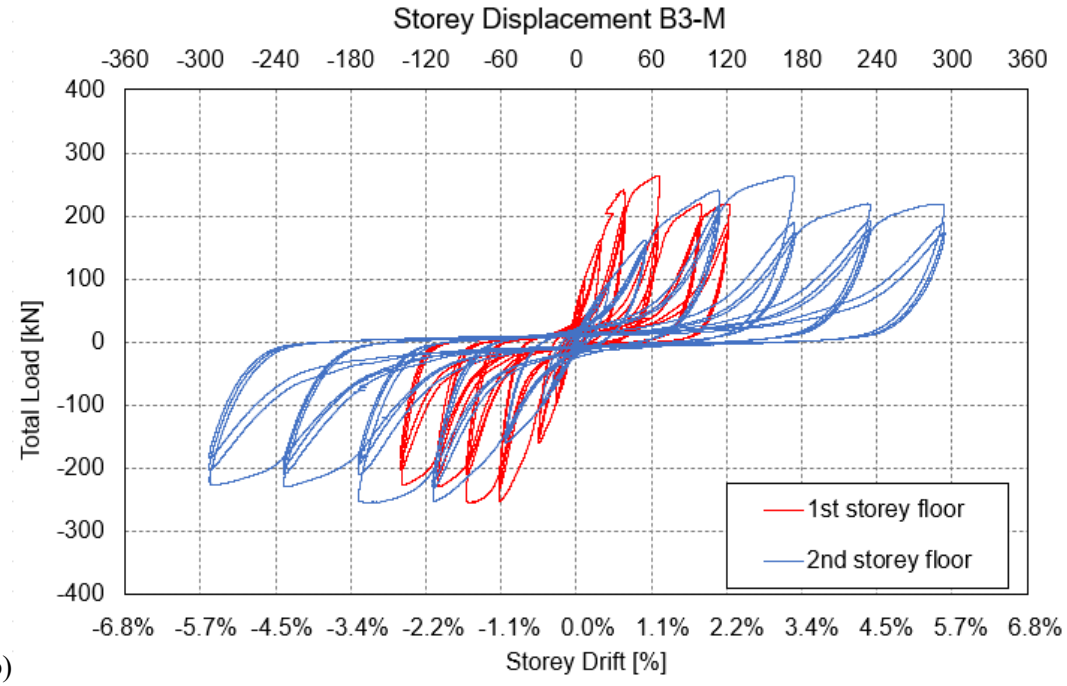

b)

Figure 17 Storey displacements; a) B3-S, b) B3- M

4.2. Hold-down uplift

The vertical uplift responses of the four HD for structures B3-S and B3-M, two on each of the north and south side shear walls, are presented in Figure 18. For Structure B3-S (Figure 18a), the load–displacement envelopes were linear up to +3.4% drift. At +5.7% drift, the HD experienced vertical uplifts of 49 mm (south-left) and 42 mm (north-left). During pull cycles at -5.7% drift, the south-right and north-right panels showed uplifts of 44 mm and 48 mm, respectively. Across all panels, negative uplifts (compression of the CLT panels) ranged between 3 mm and 4 mm. The HD initially displayed linear-elastic behavior. As drift increased, the response transitioned into the inelastic range, where the screws began to yield, leading to a reduction in both stiffness and strength. At 5.7% drift, yielding was observed in all HD screws. Due to a 20% drop from the maximum load resistance (F_{max}), the test was terminated.

For structure B3-M, which featured HD with mixed-angle STS, the HD exhibited comparable linear behavior up to +3.4% drift, as shown in Figure 18b. At this level, the north-left and south-left panels experienced uplifts of 25 mm and 27 mm. During the pull cycles, the north-right and south-right panels recorded uplifts of 26 mm and 28 mm. At +5.7% drift, all HD reached a maximum uplift of 52 mm.

The mixed angle HD exhibited higher initial stiffness compared to B3-S. At 3.4% drift during the first cycle, some angled screws began to withdraw. By the end of that drift level, several angled screws had fully withdrawn, while the bottom-row shear-installed screws started yielding. As the drift increased to 4.5%, all angled screws were fully withdrawn, and the remaining screws continued to yield, reducing the HD overall resistance. By 5.7% drift, the HD had lost its capacity to resist additional loads due to withdrawal and yielding. Notably, in both specimens, a slight increase in resistance was observed at 5.7% drift relative to 4.5%.

This is likely attributed to the engagement of shear keys in resisting uplift, as the HD had lost most of their load-carrying capacity by that stage.

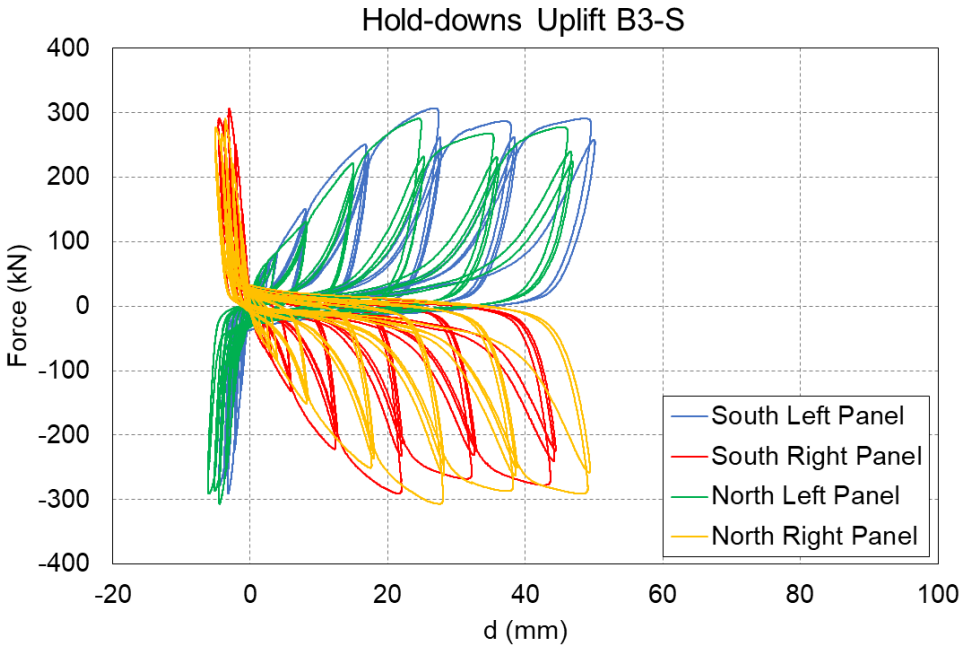

a)

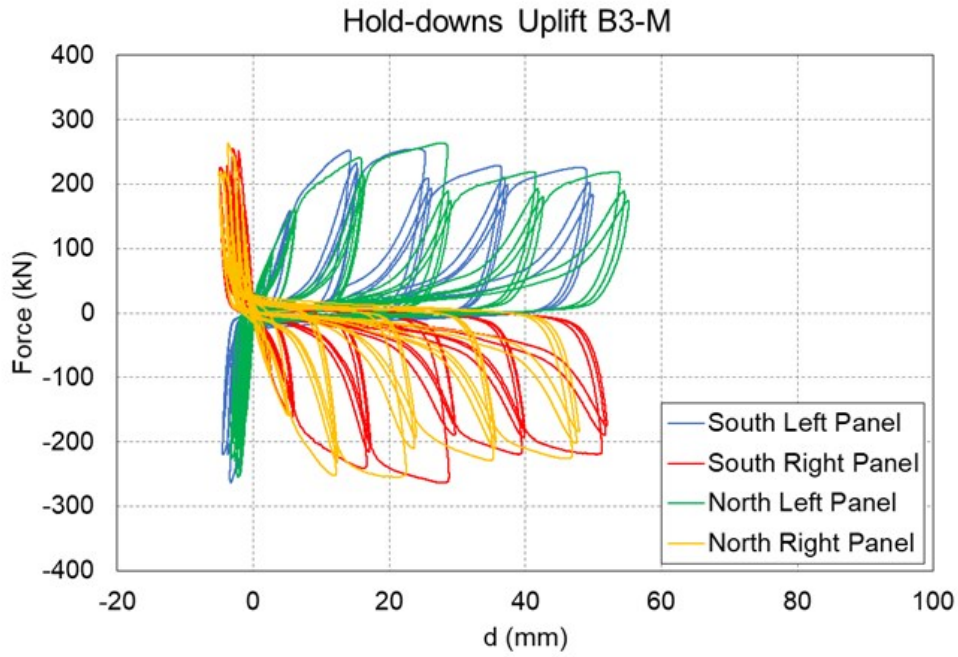

b)

Figure 18 HD uplifts; a) B3-S, b) B3-M

4.3 Inner corners uplifts

The vertical uplift behavior at the four inner corners for structures B3-S and B3-M is illustrated in Figure 19.

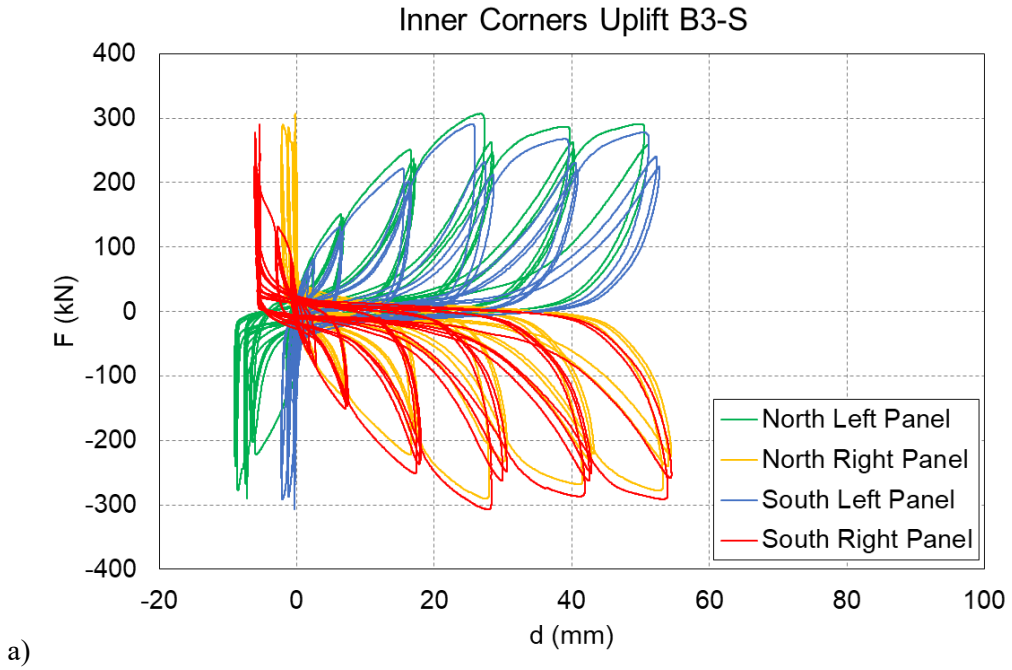

a)

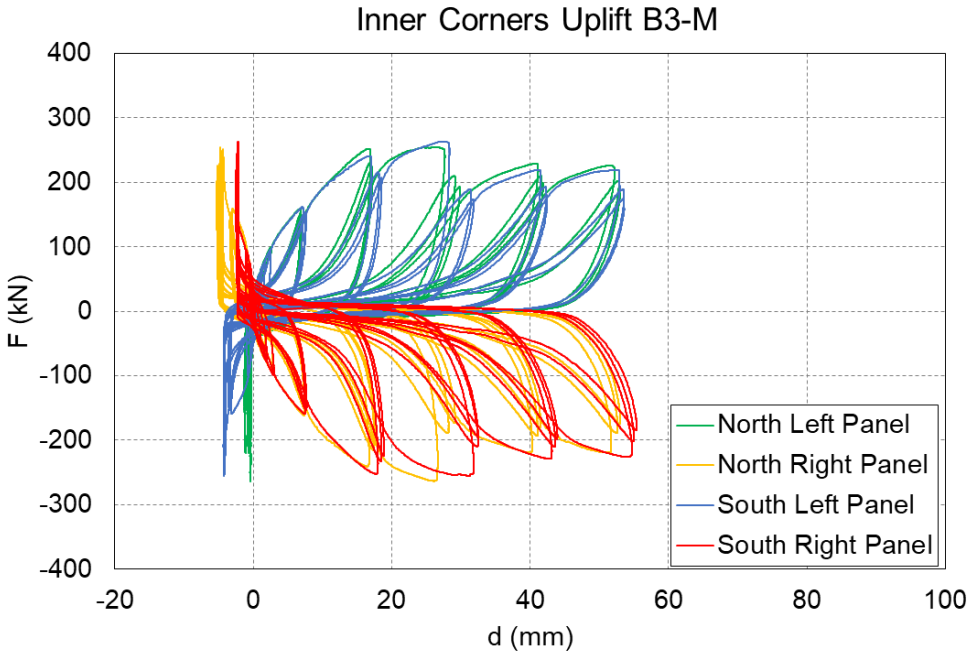

b)

Figure 19 Inner corner uplifts at base level; a) B3-S, b) B3-M

In both structures, the uplift was nearly linear up to a drift of +3.4%, with all inner corners exhibiting similar behavior. At +5.7% drift, the vertical displacement reached 50 mm in the left panels and 53 mm in the right panels. During pull (reverse) cycles, the inner corners experienced compressive displacements (negative uplift), ranging from 2 mm to 8 mm in the left panels and 2 mm to 6 mm in the right panels. For Structure B3-M (Figure 19b), the uplift deformations were slightly higher than in B3-S, with 52 mm in the left panels and 54 mm in the right panels at maximum drift. Compression during pull cycles ranged from 0 mm to 4 mm in the left panels and 2 mm to 5 mm in the right panels.

4.4 Panel sliding

The sliding displacements recorded at the base level for structures B3-S and B3-M are presented in Figure 20. During the initial drift cycles till ±2.2%, B3-S recorded an average displacement of 3 mm, whereas B3-M exhibited a lower value of 2 mm. As drift demands increased to ±3.4%, B3-S reached an average of 6 mm, while B3-M remained limited to 4 mm. At the maximum drift level of ±5.7%, sliding displacements became more pronounced: B3-S averaged approximately 11 mm under push loading and −9 mm under pull loading, whereas B3-M remained more restrained with averages of 7 mm and −6 mm, respectively. At the beginning of both tests, the shear keys were primarily resisting panel sliding. However, near 5.7% drift, the screws in the SB also began to resist uplift and contribute to HD performance. Overall, throughout testing, no shear failure of the SB screws was observed.

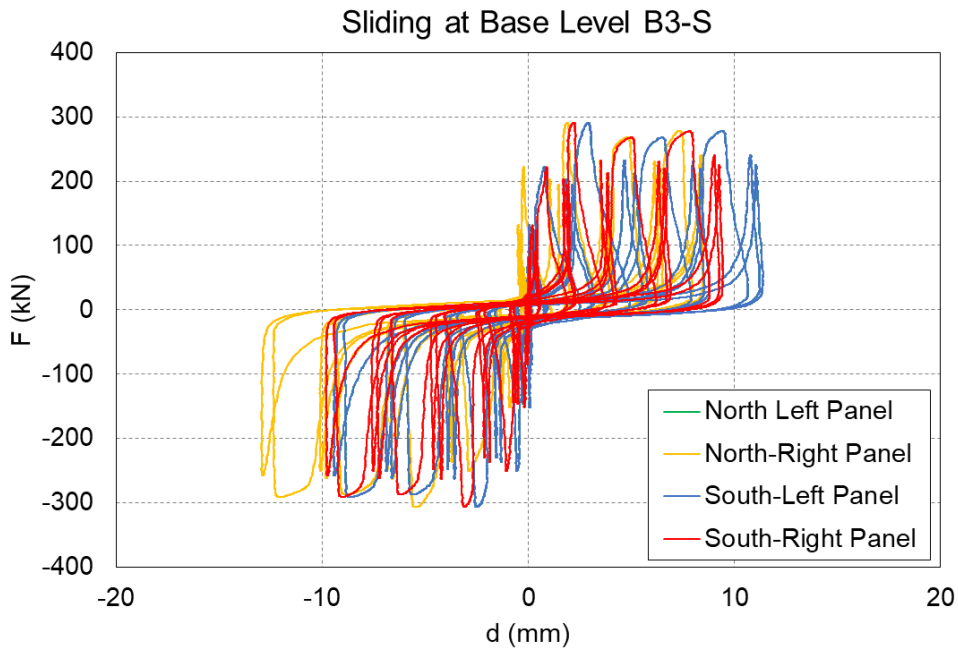

a)

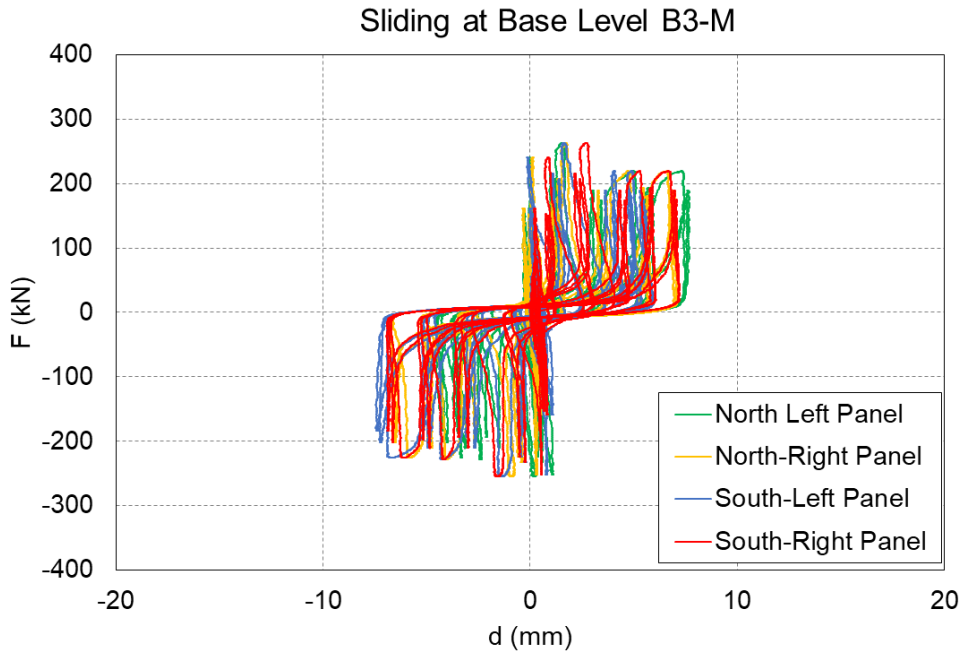

b)

Figure 20 Panel sliding at base level; a) B3-S, b) B3-M

4.5 Panel-to-panel displacement

The panel-to-panel displacements at the VJ, which serve as a key energy dissipation mechanism in coupled-panel shear walls, are illustrated for B3-S and B3-M in Figure 21.

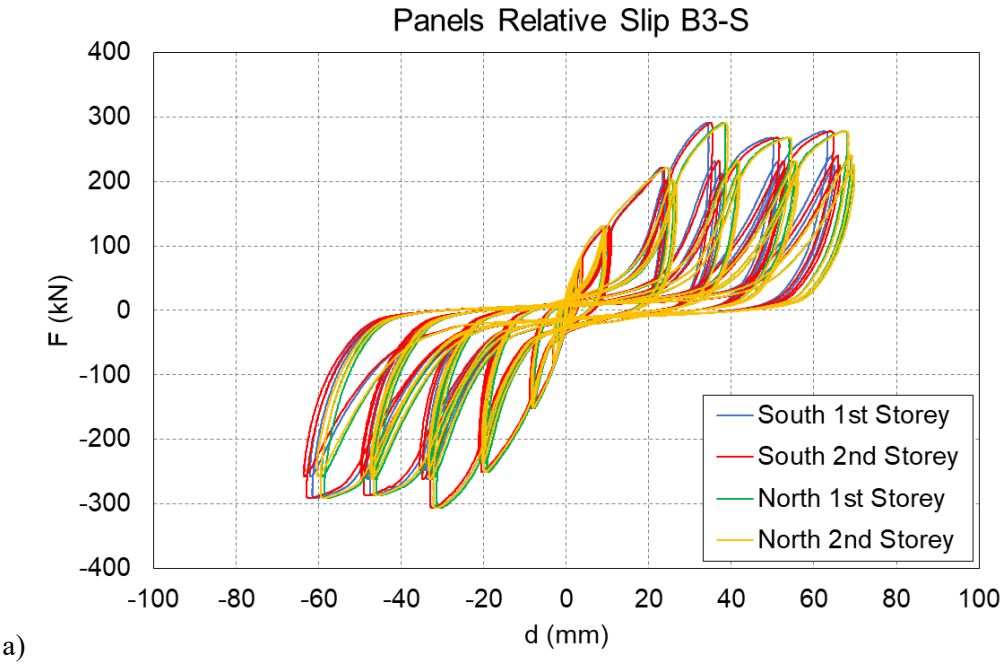

a)

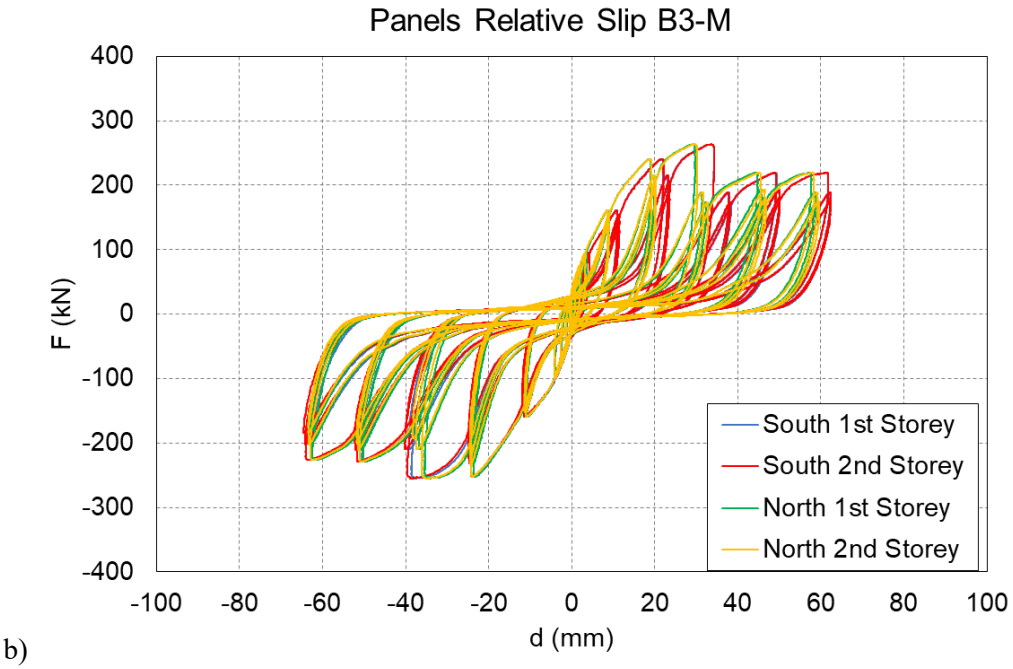

b)

Figure 21 Panels relative displacement: a) B3-S, b) B3-M

For structure B3-S, at +5.7% drift, panel-to-panel displacements ranged from 61 mm to 68 mm in the first storey and from 65 mm to 69 mm in the second storey. In B3-M, relative displacements were slightly lower, ranging from 60–62 mm in both storeys at peak drift. The

spline joint screws in B3-S and B3-M initially exhibited linear-elastic behavior with no signs of failure. At the 3.4% drift cycles, deformation in the fasteners and transitioned into inelastic domain and there was a significant amount of strength degradation. By the final cycle at this drift level, some screws had already failed, accompanied by noticeable strength degradation. With further drift increase to 5.7%, the screws experienced complete deformation and failure. At this stage, the spline joints had lost their ability to dissipate energy effectively.

4.6 Ledgers slip

The relative displacement between the ledgers and wall panels, measured at both storeys on the north and south sides of the structure, is illustrated in Figure 22. For structure B3-S, at +5.7% drift, the ledger slips at the first storey reached approximately 11 mm, while during the pull cycles, it increased slightly to -13 mm. At the second storey, the displacements were lower, ranging from 5 mm to -9 mm during push and pull cycles, respectively. In Structure B3-M, the behavior was similar. At the first storey, ledger displacements were approximately ±11 mm during both push and pull cycles, while at the second storey, the slip was consistently around ±8 mm in both directions. In both the tests, the fasteners in the ledgers behaved elastically till 3.46% drift but afterwards with an increase in drift the behavior changed and at 5.7% drift most of the ledger screws at both storey levels were either completely yielded or had failed.

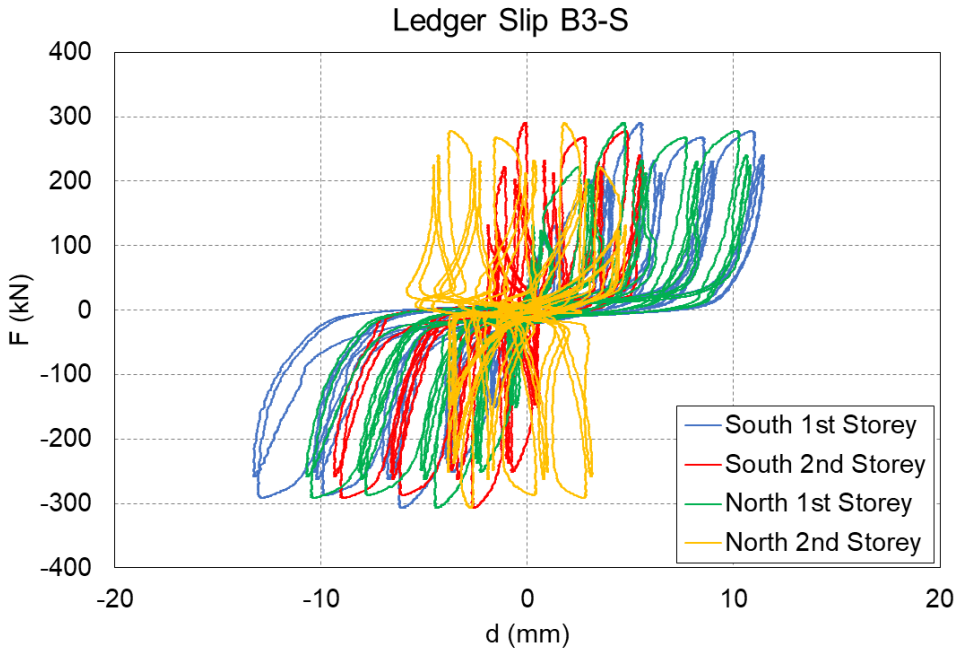

a)

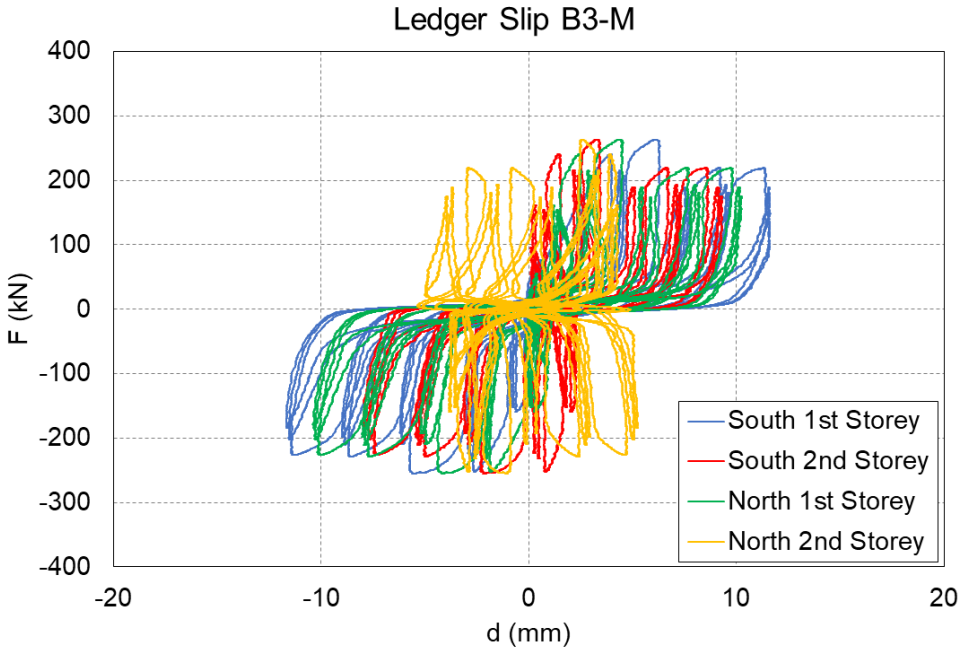

b)

Figure 22 Ledgers horizontal displacement; a) B3-S, b) B3-M

4.7 Wall displacement

The displacement of the wall panels parallel to the direction of loading was recorded at the panels opposite the applied load, as illustrated in Figure 23. For structure B3-S, at ±5.7%

drift, the displacements were +286/297 mm and -293/-282 mm for the south and north wall, respectively. For structure B3-M, the wall panels exhibited even more symmetrical displacement.

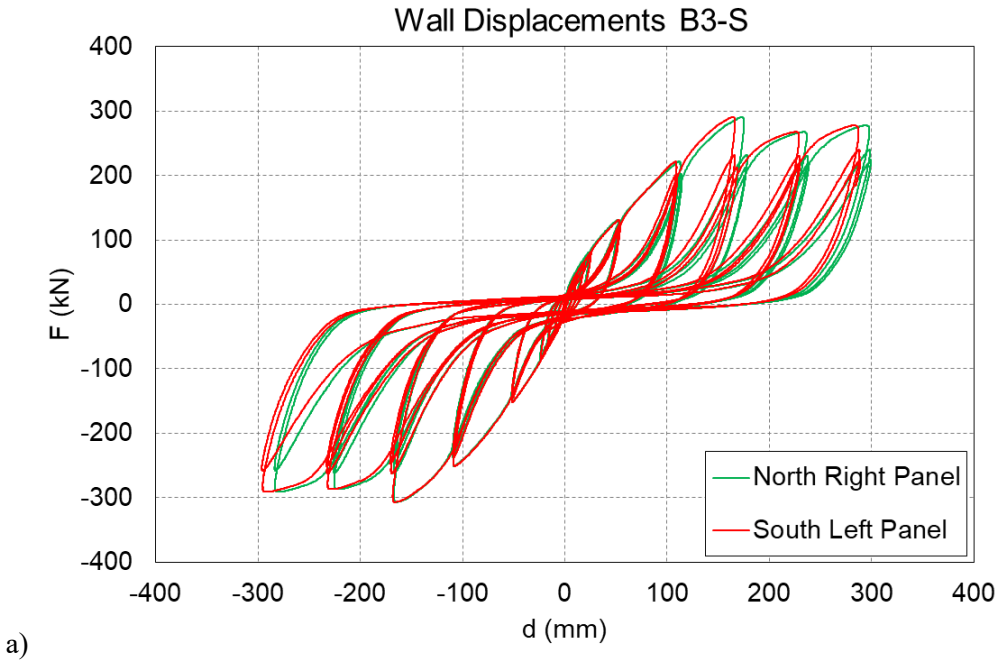

a)

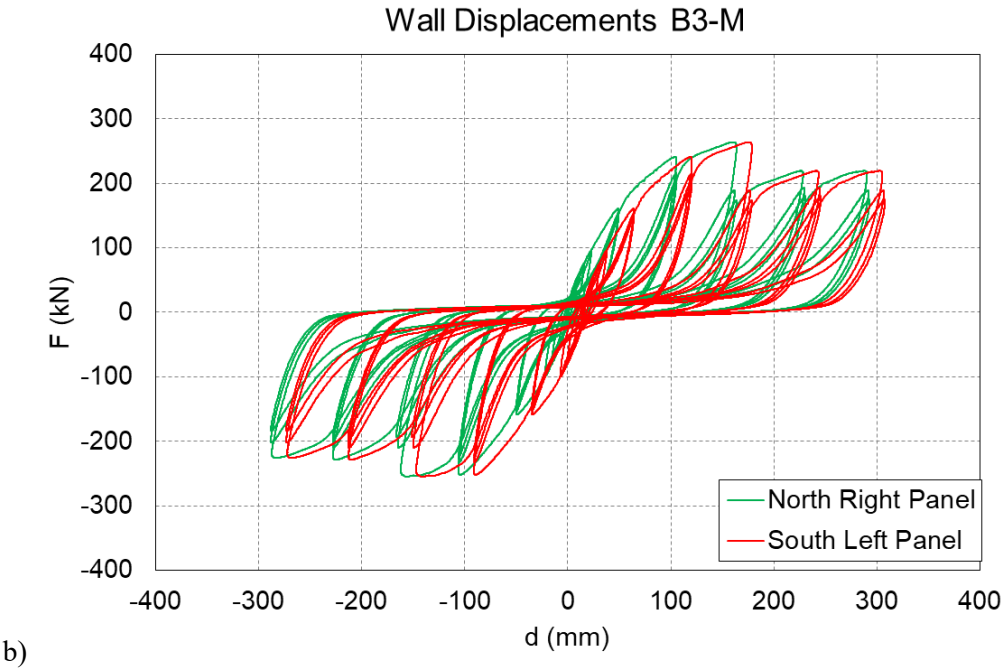

b)

Figure 23 Wall displacements; a) B3-S, b) B3-M

4.8 Panel distortion

To confirm the assumption that CLT panels behave like rigid bodies, the panel distortion was measured. The results from tests B3-S and B3-M are shown in Figure 24. Across both tests, distortions remained less than 2 mm, but the B3-S configuration exhibited slightly more distortion compared to B3-M, particularly in the south wall panels. The maximum measured distortion during tension cycles reached approximately 2 mm, primarily in the left panels of the north and south walls. In contrast, compression cycles produced near-zero displacements.

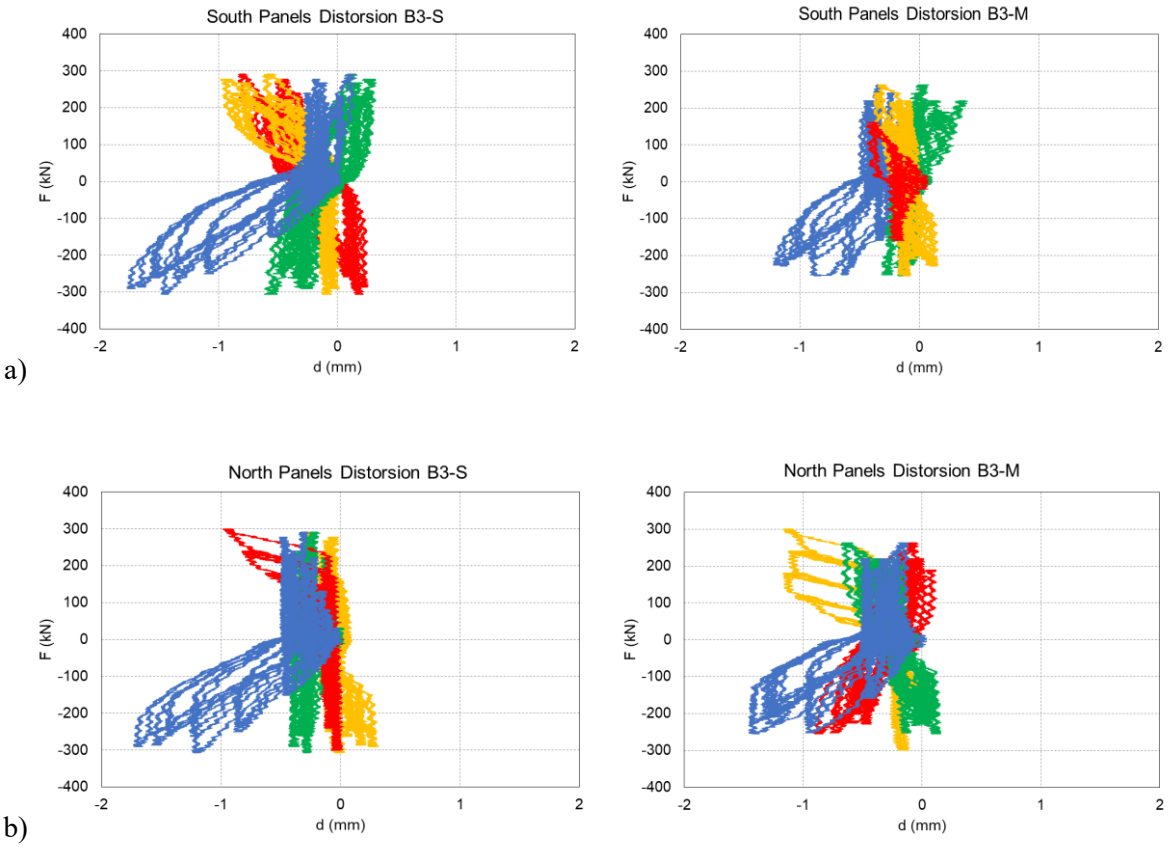

Figure 24 Panel distortion in structures B3-S and B3-M; a) south panels, b) north panels

4.7 Failure modes

4.7.1 General remarks

One of the objectives of the experimental testing was to gain insights into the failure characteristics of balloon-type CLT structures. Structures B3-S and B3-M after testing are shown Figure 25. Pre- and post-deformation images of all the structures and their connections are included in Appendices 1 and 4. Across all test configurations, although the applied load dropped to 80% or less of the peak resistance, there were no signs of global instabilities, with no occurrences of structural collapse, overturning, or full connection failure, even at drift levels reaching 5.7%.

a) 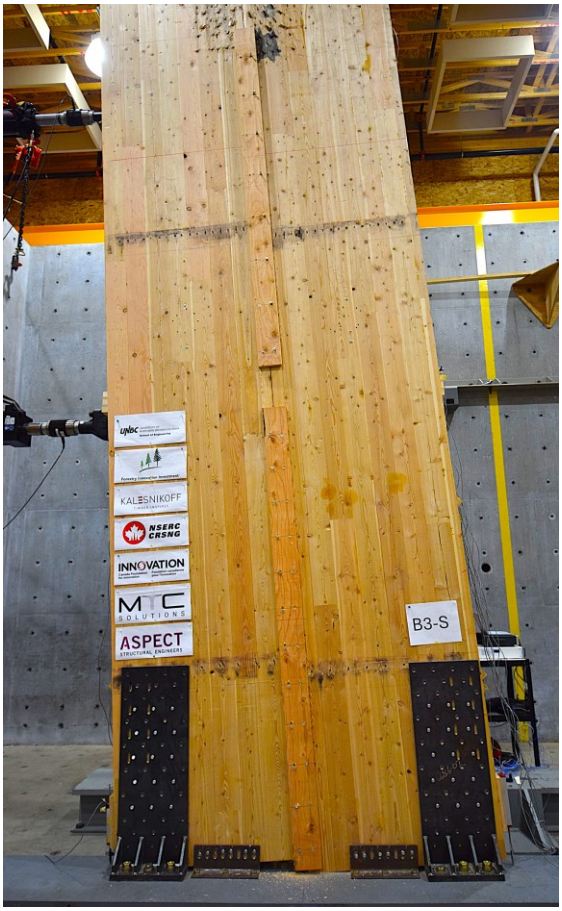

b) 

Figure 25 Structure after test: a) B3-S: b) B3-M

4.7.2 Vertical joints

The VJ were designed to enable relative vertical displacement between the segments to dissipate energy and facilitate the desired rocking mechanism. In all tests, coupled wall configurations exhibited pronounced rocking behavior under lateral loading. With an increase in drift, plastic deformations developed in the spline joints. Relative displacement between panels led to screw yielding, shear failure, or withdrawal of fasteners (Figure 26a and b), marking the initial yielding behavior of the structure. This was typically followed by localized crushing of the plywood splines as shown in Figure 26b. Screws yielding and localized crushing of plywood spines served as the primary source of energy dissipation in the CLT shear walls, validating the intended performance of the flexible spline joint design.

a)  b)  c) 

Figure 26 a) VJ screws after testing, b) spline with yielded screws, c) broken screws

4.7.3 Hold-downs

The HD screws yielded while resisting uplift in both tests; however, no shear or brittle failures were observed in any of the HD screws nor the CLT panels, as exemplary shown in

Figure 27. In mixed-angle HD configurations, some partially threaded STS installed at 45° experienced withdrawal. In most of the tests with mixed-angle HD configurations, the STS installed at 45˚ were partially threaded except in test B2-M, where 6 - ø12×200 mm fully threaded screws were used shown in Figure 27e. These screws were completely withdrawn before the test could progress beyond 3.4% drift, supporting previous research findings that fully threaded screws exhibit poor withdrawal resistance. The HD yielded screws for B3-S and B3-M are illustrated in Figure 27 (c and d).

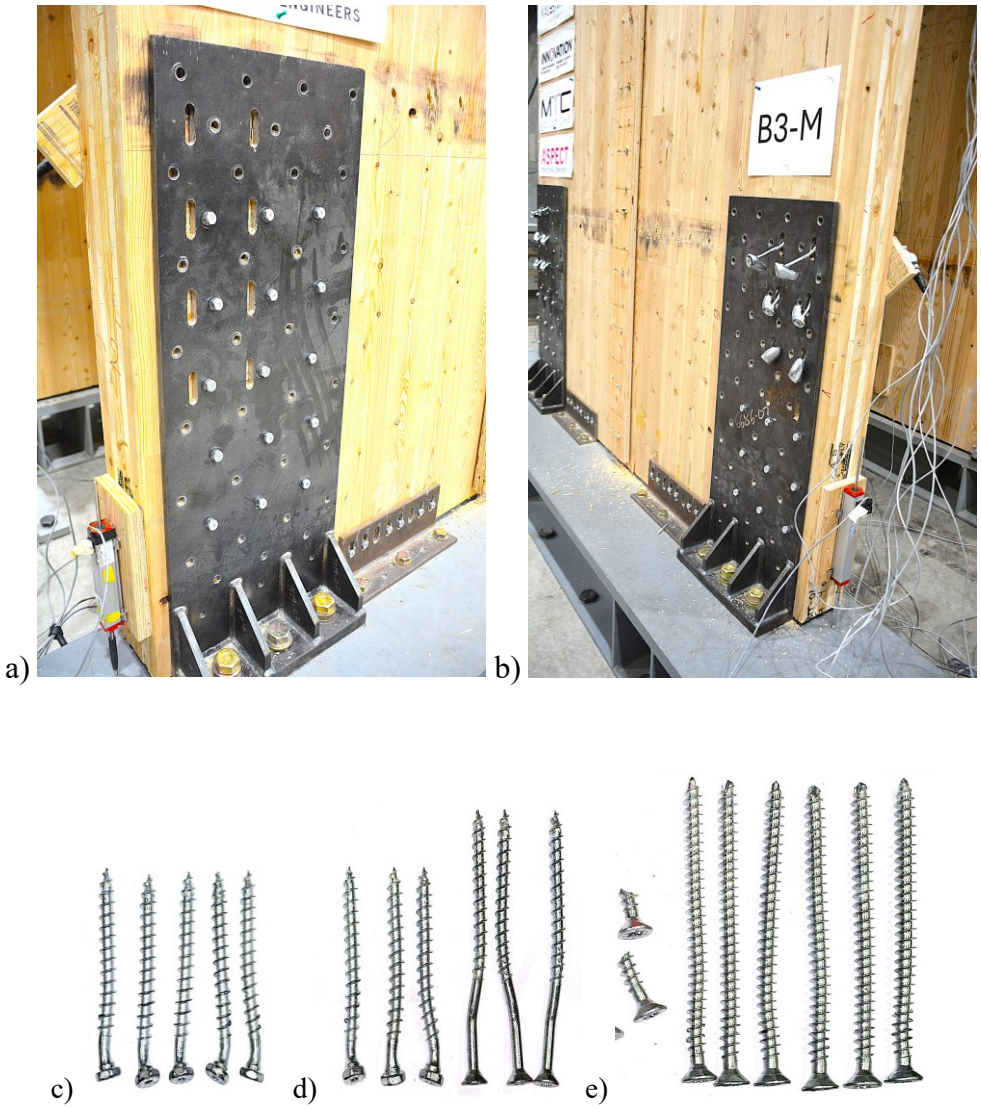

Figure 27 a) HD-S, b) HD-M, c) HD S screws, d) HD M screws, e) B2-M HD screws

4.7.4 Capacity protected connections

The SB, ledgers and TS were designed to be capacity-protected to ensured that inelastic deformations were confined to the energy-dissipating elements (VJ and HD). Up to 2.2% drift, there was no evidence of damage, yielding, or slip in these connections or their associated fasteners. When the imposed drift exceeded the code limit, some yielding was first observed in the ledger screws. With increasing drift demand, several ledger screws exhibited pronounced plastic deformation, and some fasteners ultimately fractured or pulled out, indicating local connection failure. In most cases, the ledgers yielded at higher drift levels but did not interfere with the intended rocking mechanism. However, no pull-out or fracture was observed in the fasteners associated with SB or TS, even until 5.7% drift. Moreover, no damage was observed in the CLT at the locations where these SB and TS connections were provided, even till the end of the test. The connections and their screws after testing are shown in Figure 28.

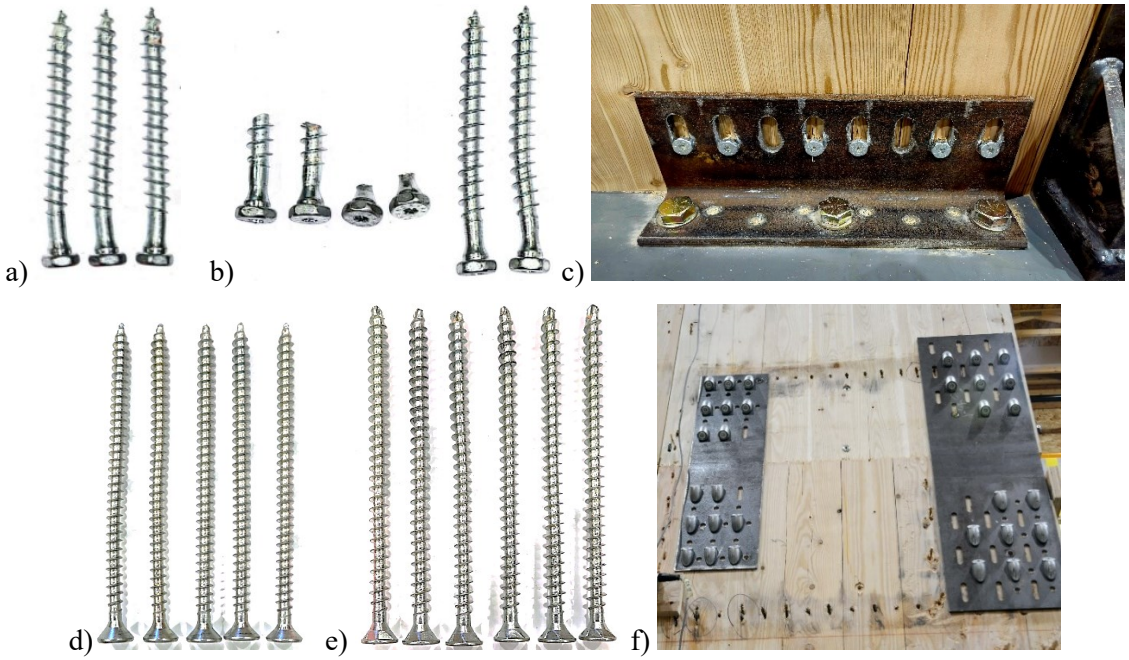

Figure 28 a) SB screws, b) ledger screws, c) SB, d) inner TS screws, e) outer TS screws, f) inner and outer TS after test

Localized damage at the panel corners—primarily due to rocking-induced bearing and crushing—was commonly observed, as illustrated in Figure 29a. After testing, 100 mm of the panel edge was trimmed to expose undamaged material for subsequent testing (Figure 29b). Out-of-plane instability was noted during test B2-S, which was subsequently addressed in later configurations by installing horizontal stiffeners between the walls at the second storey level.

a) 

b) 

Figure 29 a) Damaged panels, b) trimmed CLT panel

Chapter 5: Discussion

5.1 Shear wall resistance

The shear wall resistances at the different target drifts are illustrated in Figure 30 and summarized in Table 2. At low drifts, the mixed-angle screw variants (B2-Mi, B3-M and B4-M) consistently provided higher stiffness and lateral resistance than the shear-only variants (B2-Si, B3-S and B4-S). For instance, at 2.2% drift, B2-Mi was 35% stronger than B2-Si. Similarly, B3-M and B4-M exceeded B3-S and B4-S by 8% and 3%, respectively. While engaging HD screws in both shear and withdrawal improved initial stiffness and strength, this advantage diminished at larger drifts, where the S-variants outperformed the M-variants. For example, at 5.7% drift, B2-Si was 15% stronger than B2-Mi, B3-S exceeded B3-M by 8%, and B4-S surpassed B4-M by 2%. This indicates greater strength retention in the shear-only HD under repeated cyclic loading, whereas in the mixed angle screw HD, the screws installed at 45° experienced a large strength reduction after exceeding their withdrawal resistance.

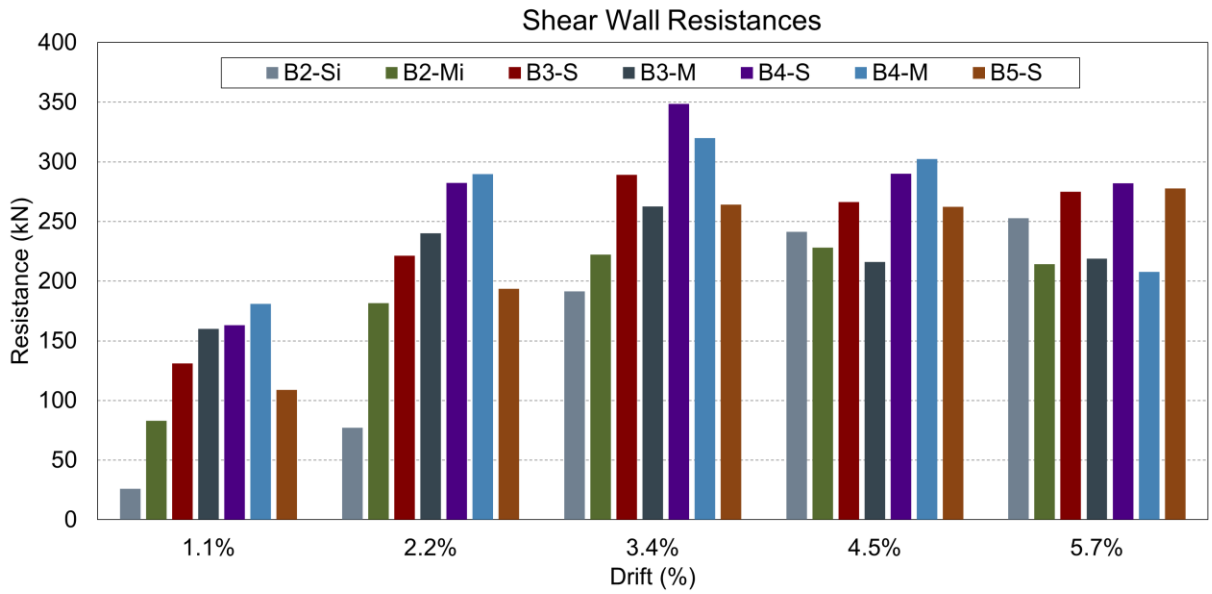

Figure 30 Shear wall resistances at target drifts

Table 2 Lateral loads at target drifts (kN)

Drift Ratios	B2-Si	B2-Mi	B3-S	B3-M	B4-S	B4-M	B5-S
1.1%	26	83.0	131	160	163	181	109
-1.1%	-34	-103	-150	-158	-183	-211	-134
2.2%	77	181	221	240	282	289	193
-2.2%	-98	-187	-247	-255	-291	-269	-232
3.4%	191	222	289	262	348	320	264
-3.4%	-217	-219	-306	-254	-345	-304	-285
4.5%	241	228	266	216	290	302	262
-4.5%	-260	-220	-286	-228	-275	-240	-279
5.7%	252	214	275	219	282	207	277
-5.7%	-268	-210	-290	-225	-277	-223	-283

The influence of VJ stiffness was critical to system resistance. At 2.2% drift, the inclusion of VJ in structures B3-S and B3-M led to resistance increases of 187% and 32%, respectively, when compared to B2-Si and B2-Mi. However, as drift increased, this advantage diminished; at 5.7% drift, B3-S and B3-M exhibited only 9% and 2% higher resistance, respectively, than B2-Si and B2-Mi. B4-S and B4-M, which incorporated stiffer joints, at 2.2% drift achieved 27% and 21% greater resistance compared to B3-S and B3-M, respectively. At 5.7% drift, B4-S was only 3% stronger than B3-S, whereas B4-M experienced a 5% reduction in resistance relative to B3-M. This drift-dependent sensitivity of wall resistance to VJ stiffness is attributed to the progressive failure of the VJ screws under increasing cyclic deformation. As drift levels increased, these screws yielded, thereby contributing less to shear wall resistance, and eventually fractured, at which point they no longer contributed to resistance. Finally, structure B5-S, which employed horizontally spliced panels and TS, exhibited the lowest initial stiffness and resistance, 17% lower than B3-S and 33% lower than B4-S at 1.1% drift. As drift increased, the TS system progressively mobilized: at 3.4% drift, B5-S trailed B3-

S and B4-S by only 9% and 24%, respectively. At 5.7% drift, B5-S effectively matched B3-S and B4-S.

5.2 Strength degradation

The different HD and VJ configurations influenced the shear wall strength degradation between cycles at each target drift, as illustrated in Figure 31 and presented Table 32 (Appendix 3). At lower drift levels (up to 2.2%), structure B2-Si, with HD screws acting in shear, exhibited the lowest strength degradation across all tests. In contrast, the structures with mixed-angle HD configurations (e.g. B2-Mi), experienced greater early-cycle degradation, with cumulative strength loss from the first to the third cycle reaching up to 11%. At 4.5% drift, B2-Mi showed the greatest overall strength degradation (−23%), followed by B2-Si (−21%).

Strength degradation trends in the B3 and B4 structures highlight the combined influence of HD configuration and VJ stiffness. At lower drift levels (1.1% and 2.2%), all configurations exhibited comparable degradation, though the stiffer VJs in the B4 series offered slight performance improvement, as reflected in marginally lower degradation values. By 3.4% drift, the benefit of increased VJ stiffness became more evident: B4-M exhibited noticeably lower degradation than B3-M despite identical HD layouts, suggesting improved energy dissipation capacity due to the stiffer VJs. However, at higher drift levels, this advantage diminished; B4-M experienced a sharp increase in degradation, likely due to localized failure in the HD connections.

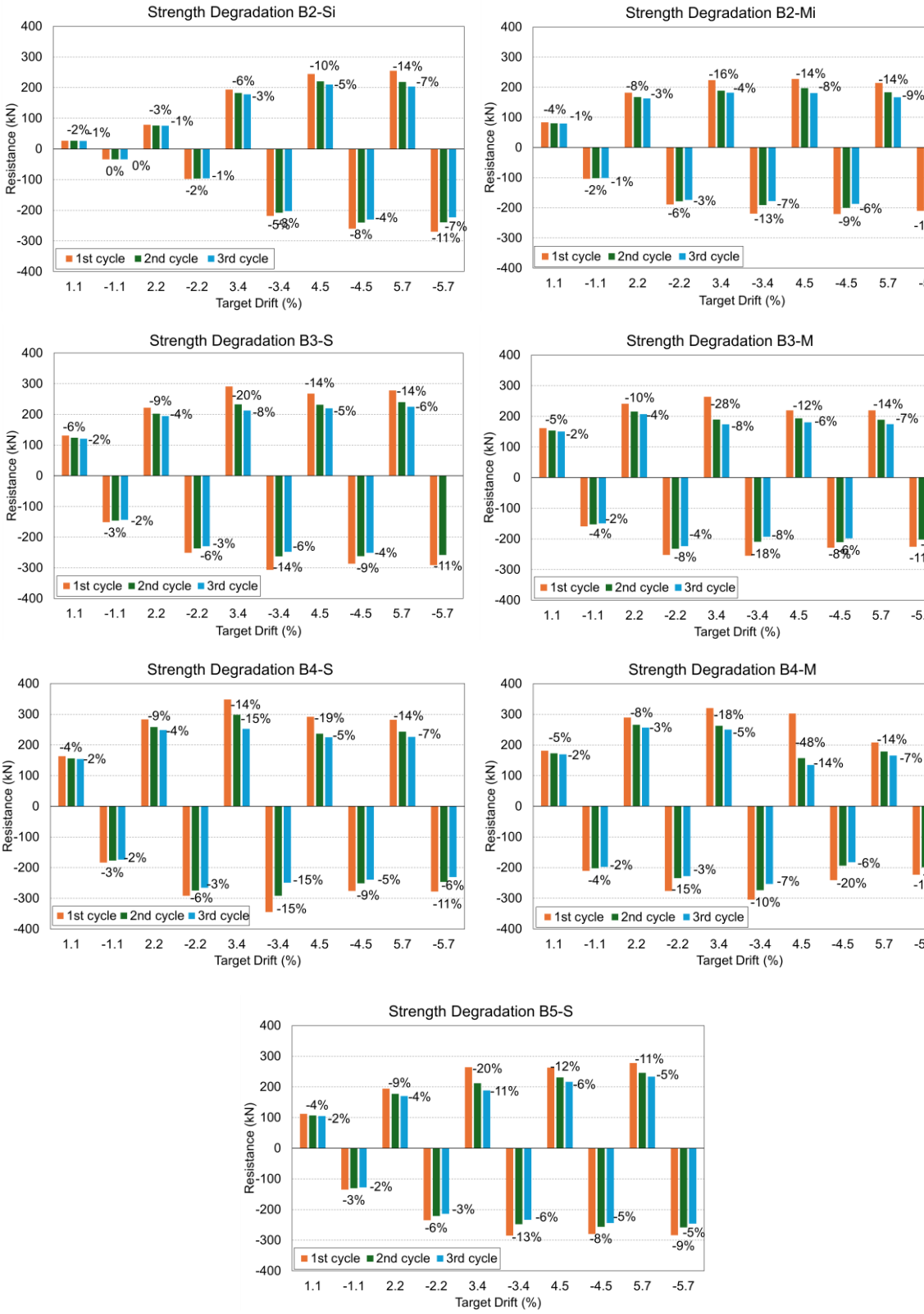

Figure 31 Strength degradation at target drifts

These findings underscore that while stiffer VJs can improve ductility particularly in walls with mixed-angle HDs at higher drift levels strength retention remains heavily dependent on HD detailing, with shear-oriented screw configurations demonstrating superior performance under large deformations. Structure B5-S exhibited strength degradation nearly identical to B4-S and comparable to B3-S, which at 3.4% drift.

B5-S experienced the highest degradation (−31%) among these configurations, indicating initial vulnerability due to panel discontinuity. However, as drift increased, B5-S had lower strength loss than B3-S and B4-S at these stages. This suggests that TS mobilization effectively stabilized the structure and limited degradation.

5.3 Energy dissipation

The dissipated energies by all structures across the target drift levels and corresponding loading cycles are illustrated in Figure 32 and presented in Table 33 (Appendix 3). Structure B2-Mi demonstrated superior energy dissipation across all drift levels and cycles compared to B2-Si, with the difference becoming more pronounced as drift demands increased. While B2-Si maintained relatively stable energy dissipation between successive cycles at small drift levels, B2-Mi continued to enhance its energy absorption with increasing deformation. This behavior can be attributed to the mixed-angle HDs configuration, where screws resisting both shear and withdrawal enabled greater deformation capacity and additional energy dissipation.

In contrast to the B2 series, the B3 and B4 structures with VJ exhibited significantly greater energy dissipation capacity. Between them, the B4 series consistently outperformed the B3 series, due to the presence of stiffer VJ. B4 structures demonstrated a more substantial increase in energy dissipation with increasing drift, whereas B3 structures exhibited slightly lower cumulative energy absorption and greater degradation between cycles at larger drifts.

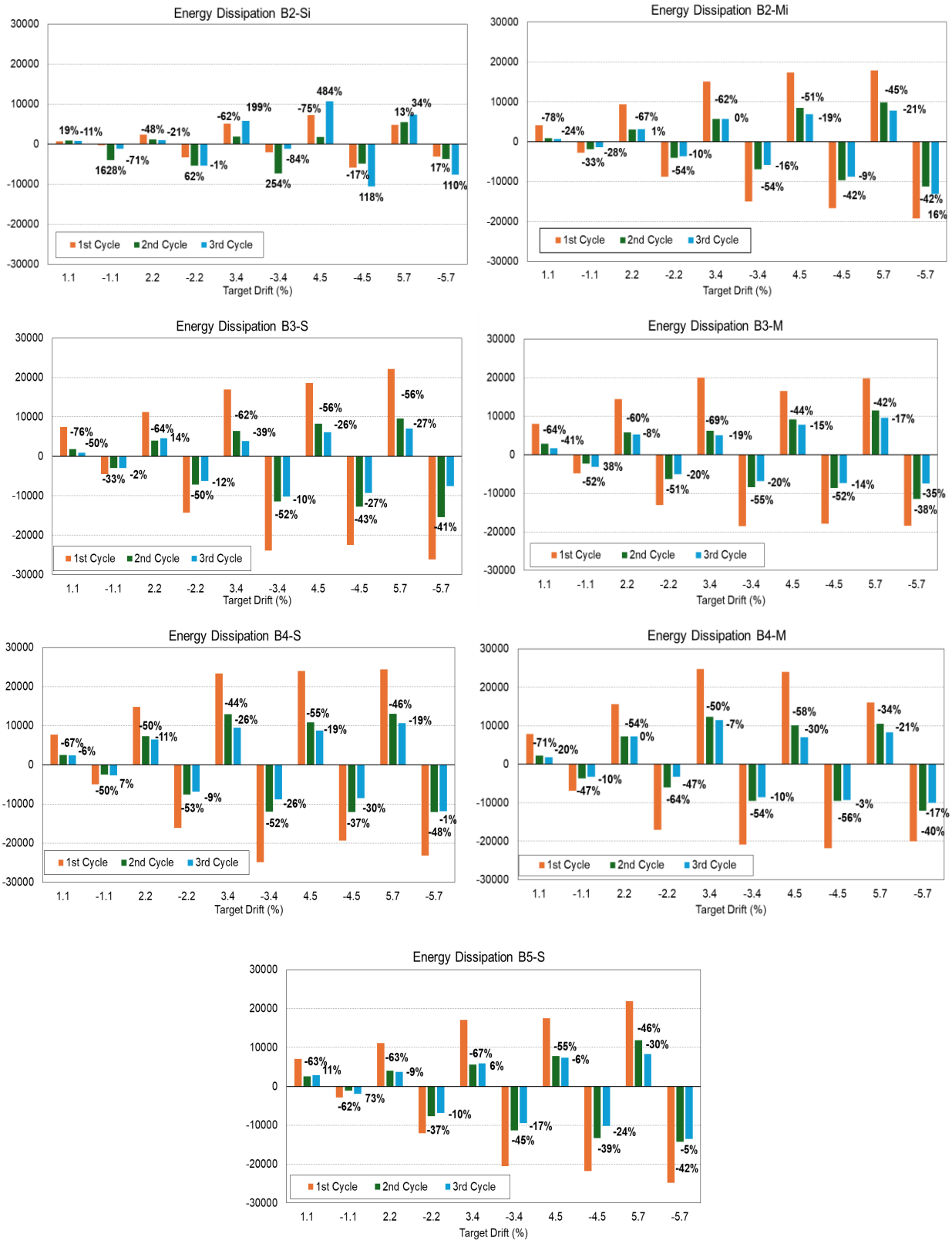

Figure 32 Energy dissipation at target drifts

Like in the B2 series, the mixed-angle configurations (B3-M and B4-M) outperformed their corresponding all-shear counterparts (B3-S and B4-S) at low to moderate drift levels. However, at larger drifts, the energy dissipation between the mixed-angle and all-shear configurations became comparable. Structure B5-S exhibited distinct energy dissipation behavior and recorded slightly lower cumulative energy absorption than the other structures.

Overall, a consistent trend in the energy dissipation behavior across loading cycles was identified. In most cases the first cycle dissipates the highest amount of energy, the second cycle shows a noticeable reduction, and the third cycle exhibits an even further decline in energy dissipation. This pattern indicates that after the initial cycle, progressive damage, such as screw yielding, wood embedment, and localized connection degradation, reduces the structure's capacity to absorb and dissipate energy.

5.4 Inter-storey drifts at target displacements

The target displacements were based on the second floor horizontal displacements; the corresponding inter-storey drift ratios of the first and second storey at 2.2% and 5.7% target drift are illustrated in Figure 33, and for all target drifts summarized in Table 34 (Appendix 3).

At the 2.2% drift level, the difference in the inter-storey drift ratios was minimal, ranging from 0% to 1%, indicating well-distributed deformation. Configurations such as B3-S, B4-S, and B4-M exhibited a 0% difference, suggesting that both storeys deformed uniformly. In contrast, B2-Mi, B3-M, and B5-S exhibited a 1% higher drift in the second storey, indicating the effect of in-plane distortion. This upward shift in drift, particularly concentrated in the second storey, reflects the contribution of panel distortion—especially in the absence of hold-downs at the upper level—which allowed the CLT panels to undergo greater in-plane deformation. With increasing drift, no abrupt changes in drift distribution were

observed; however, a gradual amplification of second-storey drift became apparent. At the 5.7% target drift, most configurations exhibited only a marginal increase in inter-storey drift difference (between 0% and 1%), maintaining a stable deformation pattern. However, B2-Si experienced a more notable increase, where the second storey inter-storey drift was 3% higher than the first. In the case of B5-S, where TS were used to connect both storeys, the second storey showed a 2% higher inter-storey drift compared to the first, which was also greater than that observed in most other configurations. It can be postulated that a stiffer TS connection would have further reduced this 2% drift differential.

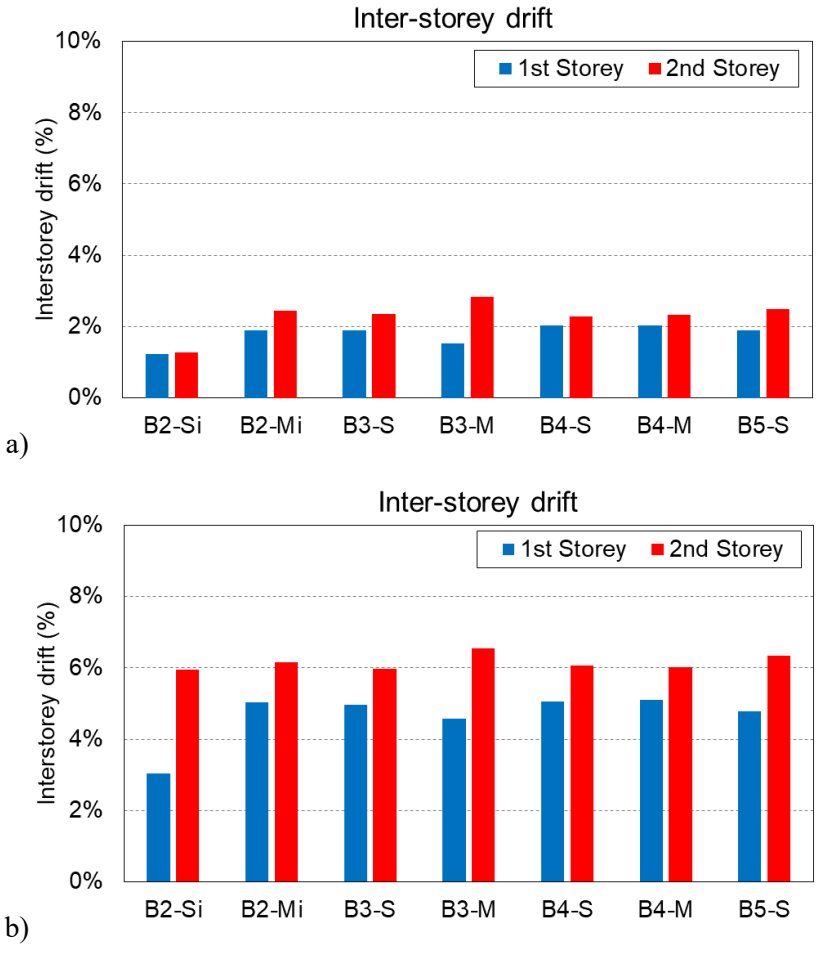

Figure 33 Inter storey drift; a) 2.2%, b) 5.7%

5.5 Hold-down and inner corner uplifts

The HD and inner corners uplifts at 2.2% and 5.7% drifts are illustrated in Figure 34. The uplift measured at each of the four HD and the inner corners for every structure at each target drift are presented in Table 8 - Table 15 (Appendix 3). At the 2.2% drift (Figure 34a), due to the increase in VJ stiffness, B4-S and B4-M exhibited the highest uplift magnitudes (20 mm), followed by B3-S and B3-M at 16 mm, and B2-Mi and B2-Si at 15 mm and 13 mm, respectively. The M variants consistently demonstrated higher lateral resistance, confirming their higher initial stiffness. It was most pronounced in the B2 series, where B2-Mi showed a 135% increase in lateral resistance compared to B2-Si. This highlights the benefit of combining screws in shear and withdrawal for improving uplift restraint at small drifts. In the B3 and B4 series, however, the gains were more modest. B3-M exhibited only an 8% improvement over B3-S, and B4-M showed a 3% increase over B4-S.

At 5.7% drift (Figure 34b), the uplifts measured at the HD increased substantially across all configurations, ranging from 44 mm to 53 mm. Notably, the M variants consistently exhibited higher uplift than their S counterparts: 52 mm vs. 44 mm in B2, 53 mm vs. 49 mm in B3, and 53 mm vs. 51 mm in B4, yet their load resistance was lower. This shift in performance is attributed to the complete yielding of the angled screws in the M variants with the increase in drift level, while these angled screws provided enhanced initial stiffness and uplift resistance at lower drift levels, their plastic deformation under increased cyclic demand resulted in a loss of effectiveness in resisting lateral load. For B5-S, the uplift in the HD was smallest (42 mm) as compared to other S variants, while resisting 10% and 2% more load than the B2-Si and B3-S structures, respectively.

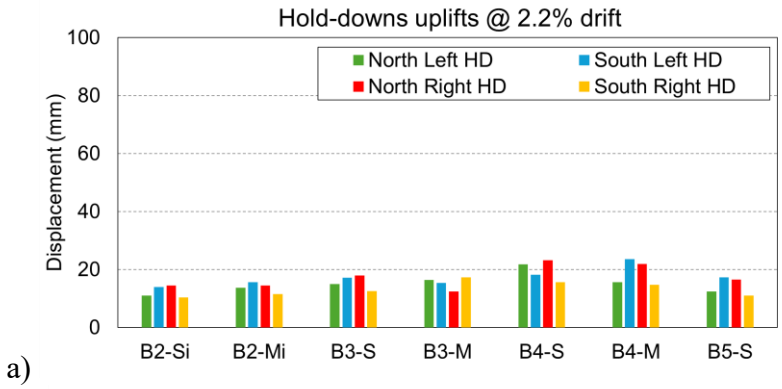

a)

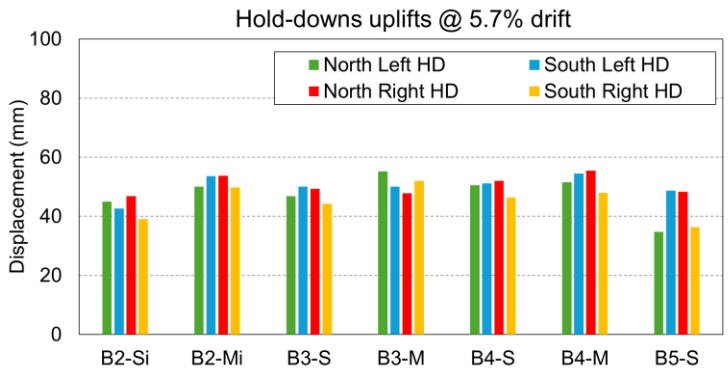

b)

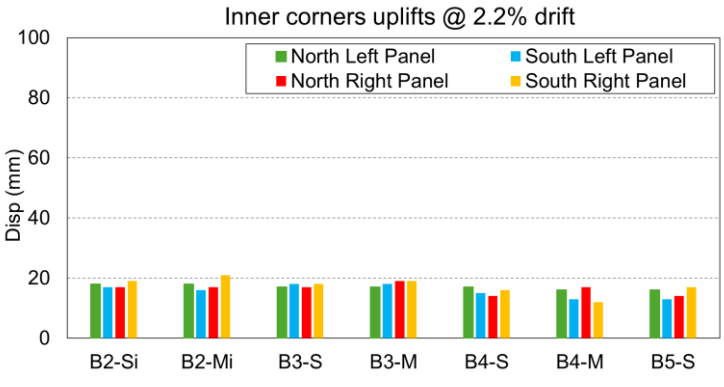

c)

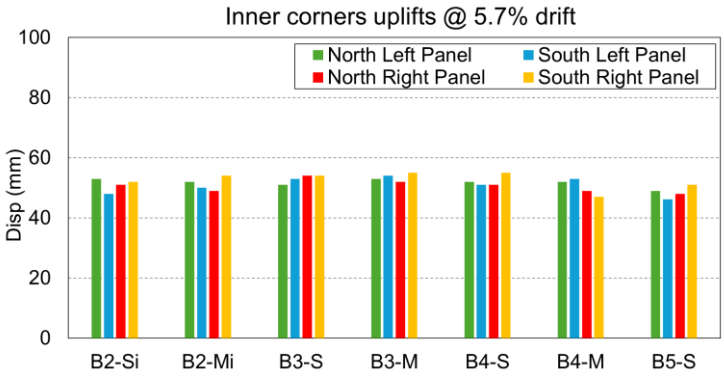

d)

Figure 34 Uplifts a) HD @ 2.2% drift, b) HD @ 5.7% drift, c) inner corners @2.2% drift, d) inner corners @ 5.7% drift

The inner corner uplift (Figure 34c and d), measured at unrestrained panel ends, was generally higher than the uplift recorded at corners restrained with HD. At 5.7% target drift, the S variants consistently showed higher inner corner uplift, with B5-S at 9%, B2-Si at 8%, and B3-S at 5%. In contrast, M variants exhibited minimal differences—B2-Mi (0%), B3-M (1%), and notably B4-M (−5%)—demonstrating more balanced uplift control.

5.6 Panel-to-panel displacement

The panel-to-panel displacements measured at the first and second storeys at 2.2% and 5.7% drift are illustrated in Figure 35, and presented for each target drift in Table 22 - Table 25 (Appendix 3). Consistent trends emerged across the tested structures: most notably, the second storey generally exhibited slightly higher panel-to-panel displacements than the first. This behavior can be attributed to differences in VJ detailing and at each level as well as the higher distortion at the second storey.

At 2.2% drift (Figure 35a), structures without vertical joints (B2-Si and B2-Mi) exhibited the largest panel-to-panel displacements. The inclusion of VJ in B3-S and B3-M led to more controlled displacements, while the use of stiffer VJ in B4-S and B4-M resulted in the most uniform panel-to-panel behavior. Across all structures, second-storey panel-to-panel displacements were either similar or greater than those in the first storey. The largest differences appeared in B2-Si and B2-Mi (with second-storey displacements 5% and 3% higher, respectively). In B3-S and B3-M, this difference was reduced, with the second storey showing only 1%, slightly higher displacement, while B4-S showed identical displacement across both storeys, while B4-M had a modest increase of 2% at the second storey.

At 5.7% drift, B2-Mi showed greater panel-to-panel displacement at the second storey compared to the first storey with a 2% increase at the second storey on both sides. B2-Si

exhibited identical panel-to-panel displacements at both storeys for both sides, reflecting uniform behavior across the height of the wall. For the other configurations, this trend of slightly higher second storey displacement generally continued, with the largest difference observed in B3-M, where the north side displacement at the second storey was 7% higher than at the first. B5-S also exhibited greater second-storey displacement on both sides, most notably with a 4% increase on the north side.

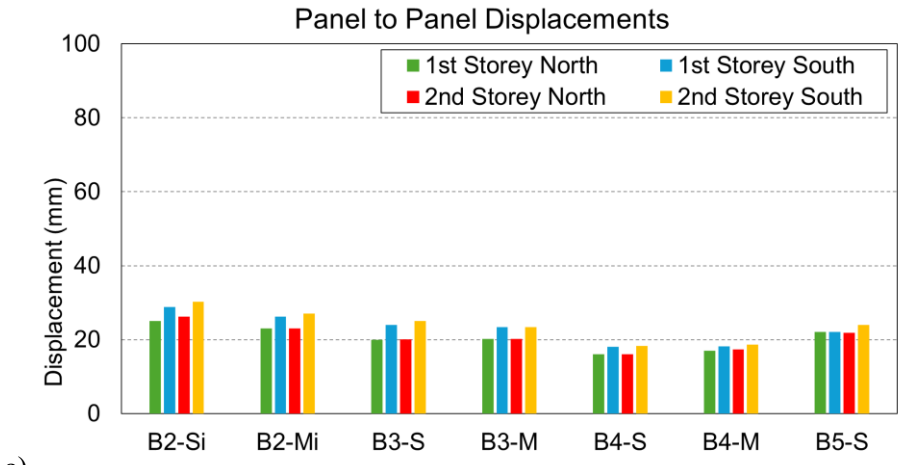

a)

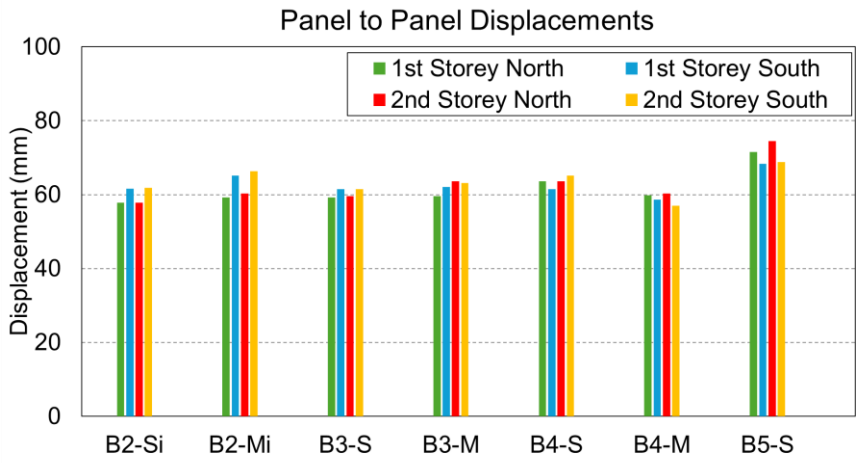

b)

Figure 35 Panel-to-panel displacements at both storeys; a) 2.2% drift, b) 5.7% drift

5.7 Shear wall sliding

The panel sliding at 2.2% and 5.7% target drift levels across all test configurations are illustrated in Figure 36 and presented for all drift levels in Table 18 - Table 21 (Appendix 3).

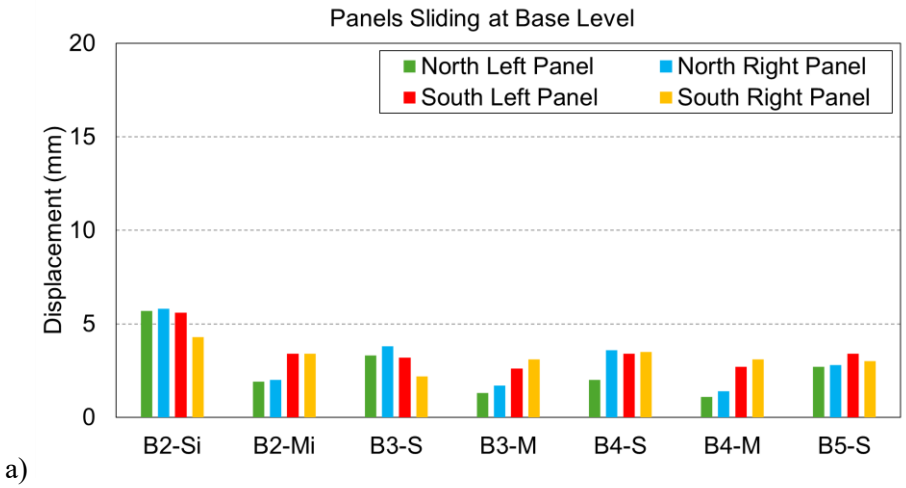

a)

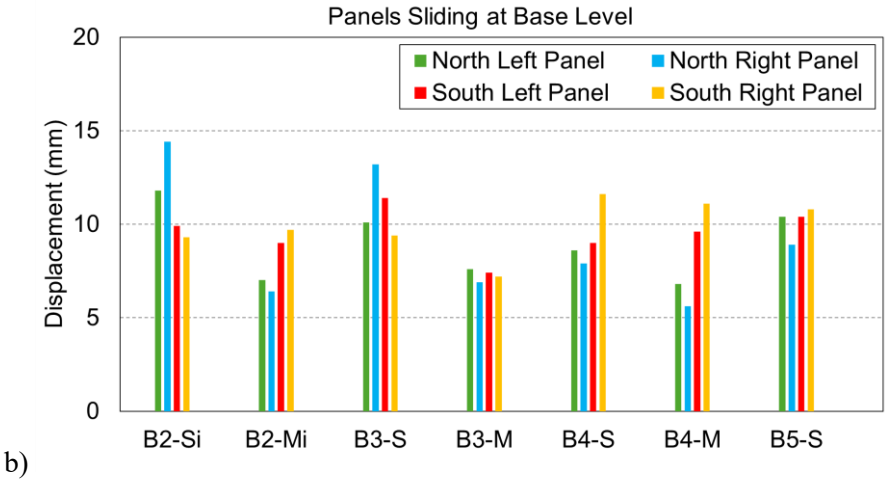

b)

Figure 36 Panels sliding at base level; a) 2.2% drift, b) 5.7% drift

At 2.2% drift, sliding remained relatively small across all specimens and varied only slightly by configuration and panel location. M variants consistently showed reduced sliding compared to their S counterparts. B2-Si had the highest sliding (close to 6 mm), while B2-Mi recorded 66% and 31% less at the north and south sides (2 mm – 3 mm). In B3-M, sliding was

2.8 mm (north) and 1.5 mm (south), which was 20% and 44% lower, respectively, than B3-S (3.5 mm and 2.7 mm). Similarly, B4-M recorded 1.2 mm (north) and 2.9 mm (south), while B4-S exhibited 55% and 16% higher sliding at 2.6 mm and 3.4 mm. These results confirm that mixed-angle HD in effectively reduced base sliding. For B5-S, sliding was balanced across all corners (2.7 mm – 3.4 mm).

At the 5.7% drift level, sliding increased notably across, with M variants consistently demonstrating improved restraint compared to their S counterparts. B2-Mi recorded 6.7 mm (north) and 9.3 mm (south), translating to 49% and 3% reductions relative to B2-Si, which exhibited 13.1 mm and 9.6 mm, respectively. Similarly, in the B3 series, B3-M recorded 7.2 mm (north) and 7.3 mm (south), showing 38% and 30% less sliding than B3-S (11.6 mm and 10.4 mm, respectively). Likewise, the B4-M exhibited 6.2 mm (north) and 10.3 mm (south), showing 25% less and 0.5% more sliding, respectively, than B4-S (8.2 mm and 10.3 mm). Lastly, B5-S, which featured tension straps exhibited relatively uniform sliding across both sides, measuring 9.6 mm (north) and 10.6 mm (south).

5.8 Ledger slip

The relative slip between the ledgers and the shear walls at both storey levels on the north and south walls for 2.2% and 5.7% target drifts are illustrated in Figure 37 and for all target drifts are presented in Table 26 - Table 29 (Appendix 3). Across all drift levels, second-storey ledger displacements were consistently lower than those at the first storey.

At 2.2% drift, B2-Si and B2-Mi exhibited the highest displacements 4.8/4.1 mm and 5.1/2.4 mm (first/second storey), respectively. In contrast, in the B3 and B4 structures, which incorporated spline joints, M variants had lower first-storey displacements, but higher second-storey values compared to their S counterparts, reflecting deformation redistribution due to

improved base restraint. For example, B3-S showed 4.3/2.0 mm, while B3-M recorded 4.0/3.0 mm; similarly, B4-S had 1.7/1.6 mm, and B4-M had 1.5/1.7 mm. The B4 series, with stiffer VJ, demonstrated overall lower displacements than B3, confirming the influence of VJ stiffness. B5-S, featuring non-monolithic panels and similar VJ detailing to B3-S, showed controlled but slightly higher displacements (2.3/1.5 mm) compared to B4.

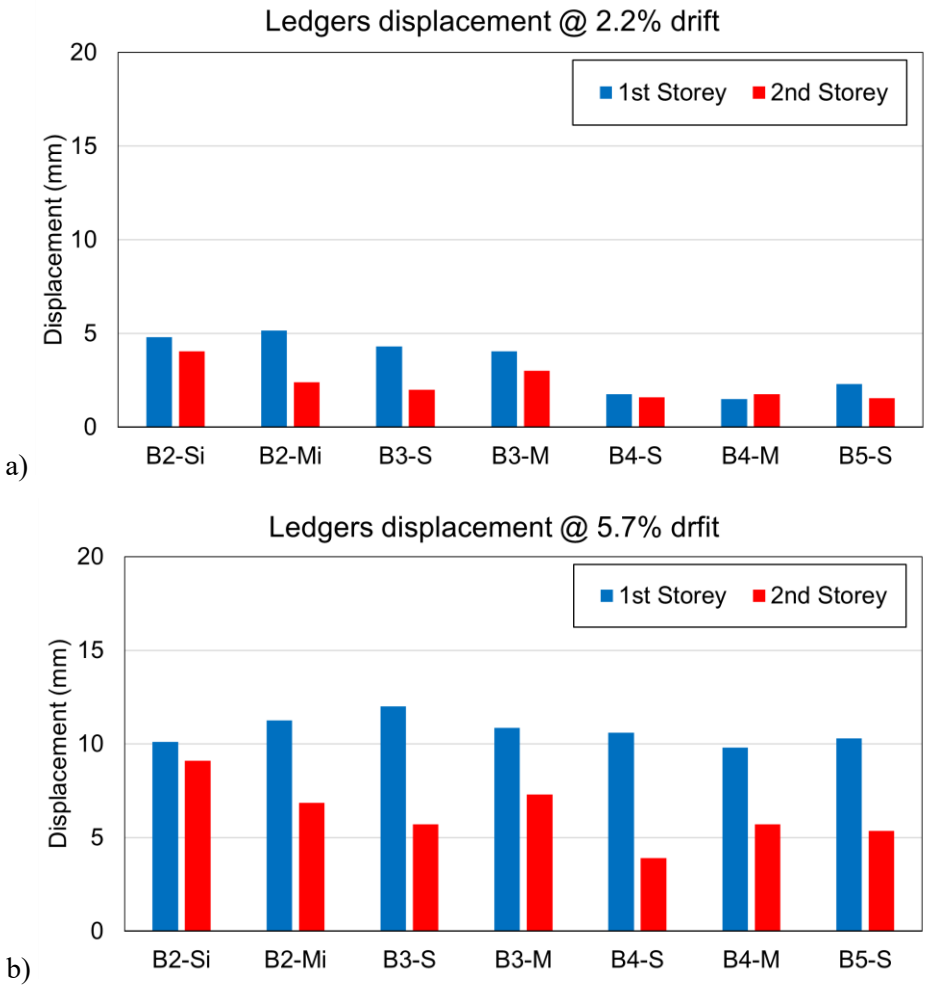

Figure 37 Ledger's displacements; a) 2.2% drift, b) 5.7% drift

At 5.7% drift, ledger displacements increased substantially, yet the trend of greater displacement at the first storey remained consistent. B3-S recorded the highest first-storey slip at 12.0 mm, followed closely by B2-Mi (11.2 mm) and B3-M (10.8 mm), while their second-

storey values were lower with 5.7 mm, 6.8 mm, and 7.3 mm, respectively. In the B2 series, B2-Si showed displacements of 10.1 mm and 9.1 mm, while B2-Mi demonstrated a sharper drop between storeys. For the B4 structures, overall displacements remained lower than other groups, with B4-S at 10.6/3.9 mm and B4-M at 9.8/5.7 mm, again highlighting the role of stiffer VJ in controlling slip. B5-S showed relatively balanced values of 10.3 mm and 5.3 mm, confirming consistent restraint despite the panel discontinuity.

5.9 Wall displacements

The individual north and south wall displacements are shown in Figure 38 and summarized in Table 30 - Table 31 (Appendix 3). Both walls displaced at an almost identical rate, indicating comparable stiffness on each side and the absence of out-of-plane distortion.

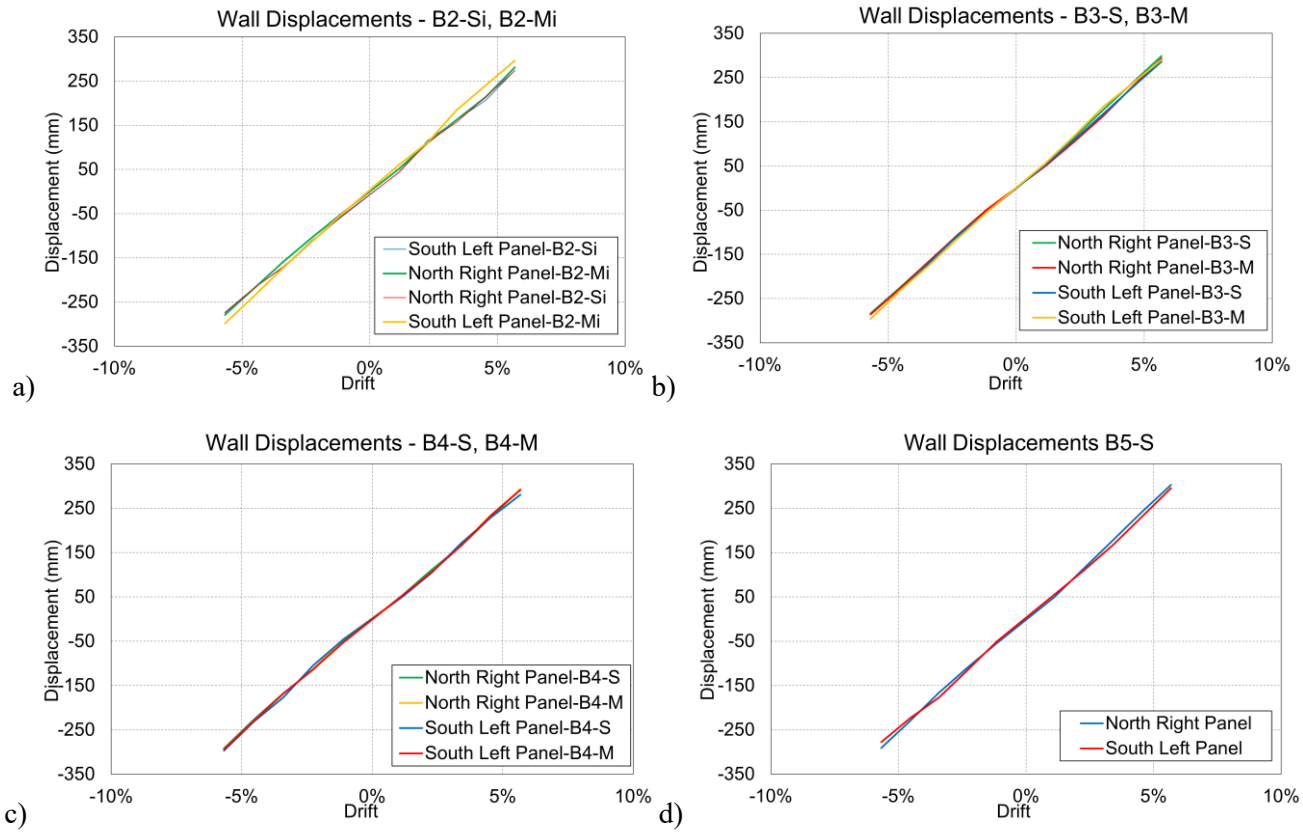

Figure 38 Wall displacements; a) B2Si, B2-Mi, b) B3-S, B3-M, c) B4-S, B4-M, d) B5-S

5.10 Tension strap uplifts

Both the inner and outer TS uplifts observed in structure B5-S at each target drift are illustrated below in Figure 39 are presented in Table 16 and Table 17. During the push cycles, the outer TS on the left panels and the inner TS on the right panels were subjected to uplift in the same direction, while the left inner TS and right outer TS were primarily in compression. At 2.2% drift, the outer TS on the left panels experienced uplifts of 2.3 mm and 3.0 mm, respectively. In contrast, the corresponding inner TS on the right panels showed lower uplift values ranging from 0.7 mm to 1.0 mm, despite being engaged in the same loading direction.

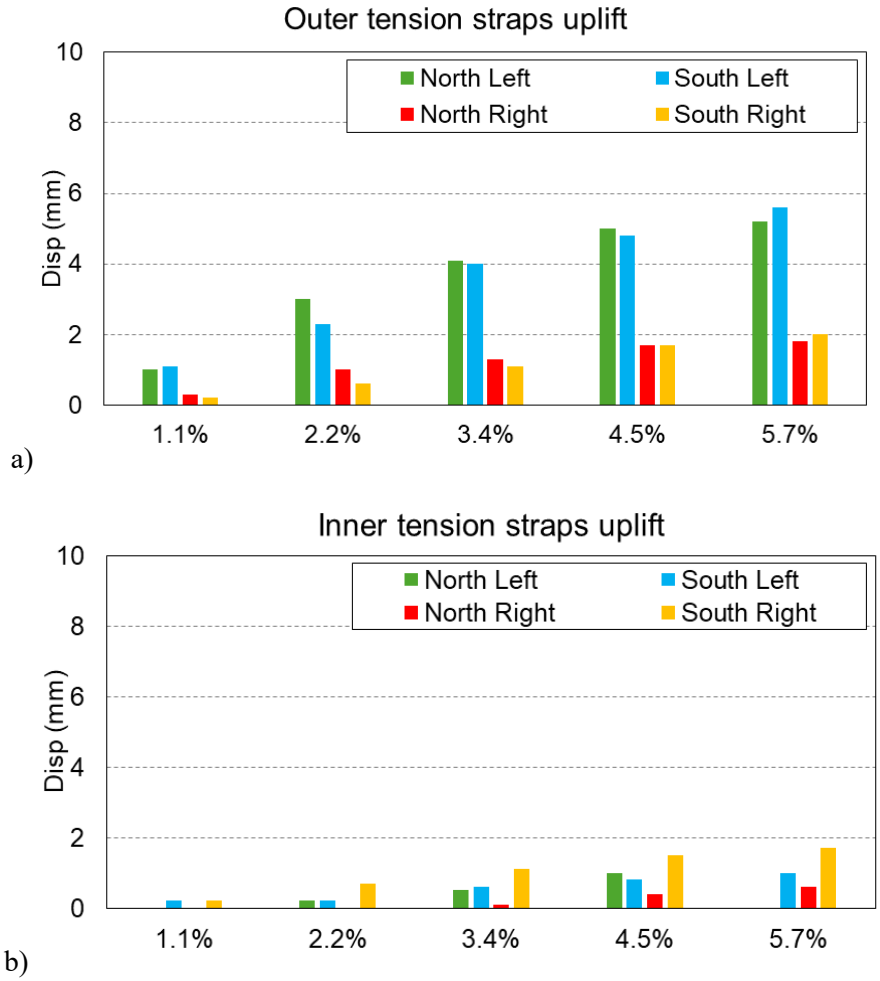

Figure 39 Uplift at tension straps; a) outer, b) inner

With an increase in drift to 5.7%, the difference in uplift became more pronounced: the uplift in the north and south left outer TS reached 5.2 mm and 5.6 mm, whereas the right inner TSs (north and south) both recorded 1.7 mm. Although the outer TS was fastened using screws of larger diameter and greater embedment length, the inner TS consistently showed better performance in limiting uplift. A similar trend was observed during the pull cycles, where the outer TS on the right panels experienced greater uplift than the inner TS on the left.

5.11 Panel distortion

The panel distortions at 2.2% and 5.7% target drift are illustrated in Figure 40. At 2.2% drift, panel distortion at the first-storey level revealed clear differences in structural response across the tested configurations. The B2-Si exhibited the highest distortion among all structures, with values ranging from 0.9 mm to 1.4 mm. In contrast, B2-Mi showed smaller distortion levels (0.2–0.5 mm), underscoring the enhanced initial stiffness provided by the angled screws in mixed-angle HD. A similar pattern was observed in the B3 and B4 series, where the M variants (B3-M and B4-M) recorded lower distortion values compared to their S counterparts. Notably, B4-M exhibited the lowest overall distortion (0.2–0.4 mm). In comparison, B5-S exhibited relatively moderate displacement values ranging from 0.5 mm to 0.8 mm, lower than B2-Si but slightly higher than both B3-S and B4-S.

At the 5.7% drift level, there was a significant escalation in deformation compared to lower drift levels, particularly within the S variants. Among all configurations, B5-S exhibited the highest distortion, with values ranging from 3.1 mm to 3.5 mm across all panels. In contrast, B4-S recorded the lowest distortion among S variants (0.7–1.0 mm), reaffirming the critical role of stiff VJs in constraining in-plane deformation under severe cyclic loading. B3-S showed intermediate performance, with distortion values between 1.0 mm and 1.1 mm. B2-Si, which

had exhibited the highest panel distortion at 2.2% drift had comparable distortion at higher drift levels as well, unlike other S variants that experienced substantial increases. At lower drift levels, where M variants typically outperformed S variants in limiting distortion due to their enhanced initial stiffness. At 5.7% drift, structures like B4-M and B2-Mi showed distortion values comparable to or exceeding their S counterparts in certain panels, suggesting that the plastic deformation of angled screws in the M variants had progressed significantly.

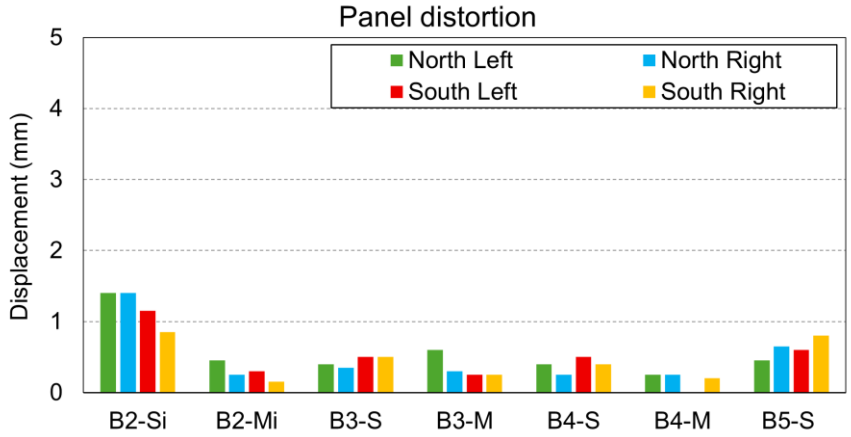

a)

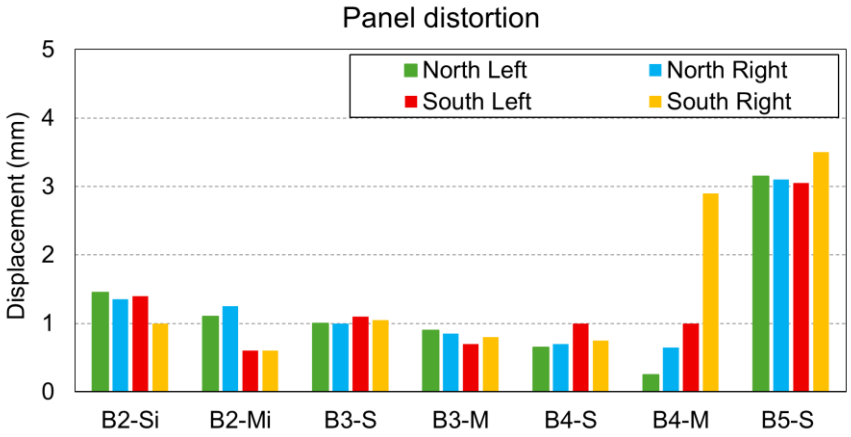

b)

Figure 40 Panel distortion in first storey panels; a) 2.2% drift, b) 5.7% drift

5.12 Contribution of individual components to lateral displacement

The contribution percentage of rocking, sliding, panel distortion, ledger slip and TS uplift for all structures at 5.7% target displacement are presented in Table 3. In this study, rocking contribution was determined using the average uplift values recorded at the HD locations and the inner panel corners at the base level. For B5-S, the average uplift of both inner and outer TSs at the second storey was also included to quantify the TS contribution. Sliding and ledger slip values were calculated as the average of measurements from the left and right panels. Panel distortion was obtained by averaging the in-plane distortions of all panels and extrapolating their cumulative effect on the total structural displacement. The rocking contribution consistently dominated overall displacement for all structures with continues shear walls with 90% to 93%. Only in structure B5-S, rocking accounted for only 78% with the difference (13%) caused by the TS uplift. Sliding and ledger slip each consistently contributed approximately 3, and the contribution of distortion was close to 2%.

Table 3 Contribution to total displacement at 5.7% drift (%)

Kinematic	B2-Si	B2-Mi	B3-S	B3-M	B4-S	B4-M	B5-S
Rocking	89.9	91.5	90.5	92.9	91.2	91.0	78.0
Sliding	4.2	2.8	3.8	2.5	3.2	3.5	3.4
Distortion	2.8	2.3	2.6	1.7	1.7	1.8	1.8
Ledger slip	3.5	3.1	3.0	3.1	3.9	3.9	3.5
TS uplift	0	0	0	0	0	0	13.3

5.13 Comparison to platform-type shear walls

Two-storey platform-type CLT shear walls were previously tested at UNBC to evaluate the impact of connection detailing (including VJ and TS configurations) on lateral performance under reversed cyclic loading [36]. In the present research, balloon-type two-storey CLT shear

walls were tested. To address the last sub-objective of this thesis, the lateral performance of the two structural configurations was compared, specifically the balloon-type structures with HD with screws acting in shear only (B2-S, B3-S, B4-S and B5-S) with the previously tested H1c platform-type structures that used a similar HD configuration. All tested structures had the same floor heights and utilized similar SB and 5-ply CLT panels of the same width. The main connection parameters are summarized in Table 4. Given the similar panel configuration and HD and SB connections, a comparison between the platform-type and balloon-type CLT walls is possible. Although these systems differ in construction methodology, the boundary conditions and connection details enable an investigation of the effects of inter-storey continuity and joint detailing on lateral performance.

Both B2-S and H1c both used HDs with 21 screws; however, in B2-S, the actuator reached its load limit before strength degradation occurred. To allow post-peak responses to be captured within actuator limits, the number of HD screws was reduced to 15 in the subsequent tests. For a more meaningful comparison with B3-S and B4-S, the structural response of B2-S and H1c, as illustrated in the envelope curves of Figure 41, were scaled down by a ratio of 15/21 to match the HD detailing of the other balloon-type structures.

Table 4 Connection parameters of two-storey platform type shear walls [36] and current study

Test	HD	SB	1st storey VJ	2nd storey VJ	Outer TS
B2-S	21-ø12×120 mm	8-ø12×120 mm	×	×	×
B3-S	15-ø12×120 mm	6-ø12×120 mm	12-ø8×100 mm	8-ø8×100 mm	×
B4-S	15-ø12×120mm	6-ø12×120 mm	24-ø8×100 mm	16-ø8×100mm	×
B5-S	15-ø12×120mm	6-ø12×120 mm	12-ø8×100 mm	8-ø8×100mm	8-ø12×200mm@45
H1c	21-ø12×120 mm	6-ø12×120 mm	16-ø8×100 mm	11-ø8×100mm	8-ø12×120mm@90

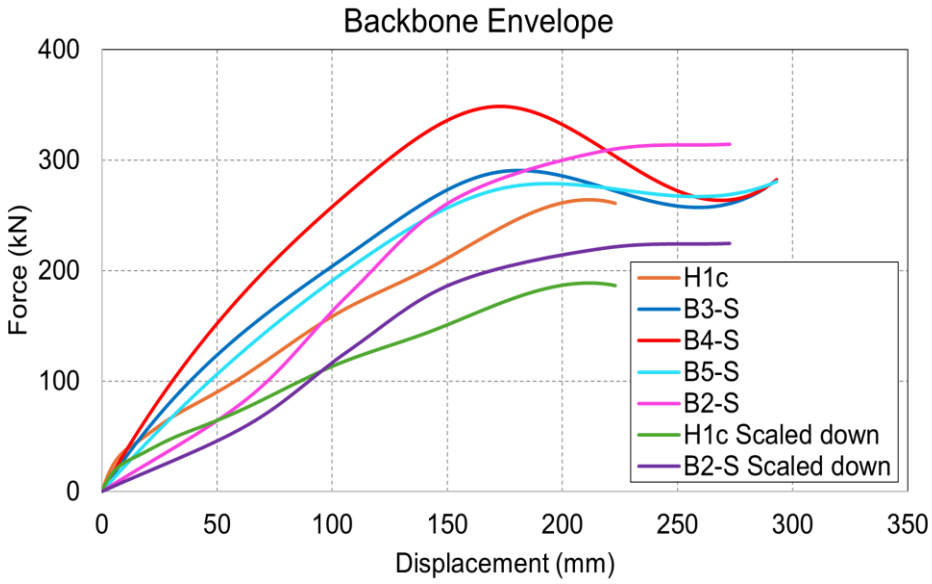

Figure 41 Envelope comparison between platform type and balloon-type shear walls

At 2.2% drift, the lateral resistance of the platform-type H1c wall was 115 kN. In comparison, the balloon-type wall without vertical joints (B2-S) exhibited a 12% higher resistance (129 kN). B3-S, despite incorporating a weaker VJ than H1c, achieved 92% greater resistance (221 kN), while B4-S, which had the stiffest VJ, reached 146% higher resistance (283 kN). B5-S, which included TS and had a more flexible VJ, also outperformed H1c with a 69% increase in resistance (194 kN). At 4.5% drift, H1c resisted 182 kN, whereas B2-S, B3-S, B4-S, and B5-S recorded 23% (224 kN), 46% (267 kN), 63% (292 kN), and 43% (262 kN) higher resistances, respectively. These results demonstrate that balloon-type configurations, even with the presence of a horizontal splice, provide better lateral resistance.

The inter-storey drifts, shown in Figure 42, revealed another advantage of the balloon-type configuration. At 2.2% target drift, H1c exhibited the lowest first-storey inter-storey drift of 1.5%, whereas the balloon-type structures, including the non-monolithic structure B5-S, showed higher first-storey inter-storey drift ratios and lower second-storey inter-storey drift of

2.5%, higher than the other balloon-type walls but still lower than H1c. At 4.5% drift, similar findings were observed. H1c exhibited the lowest first-storey drift ratio of 2.7% and the highest second-storey drift of 5.8%, indicating a pronounced deformation in the upper level. In contrast, the balloon-type structures maintained a more balanced inter-storey deformation, e.g. B3-S and B4-S showed modest differences between storeys—3.9% and 4.9%, and 4.0% and 4.8%, respectively. B5-S exhibited the highest inter-storey drift differences among balloon-type structures (5.1% vs. 3.8%). This improved performance is attributed to the use of TS on both the inner and outer panel edges in B5-S, and the absence of a floor between panels.

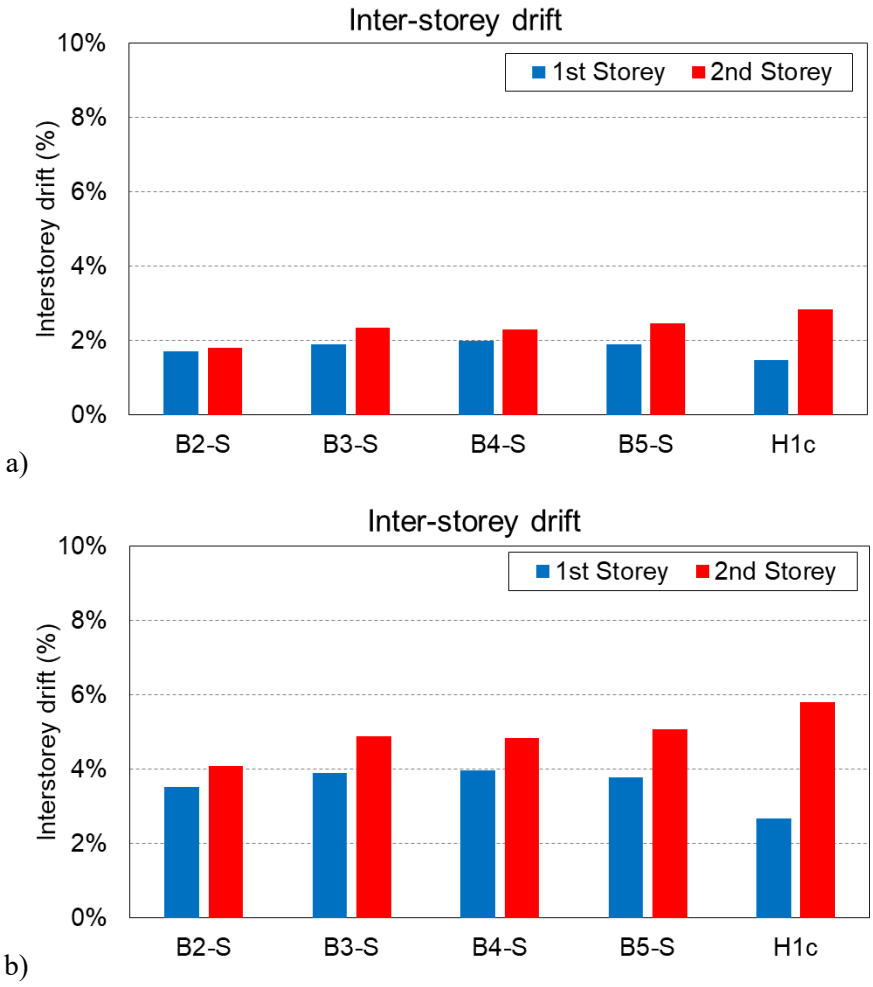

Figure 42 Inter storey drift; a) 2.2%, b) 4.5%

Chapter 6: Conclusions

6.1 Summary

This research presented in this thesis involved a comprehensive full-scale experimental investigation of two-storey balloon-type CLT shear wall structures. A total of eleven tests were conducted under both monotonic and reversed cyclic loading to evaluate the seismic performance of various connection configurations. The testing program systematically examined the influence of HD screw orientations, VJ stiffness, and the inclusion of TS in horizontally spliced panels. These variations enabled a detailed assessment of their impact on lateral strength, deformation mechanisms, and energy dissipation capacity. The main findings obtained from the analyses can be summarized as follows:

1. The two-storey balloon-framed coupled CLT shear wall systems exhibited high drift capacity and maintained global stability under large lateral deformation. All tested configurations sustained cyclic drifts up to 5.7% without exhibiting global instability or structural collapse. This was achieved through capacity protection of the CLT panels and the non-dissipative connections (SB, ledger and TS).

2. Mixed-angle HD combing screws acting in withdrawal with screws acting in shear enhanced initial stiffness and lateral resistance. At lower drift levels, structures with such HD exhibited 3% - 35% higher lateral resistance due to combined shear and withdrawal action; however, this advantage diminished at larger drifts, where shear-only HD retained 2% to 15% more strength, indicating lower degradation and superior long-term performance under cyclic loading.

3. The addition of VJ enhanced lateral resistance compared to structures without VJs, by 187% and 32% respectively at 2.2% drift for structures with shear-only and mixed-angle screw HD, respectively. This difference was no longer observed at larger drifts (5.7%) when the screws in the VJ failed.

4. In structures with stiffer VJ, S and M variants gained 27% and 21% over their counterparts with flexible VJ at low drift, but at higher drifts, the S variant retained only a 3% gain while the M variant experienced a 5% reduction—indicating VJ effectiveness is greater in S variants and primarily at lower deformation levels.

5. Structures with mixed-angle HD exhibited superior energy dissipation at low to moderate drifts, while increased VJ stiffness further amplified this effect. However, at larger drifts, the energy dissipation of mixed and shear-only variants converged, indicating that the benefits of HD detailing and VJ stiffness are most effective in the early stages of deformation.

6. Panel-to-panel displacements were consistently higher at the second storey than at the first across all configurations, due to increased panel distortion at the upper level.

7. At lower drifts, deformation was evenly distributed between the two storeys. As drift increased, the second storey consistently exhibited greater drift than the first, primarily due to panel distortion and reduced restraint at the upper level.

8. Rocking was the dominant deformation mechanism across all configurations with 90-92%, sliding and ledger drift accounting for approximately 3% and panel distortion for roughly 2% of total displacement. Horizontally splicing the panel with TS reduced the rocking contribution to 78%, indicating that the TS were not sufficiently stiff to fully maintain the balloon configuration.

9. Balloon-type CLT walls, even when constructed with more flexible vertical joints or horizontally spliced panels, consistently outperformed the platform-type configuration in both lateral resistance and inter-storey drift distribution, highlighting the benefits of continuous vertical paneling and effective connection detailing.

6.2 Future work

To further advance the work and standardization of balloon-type CLT shear wall systems, future research should build upon the current study's findings by addressing key gaps related to system behavior, connection performance, and multi-storey configurations.

At the connection level, future studies should examine HD assemblies incorporating a greater number of STS and evaluate stiffer TS to improve uplift resistance at the second storey, while maintaining uninterrupted vertical panel continuity. The current study demonstrated that mixed-angle STS in HD enhance stiffness. Future research should therefore investigate the application of angled STS configurations in vertical spline joints. A comparative study between standard and inclined screw arrangements in spline connections may reveal potential improvements in stiffness and energy dissipation across multi-storey balloon-type CLT walls.

To better simulate realistic in-service conditions, full-scale testing should consider larger vertical loads, allowing for a more accurate representation of the combined effects of rocking, sliding, and panel distortion. For more conclusive comparisons with platform-type systems, future test specimens should replicate platform-type panels geometry, inter-storey floor details, and connector configurations, thereby isolating the influence of construction methodology on overall system behavior.

While this study focused primarily on strength-related parameters, initial stiffness and ductility were not evaluated in detail. However, the experimental data generated can support such evaluations in future research, enabling a more complete assessment of lateral performance under seismic demands.

As panel segmentation and connector stiffness strongly influence lateral system behavior, future work should include full-scale tests on balloon-type CLT walls with more than two panel segments, varying parameters such as panel aspect ratio, vertical joint detailing, and ledger/diaphragm configurations. These tests will help isolate the effects of segmentation, hold-down layout, and load sharing across the height of the wall.

Experimental findings from the current and future tests should be used to calibrate analytical and finite element models. Parametric studies should explore the influence of axial load, connector stiffness, and realistic vertical loads on system behavior. In addition, nonlinear time-history analyses can be employed to simulate global structural response and investigate load redistribution mechanisms in full-scale balloon-type configurations.

Given the current lack of seismic fragility and collapse-risk assessments for balloon-type CLT shear wall systems, future research should focus on the development of probabilistic seismic models using these calibrated dynamic models. This effort can be extended to derive fragility functions for balloon-type CLT systems, contributing to performance-based seismic design frameworks—particularly in high seismic regions.

References

[1] D. of E. and S. A. United Nations, “World population projected to reach 9.8 billion in 2050, and 11.2 billion in 2100.”

[2] R. Brandner, G. Flatscher, A. Ringhofer, G. Schickhofer, and A. Thiel, “Cross laminated timber (CLT): overview and development,” *European Journal of Wood and Wood Products*, vol. 74, no. 3, pp. 331–351, May 2016, doi: 10.1007/s00107-015-0999-5.

[3] UN-Habitat, “World Cities Report 2016: Urbanization and Development – Emerging Futures,” United Nations Human Settlements Program. Accessed: Jun. 28, 2025. [Online]. Available: https://unhabitat.org/sites/default/files/download-manager-files/WCR-2016-WEB.pdf

[4] Canadian Commission on Building and Fire Codes, “National Building Code of Canada (NBCC) - 2020,” Ottawa, ON, 2020.

[5] R. J. Ross and F. P. Laboratory. USDA Forest Service., “Wood handbook: wood as an engineering material,” 2010. doi: 10.2737/FPL-GTR-190.

[6] C. D. Oliver, N. T. Nassar, B. R. Lippke, and J. B. McCarter, “Carbon, Fossil Fuel, and Biodiversity Mitigation with Wood and Forests,” *Journal of Sustainable Forestry*, vol. 33, no. 3, pp. 248–275, Apr. 2014, doi: 10.1080/10549811.2013.839386.

[7] U. Dangel, “Tall Wood Buildings: Design, Construction, and Performance” by Michael Green and Jim Taggart,” in *Technology|Architecture + Design*, Jul. 2018, pp. 254–256. doi: 10.1080/24751448.2018.1497379.

[8] E. Karacabeyli and S. Gagnon, “Canadian CLT Handbook, vol. 1. Vancouver, Canada: FPInnovations,” 2019.

[9] T. Tannert, O. A. Ajibola, and M. Popovski, "Structural performance of CLT shear walls with hyper-elastic hold downs," *Journal of Structural Engineering*, vol. 150, no. 1, Jan. 2024, doi: 10.1061/JSENDH.STENG-12703.

[10] A. M. Harte, "Mass timber – the emergence of a modern construction material," *Journal of Structural Integrity and Maintenance*, vol. 2, no. 3, pp. 121–132, Jul. 2017, doi: 10.1080/24705314.2017.1354156.

[11] T. Tannert *et al.*, "Seismic design of cross-laminated timber buildings," *Wood and Fiber Science*, vol. 50, no. Special, pp. 3–26, Aug. 2018, doi: 10.22382/wfs-2018-037.

[12] A. Ceccotti, C. Sandhaas, M. Okabe, M. Yasumura, C. Minowa, and N. Kawai, "SOFIE project – 3D shaking table test on a seven-storey full-scale cross-laminated timber building," in *Earthquake Engineering & Structural Dynamics*, Oct. 2013, pp. 2003–2021. doi: 10.1002/eqe.2309.

[13] IBC, "International Building Code (IBC) - 2021," Falls Church, VA, USA: International Code Council, 2021.

[14] Canadian Standard Association (CSA), "Engineering design in wood. CSA Standard O86-24.," 2024.

[15] D. Trutalli, L. Marchi, R. Scotta, and L. Pozza, "Capacity design of traditional and innovative ductile connections for earthquake-resistant CLT structures," *Bulletin of Earthquake Engineering*, vol. 17, no. 4, pp. 2115–2136, Apr. 2019, doi: 10.1007/s10518-018-00536-6.

[16] A. Hossain, I. Danzig, and T. Tannert, "Cross-Laminated Timber Shear Connections with Double-Angled Self-Tapping Screw Assemblies," *Journal of Structural*

Engineering, vol. 142, no. 11, Nov. 2016, doi: 10.1061/(ASCE)ST.1943-541X.0001572.

[17] J. Schneider, Y. Shen, S. F. Stiemer, and S. Tesfamariam, "Assessment and comparison of experimental and numerical model studies of cross-laminated timber mechanical connections under cyclic loading," in *Construction and Building Materials*, Feb. 2015, pp. 197–212. doi: 10.1016/j.conbuildmat.2014.12.029.

[18] I. Gavric, M. Fragiacomo, and A. Ceccotti, "Cyclic behaviour of typical metal connectors for cross-laminated (CLT) structures," in *Materials and Structures*, Jun. 2015, pp. 1841–1857. doi: 10.1617/s11527-014-0278-7.

[19] M. Shahnewaz, M. Popovski, and T. Tannert, "Resistance of cross-laminated timber shear walls for platform-type construction," *Journal of Structural Engineering*, vol. 145, no. 12, Dec. 2019, doi: 10.1061/(ASCE)ST.1943-541X.0002413.

[20] Z. Chen and M. Popovski, "Mechanics-based analytical models for balloon-type cross-laminated timber (CLT) shear walls under lateral loads," in *Engineering Structures*, Apr. 2020, p. 109916. doi: 10.1016/j.engstruct.2019.109916.

[21] X. Wang, M. He, and Z. Li, "Experimental testing of platform-type and balloon-type cross-laminated timber (CLT) shear walls with supplemental energy dissipators," *Journal of Building Engineering*, vol. 66, p. 105943, May 2023, doi: 10.1016/j.jobe.2023.105943.

[22] Canadian Standard Association (CSA), *Engineering design in wood CSA Standard O86-19*. Mississauga, Canada, 2019.

[23] H. Daneshvar, J. Niederwestberg, C. Dickof, J.-P. Letarte, and Y. H. Chui, "Cross-Laminated Timber Shear Walls in Balloon Construction: Seismic Performance of Steel Connections," *Modular and Offsite Construction (MOC) Summit Proceedings*, pp. 405–412, May 2019, doi: 10.29173/mocs120.

[24] M. Gong, "Lumber-Based Mass Timber Products in Construction," in *Timber Buildings and Sustainability*, IntechOpen, 2019. doi: 10.5772/intechopen.85808.

[25] FP-Innovations, "CLT handbook (Canadian edition), Special Publication SP-532E," Pointe-Claire, QC, Canada: FP-Innovatios, 2019. Accessed: May 27, 2024. [Online]. Available: https://web.fpinnovations.ca/wp-content/uploads/clt-handbook-complete-version-en-low.pdf

[26] A. Hossain, "Experimental investigations of shear connections with self-tapping-screws for cross-laminated-timber panels," University of British Columbia, 2019.

[27] M. Masroor, G. Doudak, and D. Casagrande, "The effect of bi-axial behaviour of mechanical anchors on the lateral response of multi-panel CLT shearwalls," in *Engineering Structures*, Dec. 2020, p. 111202. doi: 10.1016/j.engstruct.2020.111202.

[28] X. Sun, M. He, and Z. Li, "Novel engineered wood and bamboo composites for structural applications: State-of-art of manufacturing technology and mechanical performance evaluation," in *Construction and Building Materials*, Jul. 2020, p. 118751. doi: 10.1016/j.conbuildmat.2020.118751.

[29] D. Buck, X. Wang, O. Hagman, and A. Gustafsson, "Further Development of Cross-Laminated Timber (CLT): Mechanical Tests on 45° Alternating Layers," in *World Conference on Timber Engineering*, Aug. 2016.

[30] M. Shahnewaz, S. Alam, and T. Tannert, “In-Plane Strength and Stiffness of Cross-Laminated Timber Shear Walls,” *Buildings*, vol. 8, no. 8, p. 100, Aug. 2018, doi: 10.3390/buildings8080100.

[31] T. Reynolds, R. Foster, J. Bregulla, W.-S. Chang, R. Harris, and M. Ramage, “Lateral-Load Resistance of Cross-Laminated Timber Shear Walls,” *Journal of Structural Engineering*, vol. 143, no. 12, Dec. 2017, doi: 10.1061/(ASCE)ST.1943-541X.0001912.

[32] T. Connolly, C. Loss, A. Iqbal, and T. Tannert, “Feasibility Study of Mass-Timber Cores for the UBC Tall Wood Building,” *Buildings*, vol. 8, no. 8, p. 98, Aug. 2018, doi: 10.3390/buildings8080098.

[33] S. Pei *et al.*, “Cross-Laminated Timber for Seismic Regions: Progress and Challenges for Research and Implementation,” *Journal of Structural Engineering*, vol. 142, no. 4, Apr. 2016, doi: 10.1061/(ASCE)ST.1943-541X.0001192.

[34] M. A. H. Mirdad, J. Niederwestberg, A. Jucutan, and Y. H. Chui, “Prediction of withdrawal stiffness of self-tapping screws,” in *World Conference on Timber Engineering (WCTE 2023)*, Norway, 2023, pp. 1117–1122. doi: 10.52202/069179-0153.

[35] Y. Pan, T. Teflissi, and T. Tannert, “Experimental Parameter Study on CLT Shear Walls with Self-Tapping Screw Connections,” *Journal of Structural Engineering*, vol. 150, no. 1, Jan. 2024, doi: 10.1061/JSENDH.STENG-12710.

[36] M. Masroor, M. Gheisari, and T. Tannert, “Experimental Parameter Study of Two-Story Platform-Type CLT Shear Walls,” *Journal of Structural Engineering*, vol. 150, no. 8, Aug. 2024, doi: 10.1061/JSENDH.STENG-13277.

[37] A. Sandoli, C. D’Ambra, C. Ceraldi, B. Calderoni, and A. Prota, “Sustainable Cross-Laminated Timber Structures in a Seismic Area: Overview and Future Trends,” *Applied Sciences*, vol. 11, no. 5, p. 2078, Feb. 2021, doi: 10.3390/app11052078.

[38] M. Mohammad, S. Gagnon, B. K. Douglas, and L. Podesto, “Introduction to cross laminated timber,” in *Wood Design Focus*, Jan. 2012, pp. 3–12.

[39] I. Gavrić, A. Ceccotti, and M. Fragiacomo, “Investigation of seismic performance of multi-storey timber buildings within the framework of the SERIES Project,” in *Structures and Architecture*, CRC Press, 2013, pp. 110–117. doi: 10.1201/b15267-13.

[40] C. Loss, S. Pacchioli, A. Polastri, D. Casagrande, L. Pozza, and I. Smith, “Numerical Study of Alternative Seismic-Resisting Systems for CLT Buildings,” *Buildings*, vol. 8, no. 11, p. 162, Nov. 2018, doi: 10.3390/buildings8110162.

[41] I. Smith and A. Frangi, *Use of Timber in Tall Multi-Storey Buildings*. Zurich, Switzerland: International Association for Bridge and Structural Engineering (IABSE), 2014. doi: 10.2749/sed013.

[42] C. Loss and A. Frangi, “Experimental investigation on in-plane stiffness and strength of innovative steel-timber hybrid floor diaphragms,” in *Engineering Structures*, May 2017, pp. 229–244. doi: 10.1016/j.engstruct.2017.02.032.

[43] S. A. R. Z. Bruno Dujic, “Testing of wooden wall panels applying realistic boundary conditions,” in *Proceedings of the 9th World Conference on Timber Engineering*, Portland, Oregon, USA, 2006, pp. 125–142.

[44] M. Popovski, I. Gavrić, and J. Schneider, “Performance of two storey CLT house subjected to lateral loads,” in *13th World Conference on Timber Engineering (WCTE 2014)*, Quebec City, Canada, Aug. 2014. doi: 10.13140/RG.2.1.3582.9280.

[45] J. W. van de Lindt *et al.*, “Experimental seismic behavior of a two-story CLT platform building,” in *Engineering Structures*, Mar. 2019, pp. 408–422. doi: 10.1016/j.engstruct.2018.12.079.

[46] M. Popovski, J. Schneider, and M. Schweinsteiger, “Lateral load resistance of cross-laminated wood panels,” in *11th World Conference on Timber Engineering (WCTE 2010)*, Riva del Garda, Italy, Jan. 2010.

[47] M. Popovski and E. Karacabeyli, “Seismic Behaviour of Cross-Laminated Timber Structures,” in *World Conference on Timber Engineering (WCTE 2012)*, Aukland, Newzeland, Jan. 2012.

[48] I. Gavric, M. Fragiacomo, M. Popovski, and A. Ceccotti, “Behaviour of Cross-Laminated Timber Panels under Cyclic Loads,” in *Materials and Joints in Timber Structures*, Dordrecht: Springer Netherlands, 2014, pp. 689–702. doi: 10.1007/978-94-007-7811-5_62.

[49] T. Tannert and C. Loss, “Contemporary and novel hold-down solutions for mass timber shear walls,” *Buildings*, vol. 12, no. 2, p. 202, Feb. 2022, doi: 10.3390/buildings12020202.

[50] F. Benedetti, V. Rosales, A. Opazo-Vega, J. Norambuena-Contreras, and A. Jara-Cisterna, "Experimental and numerical evaluation of hold-down connections on radiata pine Cross-Laminated-Timber shear walls: a case study in Chile," *European Journal of Wood and Wood Products*, vol. 77, no. 1, pp. 79–92, Jan. 2019, doi: 10.1007/s00107-018-1365-1.

[51] L.-M. Ottenhaus, M. Li, and T. Smith, "Structural performance of large-scale dowelled CLT connections under monotonic and cyclic loading," *Eng Struct*, vol. 176, pp. 41–48, Dec. 2018, doi: 10.1016/j.engstruct.2018.09.002.

[52] N. Chan, A. Hashemi, P. Zarnani, and P. Quenneville, "Pinching-Free Connector for Timber Structures," *Journal of Structural Engineering*, vol. 147, no. 5, May 2021, doi: 10.1061/(ASCE)ST.1943-541X.0002982.

[53] A. Hashemi, P. Zarnani, R. Masoudnia, and P. Quenneville, "Seismic resistant rocking coupled walls with innovative Resilient Slip Friction (RSF) joints," in *Journal of Constructional Steel Research*, Feb. 2017, pp. 215–226. doi: 10.1016/j.jcsr.2016.11.016.

[54] R. Tomasi, A. Crosatti, and M. Piazza, "Theoretical and experimental analysis of timber-to-timber joints connected with inclined screws," in *Construction and Building Materials*, Sep. 2010, pp. 1560–1571. doi: 10.1016/j.conbuildmat.2010.03.007.

[55] K. Sullivan, T. H. Miller, and R. Gupta, "Behavior of cross-laminated timber diaphragm connections with self-tapping screws," in *Engineering Structures*, Aug. 2018, pp. 505–524. doi: 10.1016/j.engstruct.2018.04.094.

[56] J. R. Brown, M. Li, T. Tannert, and D. Moroder, “Experimental study on orthogonal joints in cross-laminated timber with self-tapping screws installed with mixed angles,” in *Engineering Structures*, Feb. 2021, p. 111560. doi: 10.1016/j.engstruct.2020.111560.

[57] A. Hossain, M. Popovski, and T. Tannert, “Cross-laminated timber connections assembled with a combination of screws in withdrawal and screws in shear,” in *Engineering Structures*, Aug. 2018, pp. 1–11. doi: 10.1016/j.engstruct.2018.04.052.

[58] M. B. I. S. Tom Joyce, “Mechanical behavior of in-plane shear connections between CLT wall panels,” in *CIB-W18 Meeting 44At: Alghero, Italy*, 2011.

[59] T. Wright, M. Li, D. Moroder, and D. M. Carradine, “Cyclic behaviour of hold-downs using mixed angle self-tapping screws in Douglas-fir CLT,” in *Proceedings of the 2021 New Zealand Society for Earthquake Engineering Annual Technical Conference*, New Zealand Society for Earthquake Engineering, Apr. 2021. Accessed: Dec. 03, 2024. [Online]. Available: https://repo.nzsee.org.nz/handle/nzsee/2403

[60] T. Wright, M. Li, D. Moroder, H. Lim, and D. Carradine, “Cyclic behaviour of CLT shear wall hold-down connections using mixed angle self-tapping screws,” in *Engineering Structures*, Jul. 2023, p. 116123. doi: 10.1016/j.engstruct.2023.116123.

[61] T. Wright, M. Li, D. Moroder, and D. M. Carradine, “Design of Mixed Angle Screw CLT Hold-Down Connections to New Zealand Timber Standards,” in *New Zeland Society for Earthquake Engineering Annual Conference*, Auckland, Apr. 2023.

[62] Standards New Zealand, “NZS3404 Part 1:2022 steel structures standard. Standards New Zealand; 2022,” 2022.

[63] B. Moerman, M. Li, T. Smith, and A. Liu, “Cyclic Testing of High-Capacity CLT Shear Walls,” *Journal of Structural Engineering*, vol. 149, no. 11, Nov. 2023, doi: 10.1061/JSENDH.STENG-12188.

[64] T. Cavanagh, “Balloon Houses: The Original Aspects of Conventional Wood-Frame Construction Re-examined,” *Journal of Architectural Education*, vol. 51, no. 1, pp. 5–15, Sep. 1997, doi: 10.1080/10464883.1997.10734741.

[65] P. E. Sprague, “The Origin of Balloon Framing,” *Journal of the Society of Architectural Historians*, vol. 40, no. 4, pp. 311–319, Dec. 1981, doi: 10.2307/989648.

[66] M. Shahnewaz, C. Dickof, and T. Tannert, “Seismic Behavior of Balloon Frame CLT Shear Walls with Different Ledgers,” *Journal of Structural Engineering*, vol. 147, no. 9, Sep. 2021, doi: 10.1061/(ASCE)ST.1943-541X.0003106.

[67] Z. Li, X. Wang, and M. He, “Experimental and Analytical Investigations into Lateral Performance of Cross-Laminated Timber (CLT) Shear Walls with Different Construction Methods,” *Journal of Earthquake Engineering*, vol. 26, no. 7, pp. 3724–3746, May 2022, doi: 10.1080/13632469.2020.1815609.

[68] X. Wang, M. He, H. Dong, and Z. Li, “Numerical modeling strategies and parametric analyses of platform-type and balloon-type cross-laminated timber (CLT) shear walls under lateral loads,” in *Engineering Structures*, Nov. 2023, p. 116857. doi: 10.1016/j.engstruct.2023.116857.

[69] H. Dong, M. He, X. Wang, C. Christopoulos, Z. Li, and Z. Shu, “Development of a uniaxial hysteretic model for dowel-type timber joints in OpenSees,” in *Construction and Building Materials*, Jun. 2021, p. 123112. doi: 10.1016/j.conbuildmat.2021.123112.

[70] X. Zhang, Y. Pan, and T. Tannert, “The influence of connection stiffness on the dynamic properties and seismic performance of tall cross-laminated timber buildings,” in *Engineering Structures*, Jul. 2021, p. 112261. doi: 10.1016/j.engstruct.2021.112261.

[71] K. Krauss, B. Moerman, M. Li, and F. Lam, “Experimental and numerical investigation of the cyclic behaviour of coupled balloon-type CLT shear walls with high-capacity base connections,” in *Engineering Structures*, Nov. 2024, p. 118860. doi: 10.1016/j.engstruct.2024.118860.

[72] D. Xing, D. Casagrande, and G. Doudak, “Investigating the deformation characteristics of balloon-type CLT shearwall,” *Canadian Journal of Civil Engineering*, vol. 51, no. 7, pp. 704–722, Jul. 2024, doi: 10.1139/cjce-2023-0233.

[73] Carla Dickof, Md Shahnewaz, Nick Bevilacqua, and Thomas Tannert, “Experimental investigation of balloon frame CLT shear walls,” in *World Conference on Timber Engineering*, Chile, Aug. 2020.

[74] Z. Chen and M. Popovski, “Structural performance of balloon mass timber shear walls under in-plane lateral loads,” *Structures*, vol. 58, p. 105643, Dec. 2023, doi: 10.1016/j.istruc.2023.105643.

[75] H. Danielsson and E. Serrano, “Cross laminated timber at in-plane beam loading – Prediction of shear stresses in crossing areas,” in *Engineering Structures*, Sep. 2018, pp. 921–927. doi: 10.1016/j.engstruct.2018.03.018.

[76] M. B. W. J. Ron DeVall; Marjan Popovski, “Technical guide for evaluation of seismic force resisting systems and their force modification factors for use in the National

Building Code of Canada with concepts illustrated using a cantilevered wood CLT shear wall example," 2022.

[77] T. Y. Yang, S. Lepine-Lacroix, J. A. R. Guerrero, J. B. W. McFadden, and M. A. Q. Al-Janabi, "Seismic performance evaluation of innovative balloon type CLT rocking shear walls," *Resilient Cities and Structures*, vol. 1, no. 1, pp. 44–52, Mar. 2022, doi: 10.1016/j.rcns.2022.03.004.

[78] Federal Emergency Management Agency (FEMA), "Quantification of Building Seismic Performance Factors," Washington, DC, USA, 2009.

[79] S. Lepine-Lacroix and T. Y. Yang, "Seismic design and performance evaluation of novel dual-pinned self-centering coupled CLT shear walls," in *Engineering Structures*, Mar. 2023, p. 115547. doi: 10.1016/j.engstruct.2022.115547.

[80] EN 1995-1, "Design of structures for earthquake resistance, Part 1: General rules, seismic actions and rules for buildings," Brussels, Belgium., 2004.

[81] M. Follesa *et al.*, "The new provisions for the seismic design of timber buildings in Europe," in *Engineering Structures*, Aug. 2018, pp. 736–747. doi: 10.1016/j.engstruct.2018.04.090.

[82] IBC, "International Building Code (IBC) 2015," Falls Church, VA, USA: International Code Council, 2015.

[83] NDS, "National Design Specification for Wood Construction," Washington, DC.: American Wood Council, 2015.

[84] American National Standard, "Standard for Performance-Rated Timber. ANSI/APA PRG 320," Tacoma, WA, 2017.

[85] American Society of Civil Engineers, “Minimum design loads for buildings and other structures,” Reston, VA.: American Society of Civil Engineers: Structural Engineering Institute, 2010.

[86] American Society of Civil Engineers, *Minimum Design Loads for Buildings and Other Structures*. Reston, VA: American Society of Civil Engineers, 2013. doi: 10.1061/9780784412916.

[87] Canadian Standard Association (CSA), “Engineering design in wood CSA standard O86-14,” Mississauga, Canada, 2014.

[88] Canadian Standard Association (CSA), “Engineering design in wood CSA standard O86-16 supplement,” Mississauga, Canada, 2016.

[89] European OrganizatIon for Technical Assessment (EOTA), “ETA-16/0906: Kombi LT, CSK, and Ecofast Screws for Structural Applications,” Brussels, 2021.

[90] American Society of Civil Engineers (ASTM) E2126-09, “Standard Test Methods for Cyclic (Reversed) Load Test for Shear Resistance of Vertical Elements of the Lateral Force Resisting Systems for Buildings,” 2009.

Appendix 1: Pictures of structures before testing

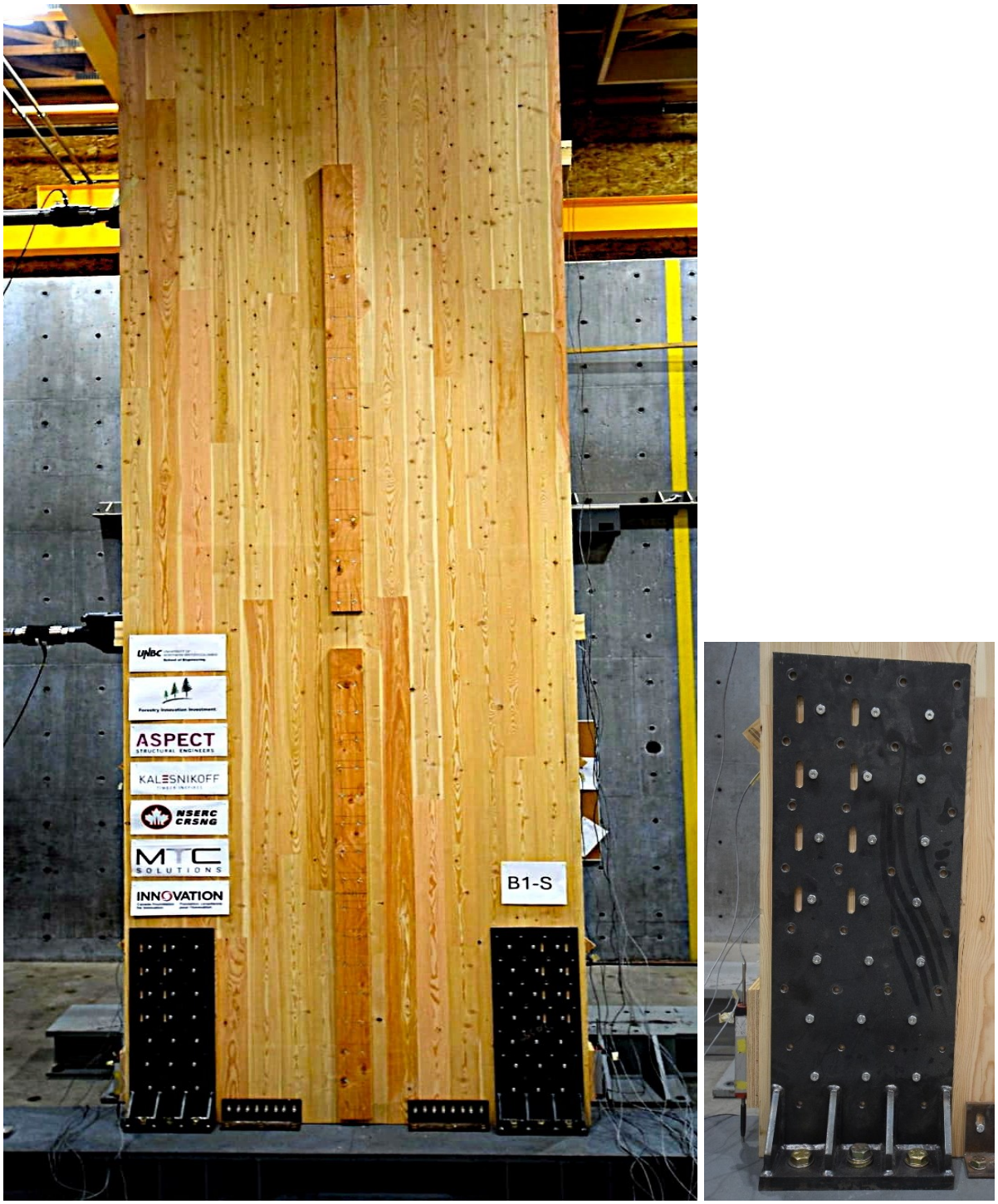

Figure 43 B1-S with perp. screws HD

Figure 44 B1-M with mixed screws HD

Figure 45 B2-S with perp. screws HD

Figure 46 B2-M with mixed screws HD

Figure 47 B2-Si with lower number perp. screws HD

Figure 48 B2-Mi with mixed screws HD and no spline joint

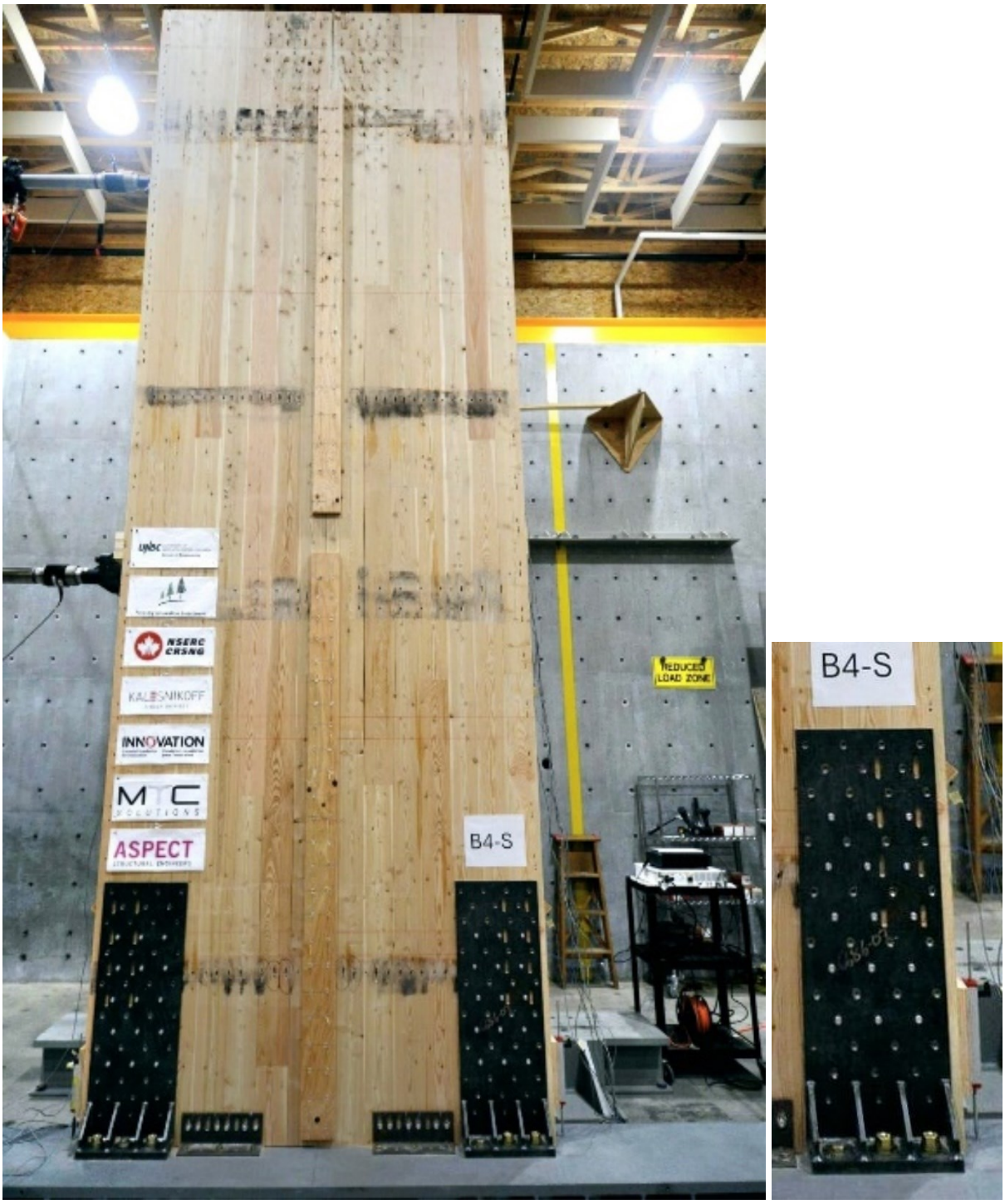

Figure 49 B4-S with perp. screws HD

Figure 50 B4-M with mixed screws HD

Figure 51 B5-S with tension straps

Appendix 2: Load-displacement curves all tests

A.2.1 Shear walls floor displacements

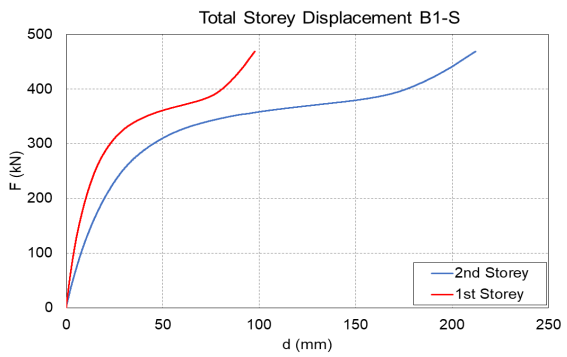

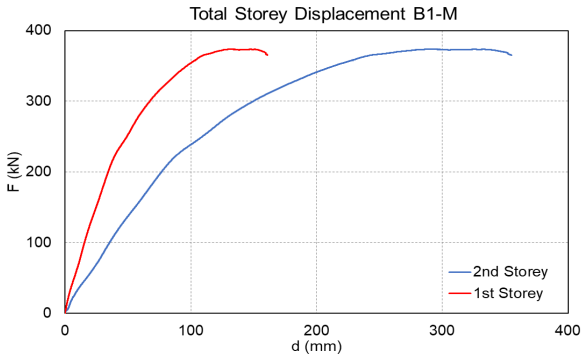

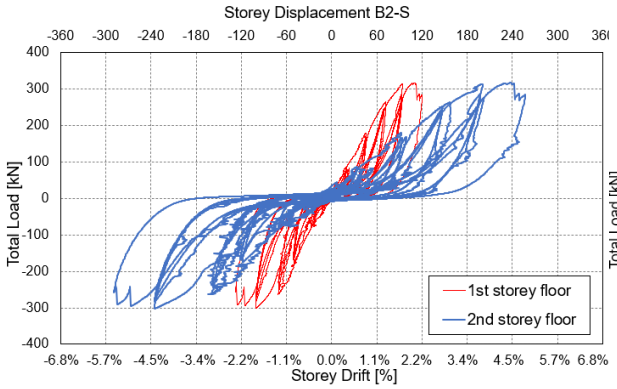

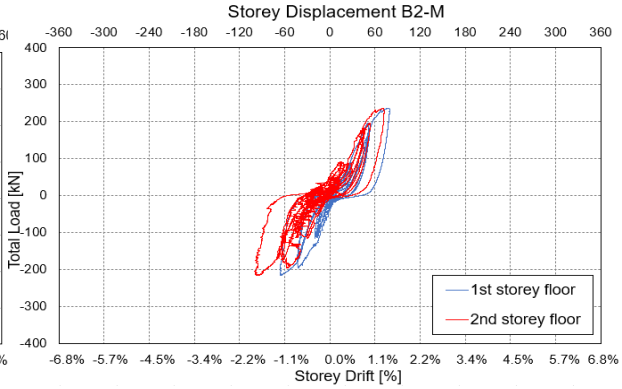

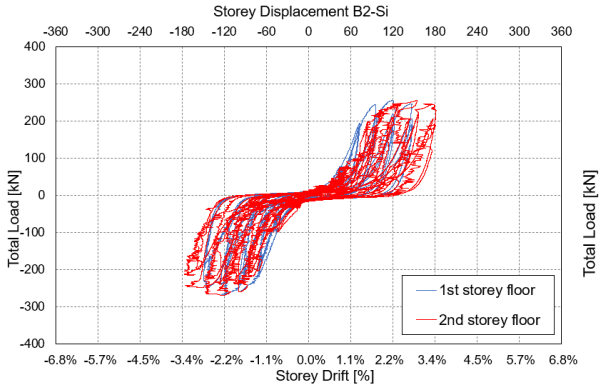

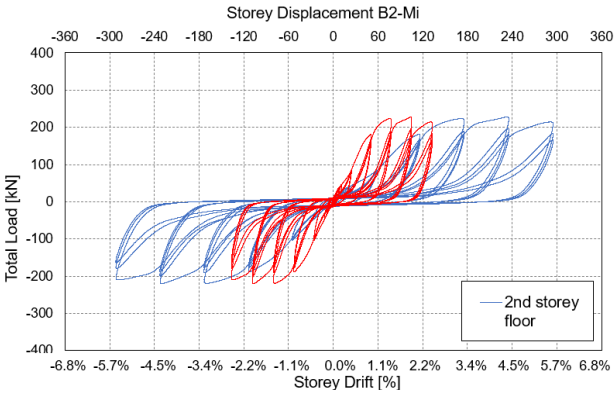

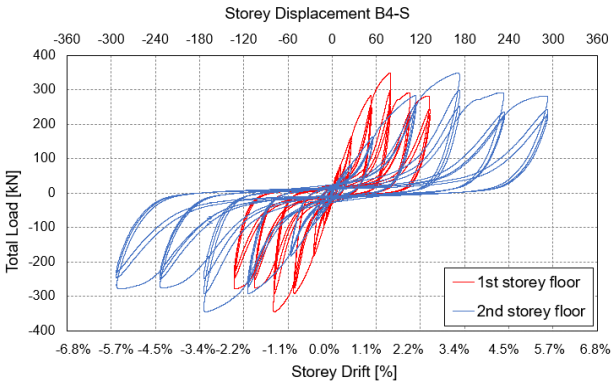
Storey Displacement B4-S
Total Load [kN]
Storey Drift [%]
1st storey floor
2nd storey floor

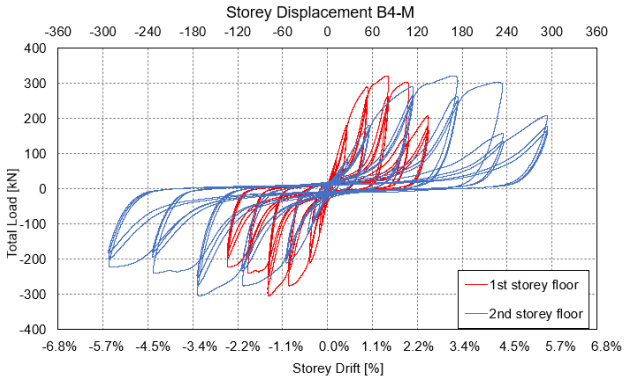
Storey Displacement B4-M
Total Load [kN]
Storey Drift [%]
1st storey floor
2nd storey floor

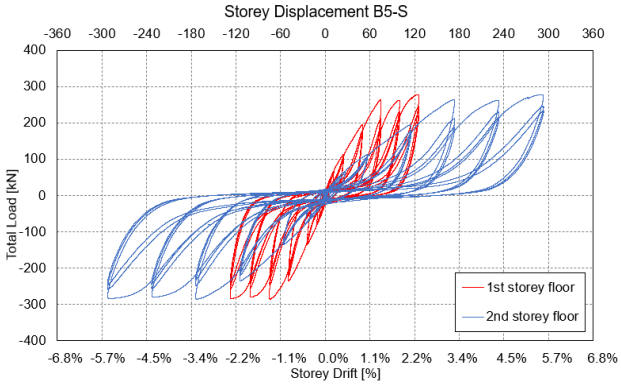
Storey Displacement B5-S
Total Load [kN]
Storey Drift [%]
1st storey floor
2nd storey floor

A.2.2 Hold-down uplifts

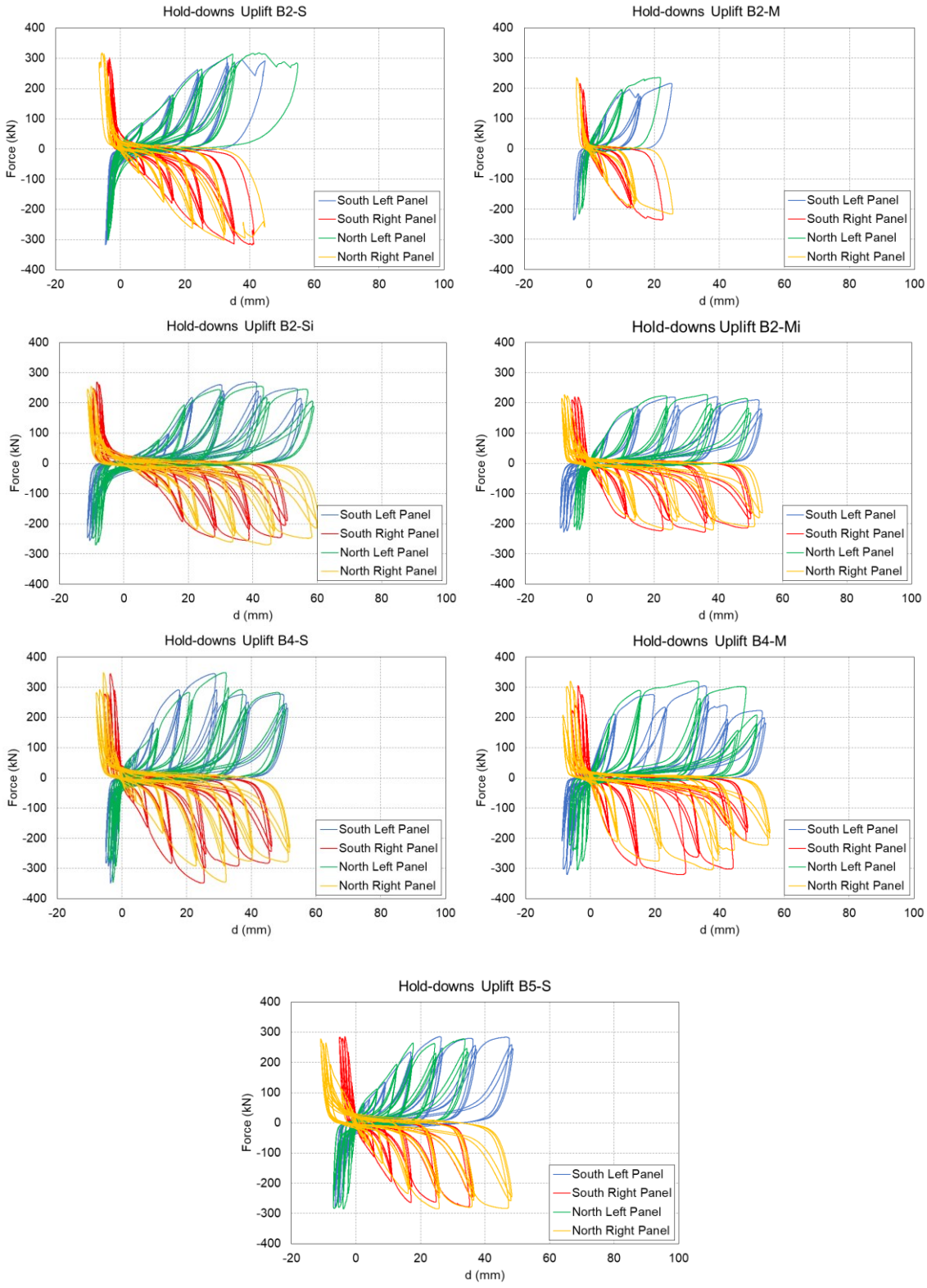

A.2.3 Tension strap uplifts

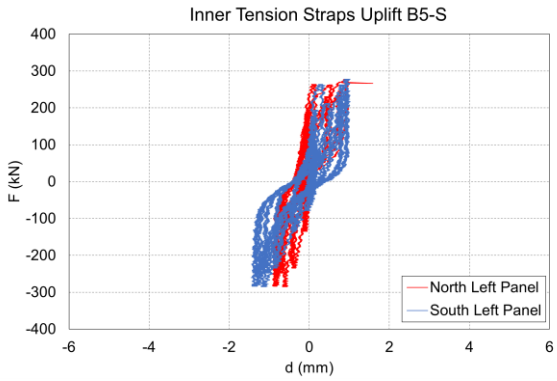

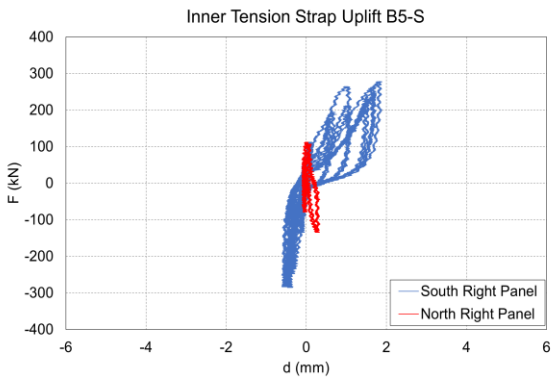

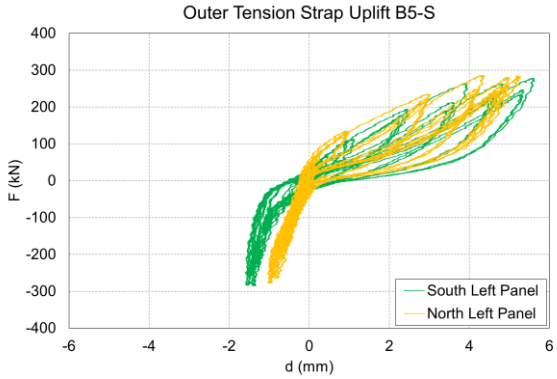

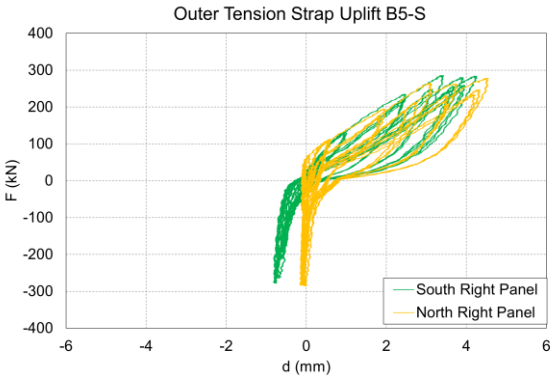

A.2.4 Shear wall uplift at inner corners

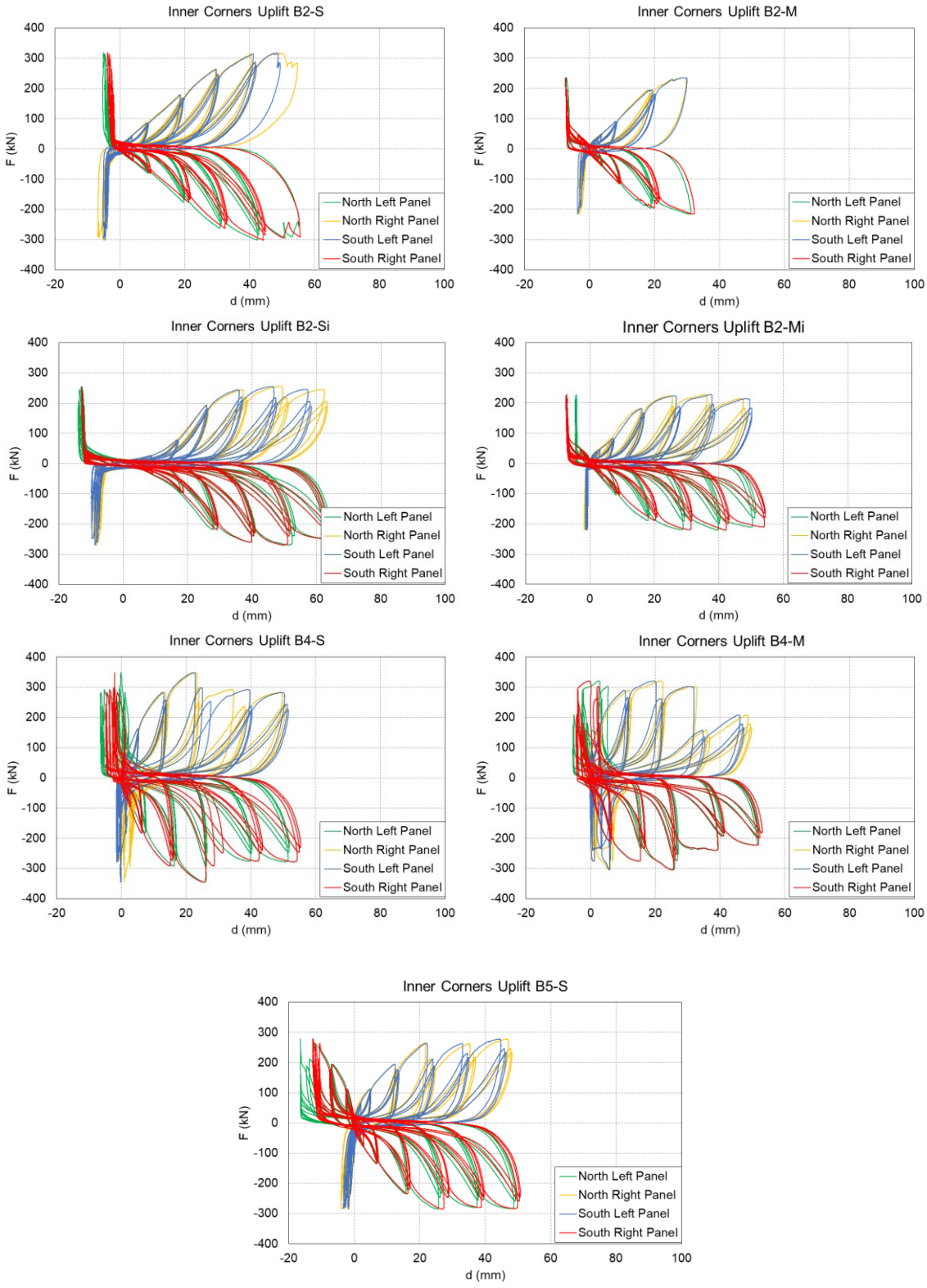

A.2.5 Panel sliding

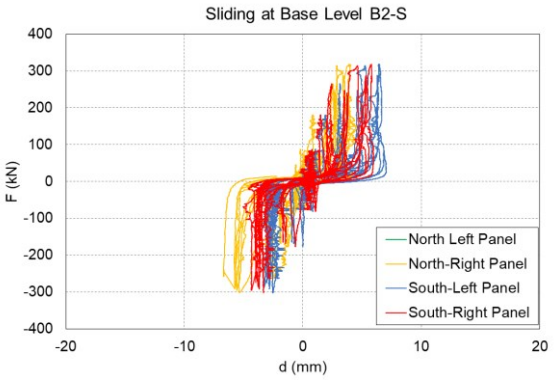

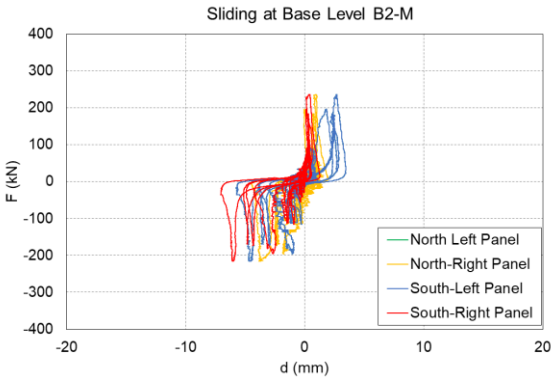

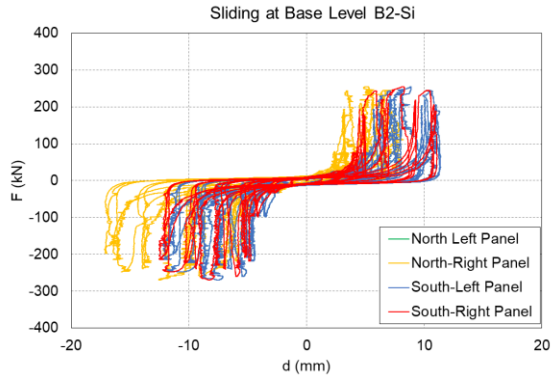

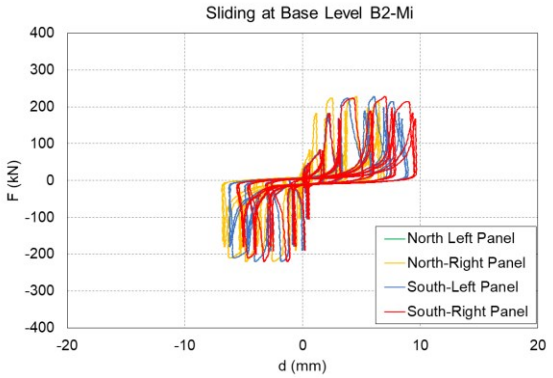

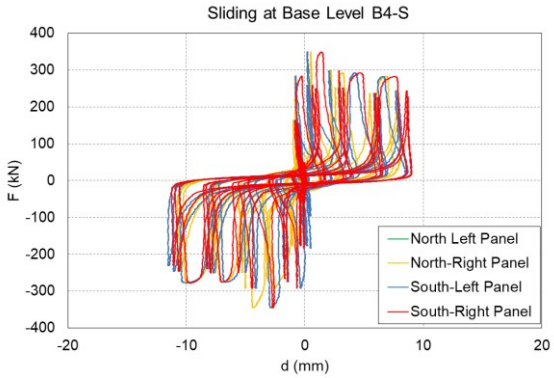

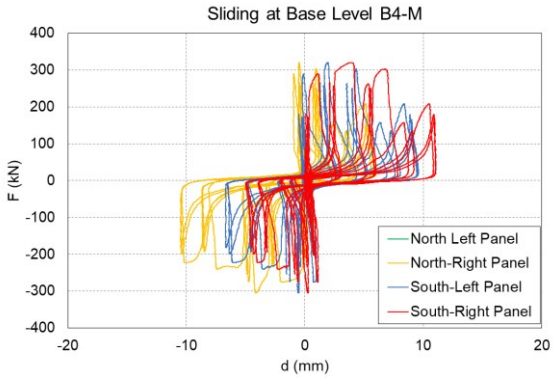

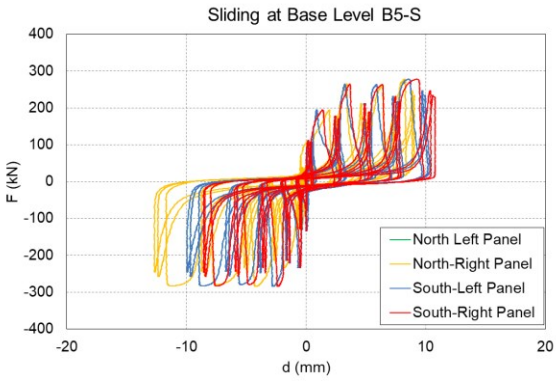

A.2.6 Panel-to-panel displacement

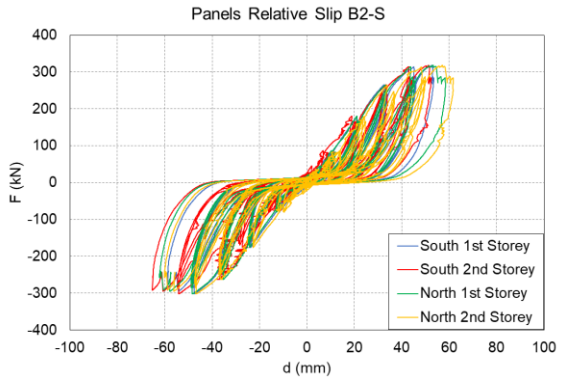

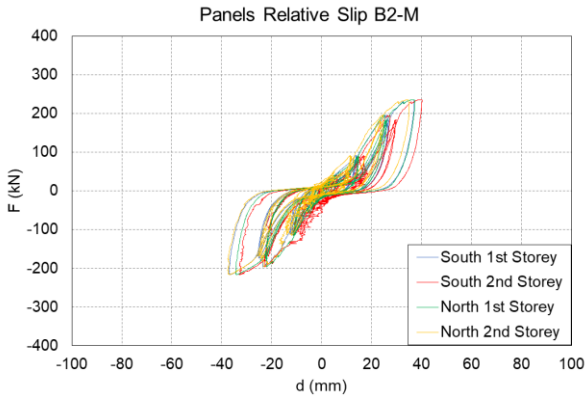

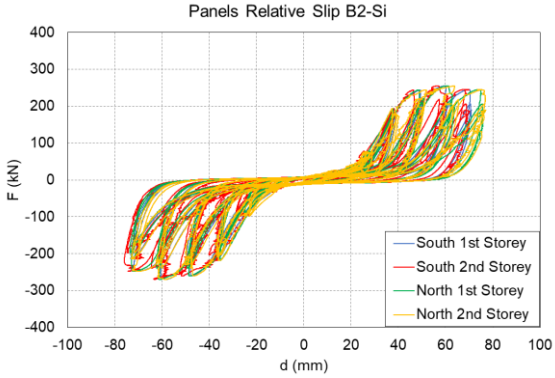

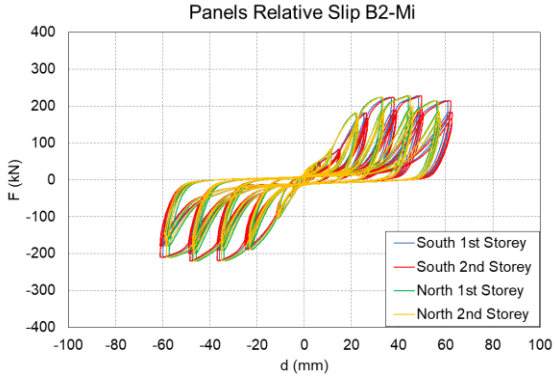

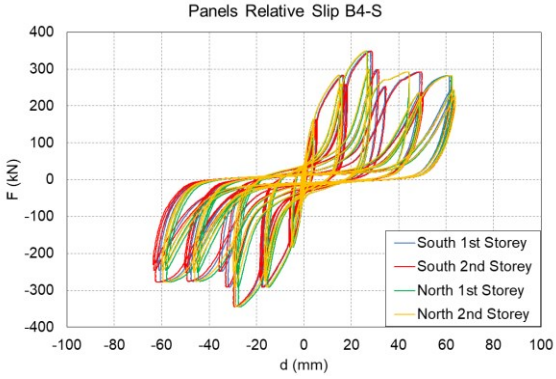

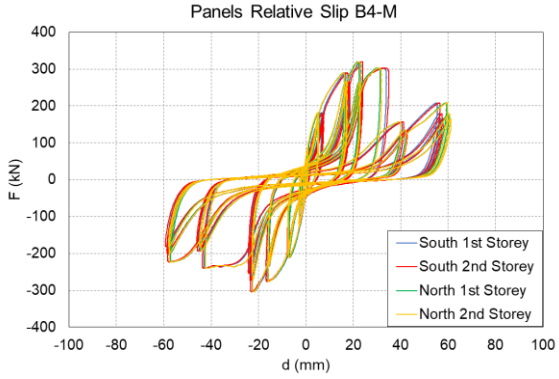

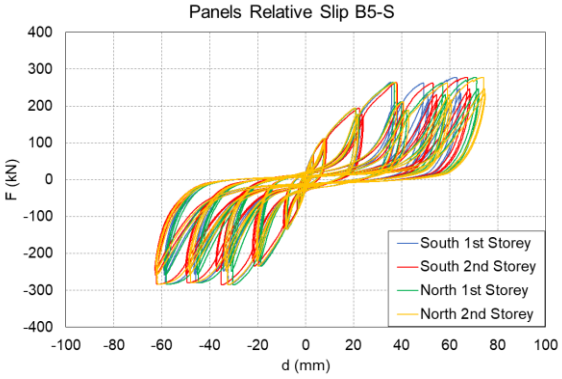

A.2.7 Ledger slip

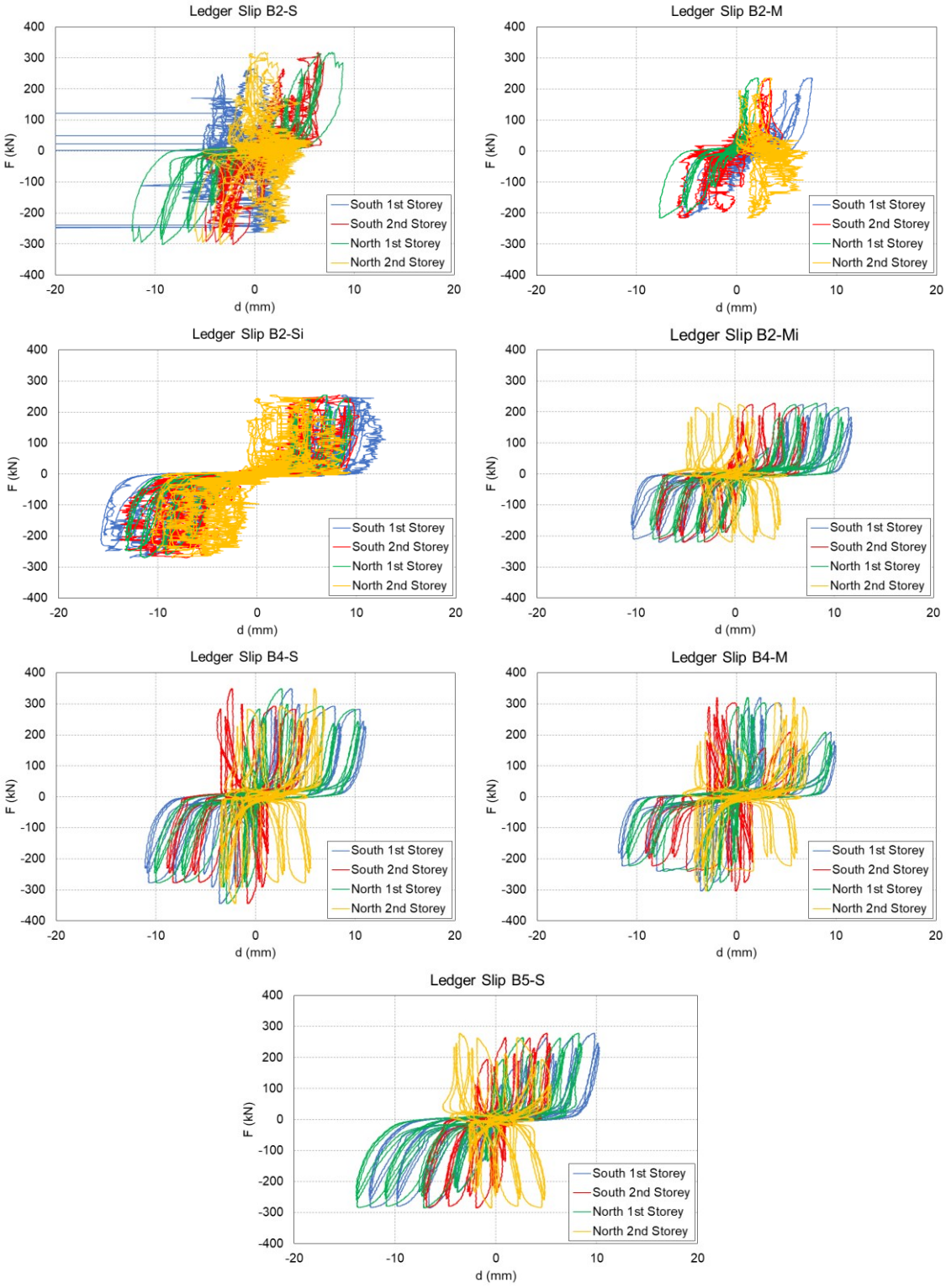

A.2.8 Wall displacements

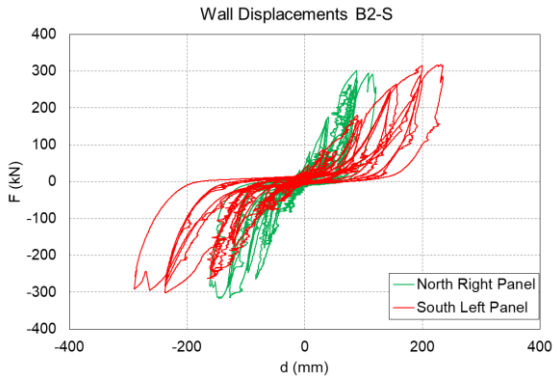

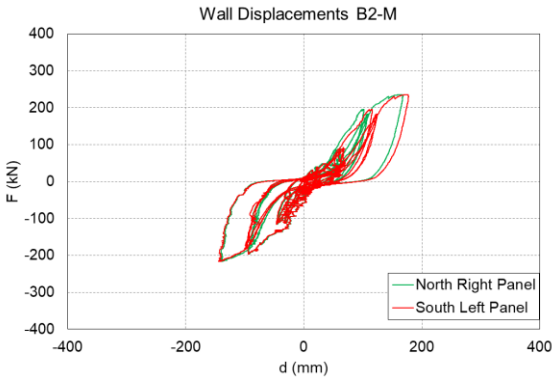

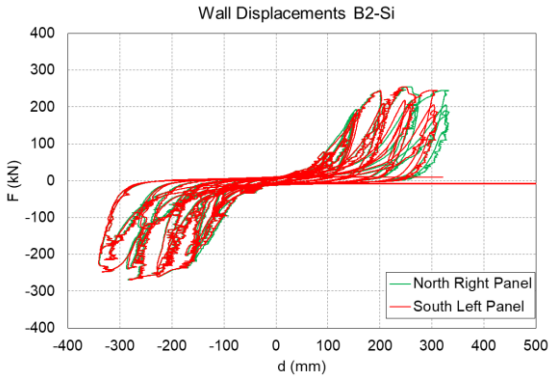

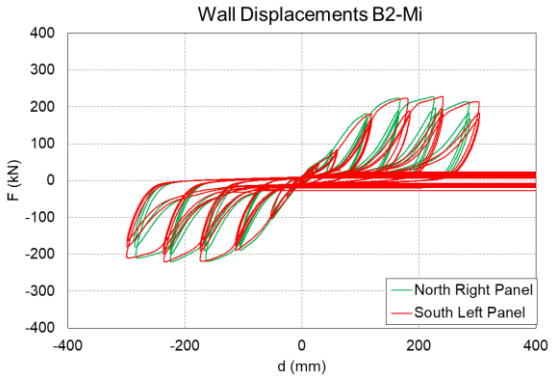

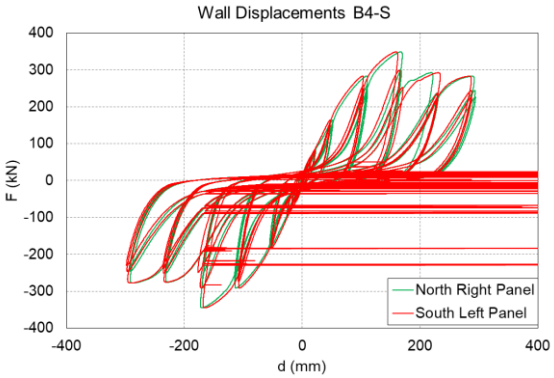

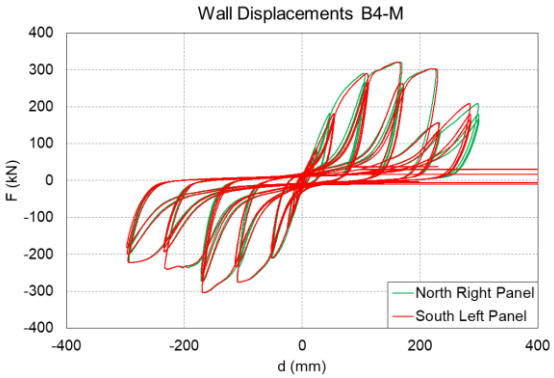

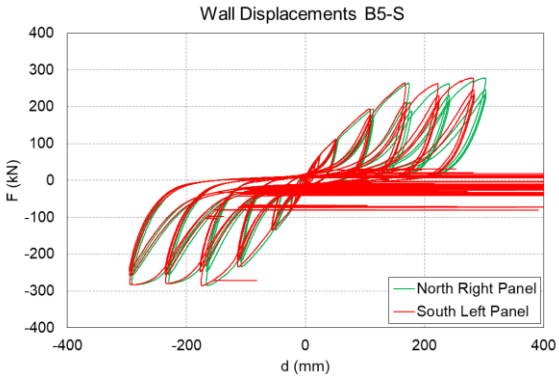

A.2.9 Panel distortion

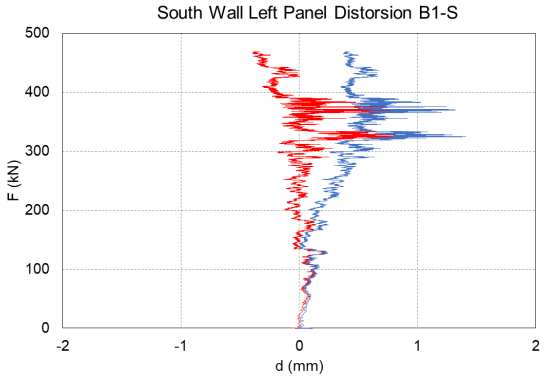

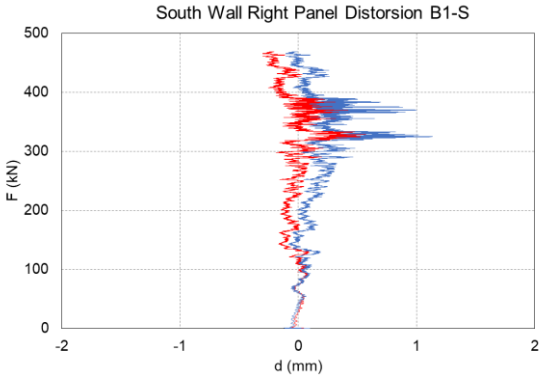

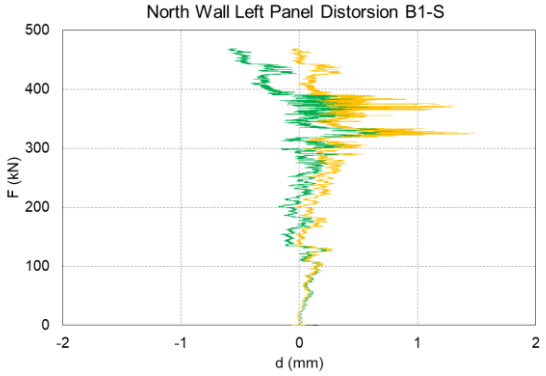

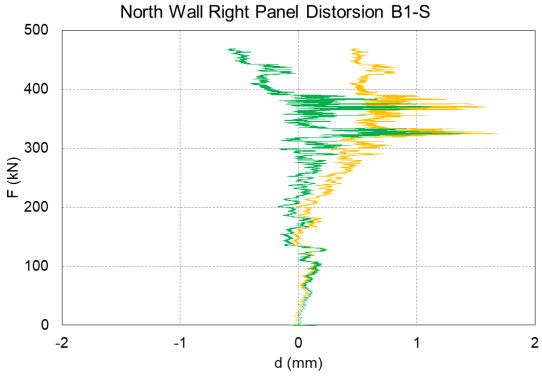

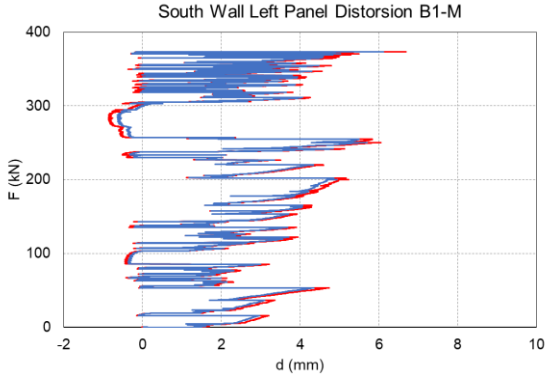

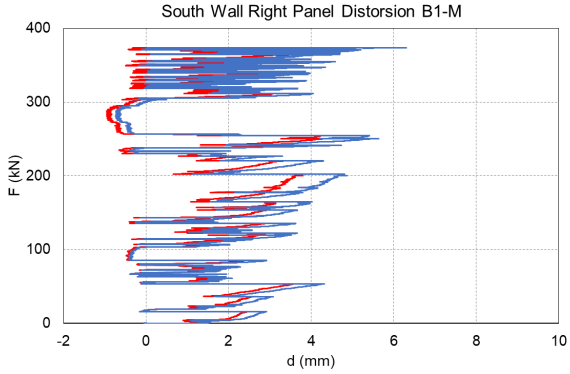

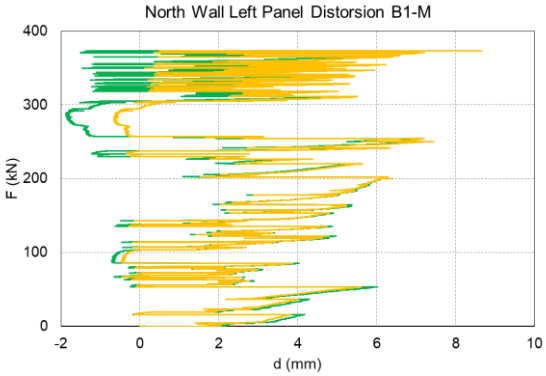

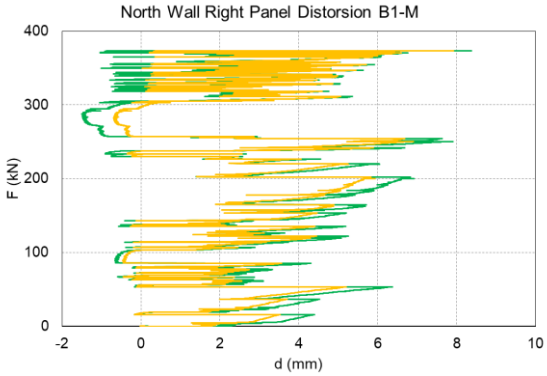

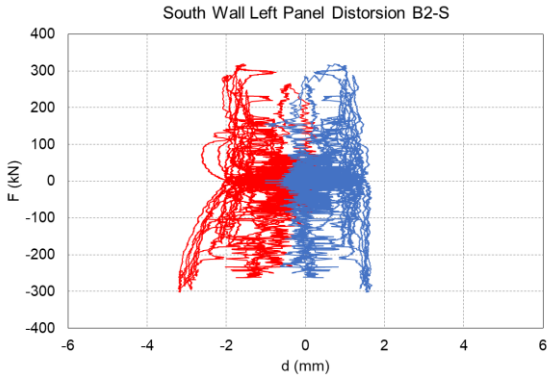
South Wall Left Panel Distorsion B2-S
F (kN)
d (mm)

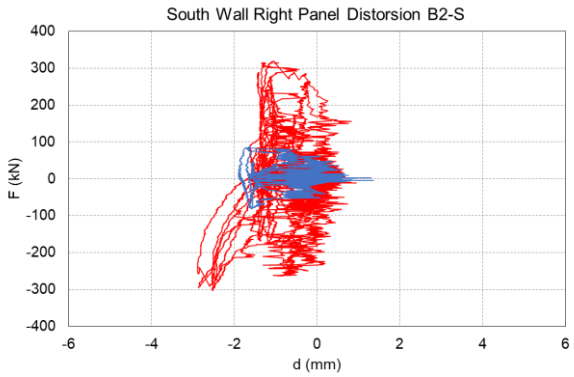
South Wall Right Panel Distorsion B2-S
F (kN)
d (mm)

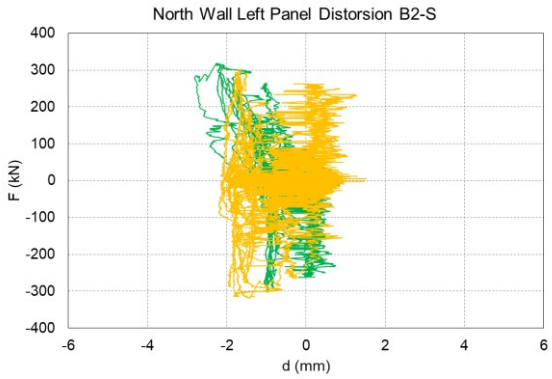
North Wall Left Panel Distorsion B2-S
F (kN)
d (mm)

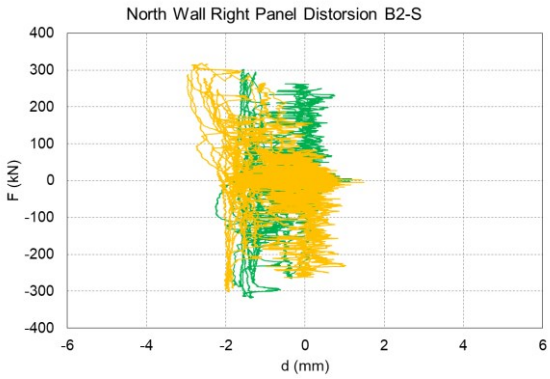
North Wall Right Panel Distorsion B2-S
F (kN)
d (mm)

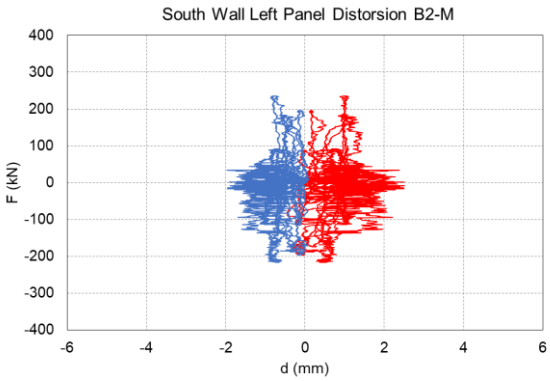
South Wall Left Panel Distorsion B2-M
F (kN)
d (mm)

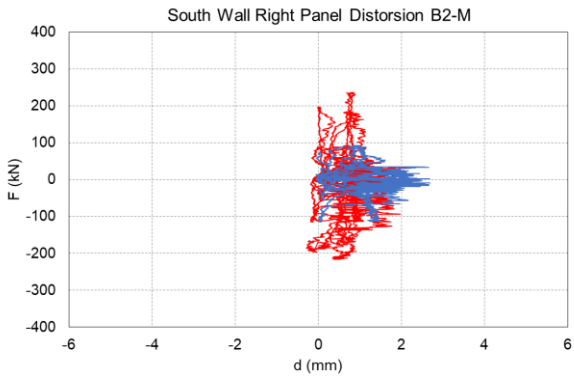
South Wall Right Panel Distorsion B2-M
F (kN)
d (mm)

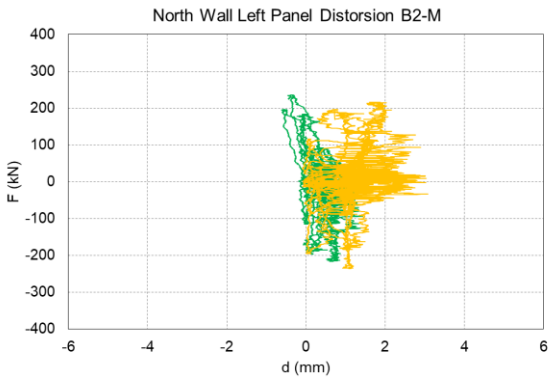
North Wall Left Panel Distorsion B2-M
F (kN)
d (mm)

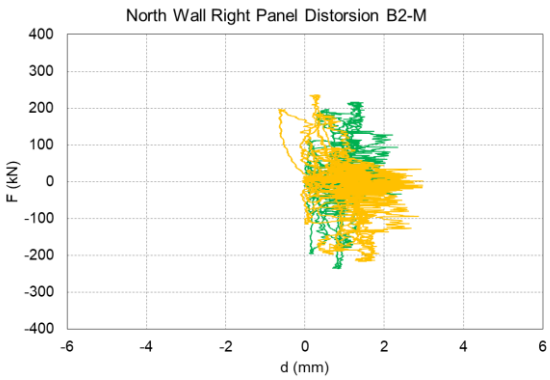
North Wall Right Panel Distorsion B2-M
F (kN)
d (mm)

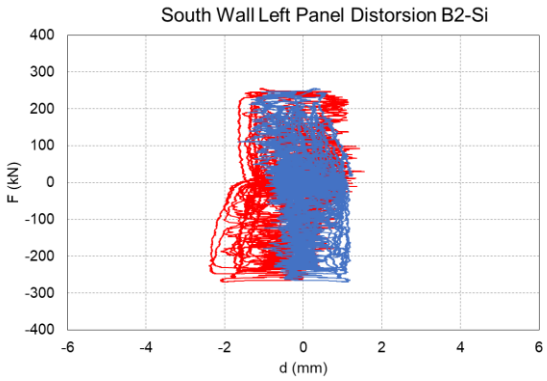
South Wall Left Panel Distorsion B2-Si
F (kN)
d (mm)

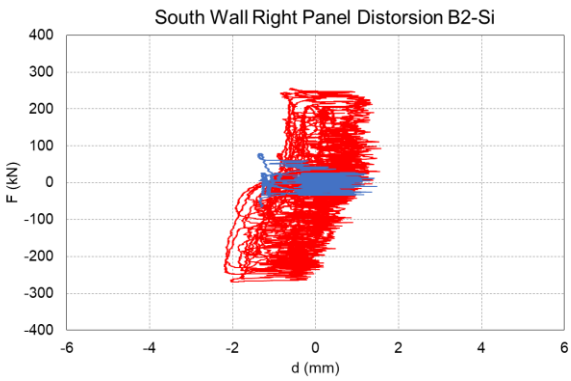
South Wall Right Panel Distorsion B2-Si
F (kN)
d (mm)

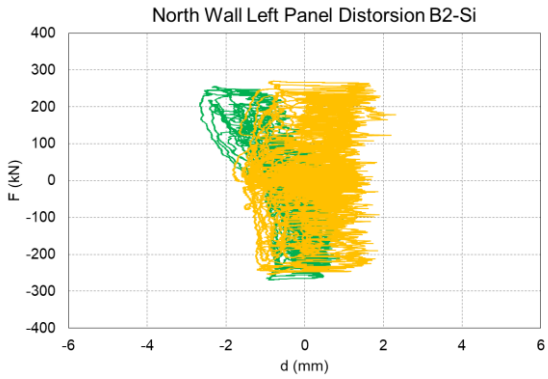
North Wall Left Panel Distorsion B2-Si
F (kN)
d (mm)

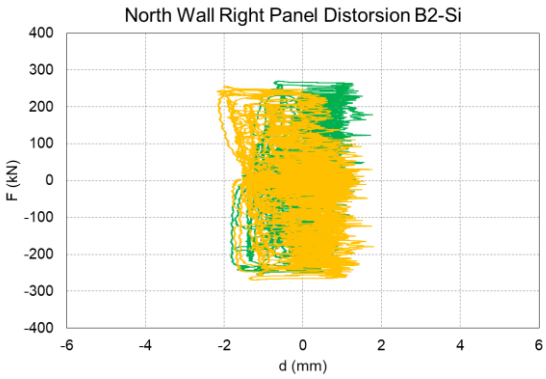
North Wall Right Panel Distorsion B2-Si
F (kN)
d (mm)

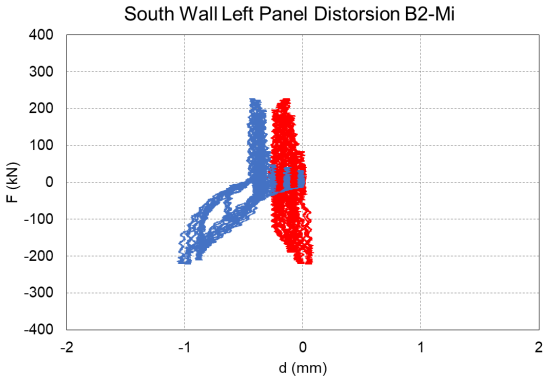
South Wall Left Panel Distorsion B2-Mi
F (kN)
d (mm)

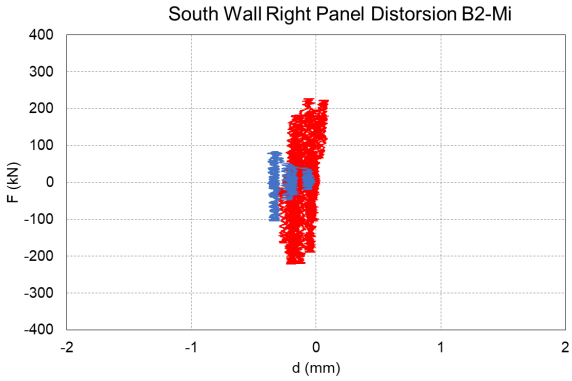
South Wall Right Panel Distorsion B2-Mi
F (kN)
d (mm)

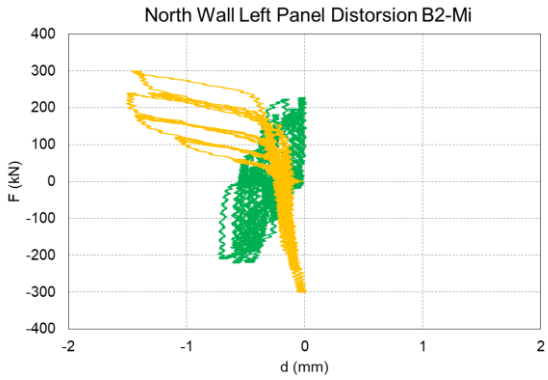
North Wall Left Panel Distorsion B2-Mi
F (kN)
d (mm)

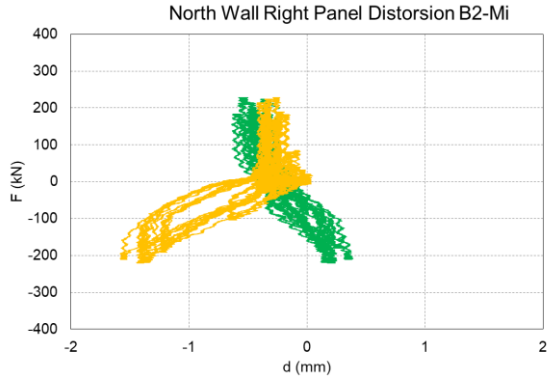
North Wall Right Panel Distorsion B2-Mi
F (kN)
d (mm)

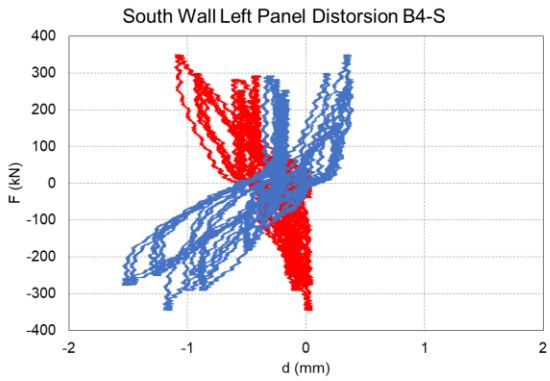
South Wall Left Panel Distorsion B4-S
F (kN)
d (mm)

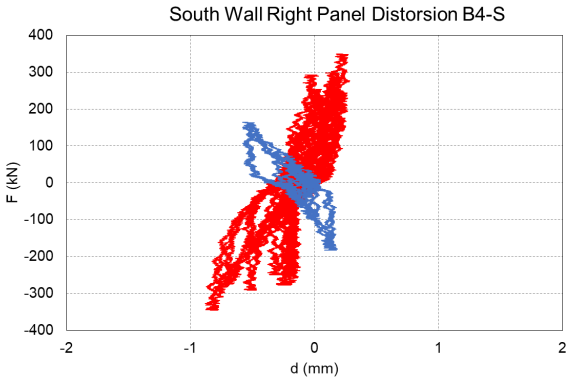
South Wall Right Panel Distorsion B4-S
F (kN)
d (mm)

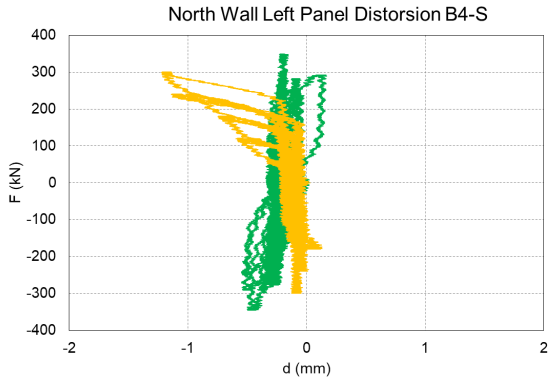
North Wall Left Panel Distorsion B4-S
F (kN)
d (mm)

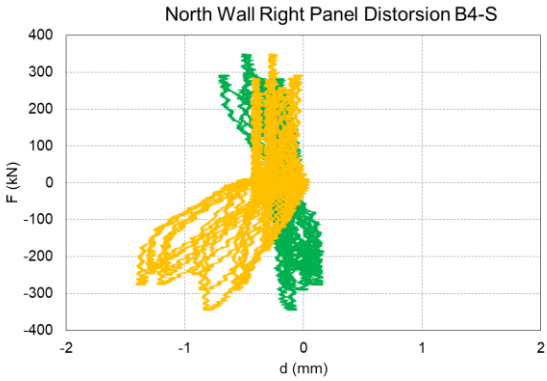
North Wall Right Panel Distorsion B4-S
F (kN)
d (mm)

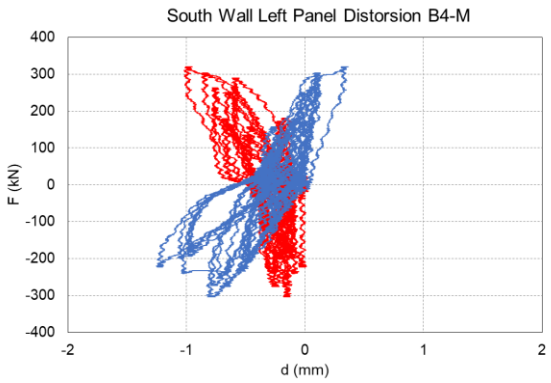
South Wall Left Panel Distorsion B4-M
F (kN)
d (mm)

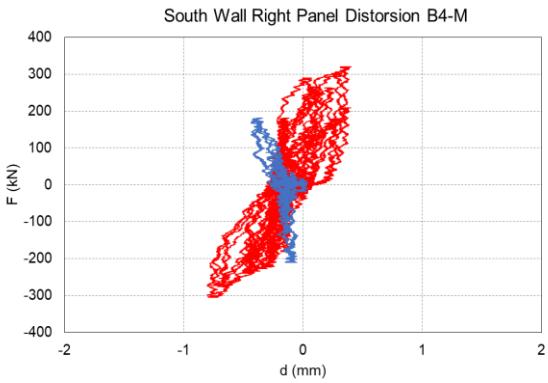
South Wall Right Panel Distorsion B4-M
F (kN)
d (mm)

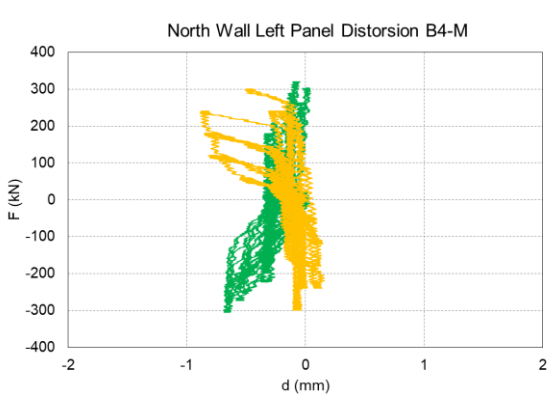
North Wall Left Panel Distorsion B4-M
F (kN)
d (mm)

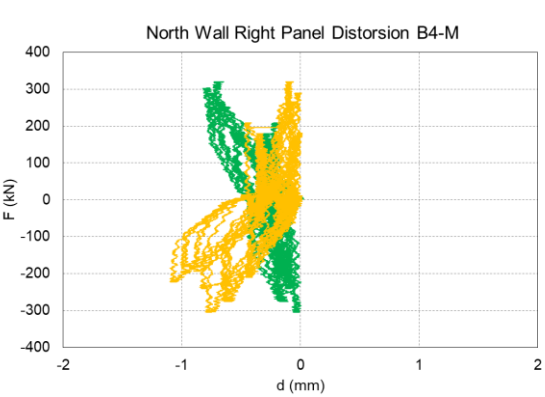
North Wall Right Panel Distorsion B4-M
F (kN)
d (mm)

Appendix 3: Detailed results

A.3.1 Load-carrying resistances and floor displacements at target drifts

Table 2 Load-carrying resistances at target drifts (kN)

Target	B2-S	B2-M	B2-Si	B2-Mi	B3-S	B3-M	B4-S	B4-M	B5-S
1.1%	85.0	91.0	26.0	83.0	131.0	160.0	163.0	181.0	109.0
1.1%	-80.0	-114.1	-34.1	-103.0	-150.0	-158.1	-183.2	-211.0	-134.3
2.2%	164.0	195.3	77.3	181.5	221.5	240.2	282.3	289.8	193.7
-2.2%	-164.7	-196.2	-98.2	-187.1	-247.4	-255.1	-291.6	-269.5	-232.1
3.4%	263.2	235.1	191.6	222.4	289.0	262.6	348.5	320.0	264.1
-3.4%	-262.6	-216.2	-217.4	-219.3	-306.7	-254.7	-345.0	-304.6	-285.2
4.5%	313.0	-	241.4	228.0	266.4	216.1	290.0	302.5	262.2
-4.5%	-301.1	-	-260.1	-220.3	-286.7	-228.6	-275.4	-240.1	-279.7
5.7%	317.0	-	252.8	214.3	275.1	219.0	282.2	207.9	277.8
-5.7%	-294.3	-	-268.1	-210.2	-290.0	-225.6	-277.6	-223.0	-283.2

Table 3 First floor displacements at target drifts (mm)

Target	B2-S	B2-M	B2-Si	B2-Mi	B3-S	B3-M	B4-S	B4-M	B5-S
1.1%	23.0	28.5	14.2	23.5	23.3	19.0	25.8	25.8	24.5
-1.1%	-25.4	-19.5	-15.3	-25.8	-25.9	-30.0	-25.0	-24.2	-24.0
2.2%	45.5	53	32.3	49.8	49.7	40.0	53.4	53.4	49.8
-2.2%	-45.15	-41	-31.8	-51.8	-52.9	-61.0	-52.2	-51.2	-48.8
3.4%	70.3	73.1	46.7	76.8	76.7	65.3	78.7	81.0	74.8
-3.4%	-70.0	-65.4	-48.3	-78.9	-79.3	-86.7	-78.7	-80.0	-74.3
4.5%	93.6	-	62.8	105.2	103.0	100.0	105.1	108.0	99.7
-4.5%	-100.5	-	-63.2	-107.9	-106.0	-112.0	-105.9	-105.9	-99.9
5.7%	120.2	-	79.9	132.8	131.0	121.0	133.2	134.9	125.9
-5.7%	-127.3	-	-77.9	-136.4	-133.0	-140.0	-133.0	-134.0	-126.6

Table 4 Second floor displacements at target drifts (mm)

Target	B2-S	B2-M	B2-Si	B2-Mi	B3-S	B3-M	B4-S	B4-M	B5-S
1.1%	55.1	24.8	36	57.6	54	55	54.5	55.8	56.7
-1.1%	-71	-45.12	-43	-55.1	-57	-56	-55.2	-55.6	-60
2.2%	93	48.5	66.2	114.1	112	114.5	113.8	114.7	115.2
-2.2%	-121.2	-70.1	-67.9	-113.6	-116	-112	-114.2	-114.2	-114.7
3.4%	146.3	80	97.4	175.7	171.6	172	173.5	174.2	174.1
-3.4%	-159.1	-100	-91.6	-170.1	-175.8	-173.1	-174.2	-174.4	-174.6
4.5%	201.1	-	127	235.7	232	234.4	233.3	235	233.6
-4.5%	-234.5	-	-108	-227.2	-235.4	-230	-233.8	-232.8	-232.7
5.7%	256.2	-	156.8	295.3	288.4	294.1	293.1	293.5	293.4
-5.7%	-289.2	-	-148.9	-291.8	-295.4	-292	-292.9	-292.1	-292.5

A.3.2 Hold-down uplifts

Table 5 HD north-left uplifts (mm)

Target	B2-S	B2-M	B2-Si	B2-Mi	B3-S	B3-M	B4-S	B4-M	B5-S
2.2%	16.8	11.3	10.9	13.7	15.0	16.4	21.8	15.6	12.5
-2.2%	-2.2	-2.7	-5.7	-2.4	-3.4	-1.5	-2.0	-2.6	-2.5
3.4%	25.3	21.8	19.0	24.4	25.2	29.0	32.2	34.1	17.3
-3.4%	-2.9	-3.1	-7.1	-3.2	-4.4	-1.9	-2.7	-4.2	-4.0
4.5%	35		30.9	38.3	36.2	42.6	38.5	44.7	24.8
-4.5%	-3.6		-7.7	-3.9	-5.1	-2.2	-3.3	-5.2	-5.6
5.7%	54		45.1	50.0	46.9	55.2	50.5	51.5	34.7
-5.7%	-3.8		-8.7	-4.6	-6.1	-2.9	-4.2	-6.4	-7.2

Table 6 HD north-right uplifts (mm)

Target	B2-S	B2-M	B2-Si	B2-Mi	B3-S	B3-M	B4-S	B4-M	B5-S
2.2%	13.7	13.6	14.5	14.5	18.0	12.4	23.2	21.9	16.6
-2.2%	-3.2	-3.9	-8.4	-5.8	-2.5	-2.0	-4.0	-5.0	-8.0
3.4%	22.1	25.5	23	27.7	28.1	24.0	31.1	39.7	26
-3.4%	-4.1	-3.9	-9.3	-6.8	-3.4	-2.5	-5.4	-6.2	-9.1
4.5%	32.4		34.6	38.8	38.4	35.3	40.4	44.0	36.2
-4.5%	-5.0		-10.1	-7.2	-3.3	-4.0	-6.7	-6.5	-9.7
5.7%	44.7		46.8	53.7	49.3	47.8	52.0	55.5	48.3
-5.7%	-6.5		-11.3	-8.0	-4.7	-4.5	-7.8	-8.3	-10.6

Table 7 HD south-left uplifts (mm)

Target	B2-S	B2-M	B2-Si	B2-Mi	B3-S	B3-M	B4-S	B4-M	B5-S
2.2%	15.6	12.3	14.0	15.6	17.2	15.4	18.2	23.6	17.3
-2.2%	-2.6	-4.6	-9.0	-6.0	-2.1	-2.2	-2.5	-6.1	-4.0
3.4%	24.3	25.2	21.3	28.0	27.8	26.2	29.5	36.5	26.8
-3.4%	-3.2	-4.7	-10.0	-7.2	-3.0	-3.0	-3.5	-7.3	-4.8
4.5%	33.4	-	31.1	40.3	38.7	37.1	39.5	42.1	37.3
-4.5%	-4.1	-	-10.6	-8.0	-3.5	-3.2	-3.8	-7.8	-5.3
5.7%	44.7	-	42.6	53.6	50.1	50.0	51.2	54.5	48.7
-5.7%	-4.4	-	-11.3	-9.0	-4.3	-4.2	-4.8	-8.3	-6.2

Table 8 HD south-right uplifts (mm)

Target	B2-S	B2-M	B2-Si	B2-Mi	B3-S	B3-M	B4-S	B4-M	B5-S
2.2%	16.4	13.0	10.4	11.5	12.6	17.3	15.6	14.8	11.1
-2.2%	-1.6	-2.0	-6.0	-2.7	-2.2	-2.1	-2.3	-2.5	-2.4
3.4%	25.6	22.6	-18.4	25.0	22.1	29.7	26.0	38.2	17.1
-3.4%	-2.4	-2.9	-6.9	-3.5	-3.1	-3.0	-3.5	-3.8	-3.4
4.5%	35.3	-	28.7	36.9	32.8	39.9	36.0	44.1	26
-4.5%	-2.6	-	-7.5	-4.4	-3.7	-3.8	-4.1	-4.5	-4.1
5.7%	41.4	-	39.1	49.8	44.3	52.0	46.4	48.0	36.4
-5.7%	-4.0	-	-8.4	-5.4	-4.6	-4.8	-5.5	-5.6	-5.0

A.3.3 Shear wall uplifts at inner corners

Table 9 Inner corner uplifts north-left (mm)

Target	B2-S	B2-M	B2-Si	B2-Mi	B3-S	B3-M	B4-S	B4-M	B5-S
2.2%	19.9	18.92	17.9	18.4	17.2	17.2	17.1	15.8	16.2
-2.2%	-3.5	-6.3	-12.2	-4.5	-6.8	-0.5	-0.2	-2.4	-7.2
3.4%	31.35	31.2	28.5	29.2	28.6	29.9	26.4	27.1	26.6
-3.4%	-3.9	-7.1	-12.7	-4.2	-7.3	-0.3	-1.4	-1.4	-14.6
4.5%	42.8	-	41.0	40.1	40.4	41.9	40.0	40.5	-38.0
-4.5%	-4.4	-	-12.8	-4.2	-7.6	-0.8	-5.9	-1.2	-16.0
5.7%	55.3	-	53.4	51.6	50.8	53.0	52.0	51.8	49.0
-5.7%	-5.2	-	-13.7	-4.3	-9.1	-1.3	-6.5	-5.5	-16.0

Table 10 Inner corner uplifts north-right (mm)

Target	B2-S	B2-M	B2-Si	B2-Mi	B3-S	B3-M	B4-S	B4-M	B5-S
2.2%	19.1	19.0	16.8	16.3	17.7	17.7	14.5	12.6	13.1
-2.2%	-3.4	-2.5	-5.7	-1.6	-0.1	-4.4	-1.5	-0.2	-1.0
3.4%	30.2	31.4	26.4	26.1	30.6	29.2	24.0	23.0	24.7
-3.4%	-4.4	-2.8	-7.2	-1.5	-0.5	-4.6	-0.6	-0.1	-1.7
4.5%	41.8	-	38.4	37.5	43.2	41.4	38.7	36.8	37.2
-4.5%	-5.4	-	-7.8	-1.5	-1.4	-5.1	-0.8	-0.1	-2.8
5.7%	54.7	-	51.3	48.6	54.4	52.4	51.0	49.2	48.0
-5.7%	-6.6	-	-14.1	-1.5	-2.3	-5.3	-1.3	-0.1	-4.0

Table 11 Inner corner uplifts south-left (mm)

Target	B2-S	B2-M	B2-Si	B2-Mi	B3-S	B3-M	B4-S	B4-M	B5-S
2.2%	19.4	20.3	17.1	17.0	17.2	18.5	13.9	16.9	14.0
-2.2%	-3.5	-3.2	-7.1	-1.3	-0.1	-4.2	-0.5	-4.1	-1.2
3.4%	30.2	30.2	26.1	28.1	29.1	31.8	27.6	26.5	24.0
-3.4%	-3.7	-3.6	-7.6	-1.1	-0.5	-4.3	-0.5	-0.3	-2.0
4.5%	41.8	-	36.9	38.8	41.2	42.4	40.4	41.1	35.0
-4.5%	-4.4	-	-8.2	-1.1	-1.4	-4.3	-1.1	-3.0	-3.0
5.7%	49.3	-	47.7	50.3	52.9	53.6	51.5	52.9	46.2
-5.7%	-5.3	-	-8.8	-1.1	-2.3	-4.2	-1.5	-4.5	-3.1

Table 12 Inner corner uplifts south-right (mm)

Target	B2-S	B2-M	B2-Si	B2-Mi	B3-S	B3-M	B4-S	B4-M	B5-S
2.2%	21.7	21.6	18.5	20.8	18.1	18.9	16.0	11.8	17.0
-2.2%	-2.1	-7.4	-12.3	-7.5	-5.5	-2.4	-1.9	-0.1	-7.5
3.4%	33.1	32.5	29.3	31.7	30.8	32.6	31.3	22.5	29.0
-3.4%	-3.2	-7.2	-12.7	-7.2	-5.7	-2.2	-2.3	-0.3	-11.0
4.5%	44.8	-	40.7	42.8	42.8	43.6	43.3	35.3	40.0
-4.5%	-3.6	-	-12.8	-7.0	-5.9	-2.3	-3.6	-0.2	-12.0
5.7%	55.5	-	52.0	54.4	54.4	55.4	55.3	47.3	51.0
-5.7%	-3.78	-	-12.9	-7.0	-6.1	-2.3	-4.8	-0.1	-12.0

A.3.4 Tension strap uplifts

Table 13 Uplifts at outer TS in B5-S (mm)

Target	2.2%	-2.2%	3.4%	-3.4%	4.5%	-4.5%	5.7%	-5.7%
North-left	1	-0.5	4.1	-0.7	5.0	-1.0	5.2	-1.0
north-right	1.8	-0.1	1.3	0	1.7	0	1.8	-0.1
south-left	2.3	-1.3	3.9	-1.4	4.5	-1.5	5.6	-1.5
south-right	0.6	-2.4	1.1	-0.6	1.7	-0.5	2.0	-0.6

Table 14 Uplifts at inner TS in B5-S (mm)

Target	2.2%	-2.2%	3.4%	-3.4%	4.5%	-4.5%	5.7%	-5.7%
North-left	0.0	-0.5	0.0	-0.7	0.5	-0.9	0.8	-0.9
north-right	0.1	-0.9	0.1	-1.5	0.4	-1.7	0.6	-1.8
south-left	0.2	-0.9	0.6	-1.2	0.8	-1.3	1.0	-1.4
south-right	0.7	-0.4	1.1	-0.4	1.5	-0.5	1.7	-0.6

A.3.5 Shear wall siding

Table 15 Shear wall sliding north-left panel (mm)

Target	B2-S	B2-M	B2-Si	B2-Mi	B3-S	B3-M	B4-S	B4-M	B5-S
2.2%	2.2	0.82	5.7	1.9	3.3	1.3	2.0	1.1	2.7
-2.2%	-2.4	-1.25	-3.6	-1.4	-2.5	-0.9	-2.7	-2.6	-3.0
3.4%	3.7	1.7	6.8	3.8	5.4	3.3	3.7	2.3	5.4
-3.4%	-3.3	-2.54	-4.3	-3.8	-4.8	-2.8	-4.8	-4.5	-5.1
4.5%	5.4	-	8.8	6.1	8.0	5.9	6.3	5.0	8.4
-4.5%	-4.5	-	-5.7	-5.0	-7.8	-3.9	-6.9	-7.5	-7.9
5.7%	6.7	-	11.8	7.0	10.1	7.6	8.6	6.8	10.4
-5.7%	-5.4	-	-7.9	-5.6	-10.3	-4.7	-9.2	-8.8	-11.3

Table 16 Shear wall sliding north-right panel (mm)

Target	B2-S	B2-M	B2-Si	B2-Mi	B3-S	B3-M	B4-S	B4-M	B5-S
2.2%	2.1	0.8	5.8	2.0	3.8	1.7	3.6	1.4	2.8
-2.2%	-2.4	-1.7	-3.4	-1.7	-1.8	-1.1	-1.2	-3.3	-3.1
3.4%	3.7	1.0	7.5	3.7	6.7	3.7	3.1	2.7	5.5
-3.4%	-3.3	-3.8	-4.2	-4.1	-4.0	-3.5	-5.7	-5.3	-5.3
4.5%	5.7	-	10.4	5.8	9.8	5.7	6.0	4.2	7.5
-4.5%	-4.4	-	-6.6	-5.6	-6.4	-5.3	-8.0	-8.7	-8.8
5.7%	6.7	-	14.4	6.4	13.2	6.9	7.9	5.6	8.9
-5.7%	-4.3	-	-7.2	-6.9	-8.4	-6.8	-10.8	-10.5	-12.7

Table 17 shear wall sliding south-left panel (mm)

Target	B2-S	B2-M	B2-Si	B2-Mi	B3-S	B3-M	B4-S	B4-M	B5-S
2.2%	3.6	1.8	5.6	3.4	3.2	2.6	3.4	2.7	3.4
-2.2%	-1.0	-3.6	-4.8	-1.1	-1.9	-0.6	-2.9	-1.2	-2.1
3.4%	5.8	2.71	6.6	5.8	5.9	4.5	4.0	5.3	5.8
-3.4%	-3.2	-4.5	-5.5	-3.2	-3.6	-2.9	-6.1	-2.3	-4.0
4.5%	6.8	-	9.8	7.5	8.8	5.4	6.5	8.0	8.1
-4.5%	-3.6	-	-9.4	-5.0	-6.5	-5.0	-8.4	-4.2	-6.4
5.7%	7.0	-	9.9	9.0	11.4	7.4	9.0	9.6	10.4
-5.7%	-3.8	-	-10.2	-6.2	-9.2	-5.9	-11.1	-6.7	-10.0

Table 18 Shear wall sliding south-right panel (mm)

Target	B2-S	B2-M	B2-Si	B2-Mi	B3-S	B3-M	B4-S	B4-M	B5-S
2.2%	2.5	0.5	4.3	3.4	2.2	3.1	3.5	3.1	3.0
-2.2%	-1.8	-4.8	-4.7	-1.0	-2.5	-1.3	-2.2	-1.2	-2.1
3.4%	3.9	1.2	5.0	5.7	4.5	4.8	4.6	6.0	5.5
-3.4%	-3.7	-6.5	-5.6	-3.0	-4.7	-3.7	-5.1	-2.2	-3.7
4.5%	5.5	-	7.0	7.9	6.8	6.0	7.0	9.2	8.1
-4.5%	-4.6	-	-7.9	-4.5	-7.6	-5.4	-8.0	-3.9	-5.8
5.7%	6.0	-	9.3	9.7	9.4	7.2	11.6	11.1	10.8
-5.7%	-5.1	-	-10.4	-5.4	-9.8	-6.8	-8.7	-5.1	-8.4

A.3.6 Panel-to-panel displacement

Table 19 Panel-to-panel displacement first storey north side (mm)

Target	B2-S	B2-M	B2-Si	B2-Mi	B3-S	B3-M	B4-S	B4-M	B5-S
2.2%	21.0	24.4	25.0	23.0	19.8	20.2	16.0	17.0	22.1
-2.2%	-25.2	-25.8	-28.3	-22.8	-26.5	-24.5	-15.9	-16.0	-19.4
3.4%	36.2	37.3	36.5	33.6	41.6	31.5	28.1	22.4	42.1
-3.4%	-39.3	-37.4	-38.3	-34.2	-32.5	-37.4	-29.3	-22.8	-31.6
4.5%	43.6	-	49.3	46.1	46.3	46.8	49.4	42.0	58.8
-4.5%	-48.0	-	-50.4	-46.6	-55.7	-51.5	-46.0	-44.5	-45.2
5.7%	54.4	-	62.2	57.8	59.2	59.6	63.6	59.8	71.5
-5.7%	-57.8	-	-63.3	-57.6	-69.6	-63.4	-59.5	-57.8	-58.9

Table 20 Panel-to-panel displacement first storey south side (mm)

Target	B2-S	B2-M	B2-Si	B2-Mi	B3-S	B3-M	B4-S	B4-M	B5-S
2.2%	22.8	26.7	28.8	26.2	23.7	23.4	18.1	18.2	22.1
-2.2%	-26.5	-25.8	-26.2	-23.5	-20.5	-24.3	-18.0	-15.5	-19.8
3.4%	32.3	36.9	39.0	38.5	37.2	38.2	33.9	23.1	37.1
-3.4%	-36.1	-37.0	-37.6	-35.6	-34.3	-38.7	-35.2	-24.2	-33.3
4.5%	45.0	-	49.8	48.0	50.9	50.0	50.0	42.5	51.3
-4.5%	-47.2	-	-50.1	-47.9	-48.3	-52.0	-49.8	-45.8	-46.8
5.7%	53.1	-	60.4	61.6	65.2	61.5	62.1	56.8	65.2
-5.7%	-56.3	-	-59.7	-58.8	-62.4	-64.1	-63.0	-59.2	-59.5

Table 21 Panel-to-panel displacement second storey north side (mm)

Target	B2-S	B2-M	B2-Si	B2-Mi	B3-S	B3-M	B4-S	B4-M	B5-S
2.2%	24.2	25.3	26.2	23.0	20.1	20.2	16.0	17.3	21.8
-2.2%	-25.6	-24.1	-28.4	-23.5	-27.2	-24.5	-16.7	-16.0	-20.6
3.4%	33.9	37.5	37.5	33.6	42.0	31.5	28.1	22.9	42.8
-3.4%	-38.1	-34.8	-40.0	-35.2	-33.1	-37.4	-30.0	-22.8	-33.9
4.5%	48.2	-	50.6	46.1	47.0	46.8	49.4	42.3	60.7
-4.5%	-46.4	-	-51.3	-47.2	-56.1	-51.5	-46.5	-44.5	-48.7
5.7%	57.9	-	62.4	57.8	60.3	59.6	63.6	60.3	74.5
-5.7%	-58.7	-	-63.1	-59.0	-69.9	-63.4	-60.0	-57.8	-62.4

Table 22 Panel-to-panel displacement second storey south side (mm)

Target	B2-S	B2-M	B2-Si	B2-Mi	B3-S	B3-M	B4-S	B4-M	B5-S
2.2%	18.6	29.4	30.2	27.0	24.7	23.4	18.3	18.6	24.0
-2.2%	-21.0	-22.2	-27.9	-25.1	-21.2	-24.8	-18.0	-15.5	-22.3
3.4%	33.8	40.2	38.6	39.1	38.5	38.2	34.2	23.6	40.9
-3.4%	-37.8	-32.9	-40.2	-36.9	-35.3	-39.1	-35.8	-24.2	-37.5
4.5%	42.5	-	48.7	50.5	52.9	50.0	50.3	42.7	54.8
-4.5%	-53.8	-	-50.9	-48.6	-49.8	-52.4	-50.0	-45.8	-49.7
5.7%	53.0	-	59.8	61.6	66.3	61.5	62.8	57.0	68.8
-5.7%	-65.0	-	-61.9	-60.8	-63.4	-64.6	-63.6	-59.2	-62.4

A.3.7 Ledger slip

Table 23 First storey ledger slip north side (mm)

Target	B2-S	B2-M	B2-Si	B2-Mi	B3-S	B3-M	B4-S	B4-M	B5-S
2.2%	4.2	1.04	3.6	5.0	4.6	3.6	1.2	1.4	1.4
-2.2%	-3.1	-4.8	-4.8	-1.5	-2.6	-2.2	-1.2	-1.9	-4.1
3.4%	6.8	2.2	4.0	6.5	5.8	6.1	3.7	2.0	4.2
-3.4%	-4.8	-7.6	-6.9	-3.9	-5.1	-5.2	-3.6	-3.2	-7.6
4.5%	9.5	-	5.5	8.8	8.4	8.2	8.1	6.7	6.8
-4.5%	-6.7	-	-9.6	-6.2	-8.1	-8.0	-7.4	-8.4	-10.9
5.7%	8.8	-	7.5	10.8	10.7	10.1	10.1	9.6	8.4
-5.7%	-12.2	-	-11.2	-8.6	-10.8	-10.3	-10.5	-11.0	-13.9

Table 24 First storey ledger slip south side (mm)

Target	B2-S	B2-M	B2-Si	B2-Mi	B3-S	B3-M	B4-S	B4-M	B5-S
2.2%	-	6.2	6.0	5.3	-4.0	4.5	2.3	1.6	3.2
-2.2%	-	-3.6	-6.4	-3.1	-5.5	-2.8	-2.1	-2.4	-4.1
3.4%	-	7.6	8.3	7.5	7.0	7.8	5.2	2.7	6.0
-3.4%	-	-5.3	-7.5	-5.5	-6.5	-6.1	-5.2	-4.0	-7.2
4.5%	-	-	10.0	9.5	10.3	9.7	8.3	7.3	8.1
-4.5%	-	-	-8.6	-7.5	-9.0	-9.0	-8.5	-9.0	-9.6
5.7%	-	-	12.7	11.7	13.3	11.6	11.1	10.0	12. 2
-5.7%	-	-	-10.5	-10.5	-11.5	-11.7	-11.1	-11.8	-10.2

Table 25 Second storey ledger slip north side (mm)

Target	B2-S	B2-M	B2-Si	B2-Mi	B3-S	B3-M	B4-S	B4-M	B5-S
2.2%	1.4	-	1.4	3.0	3.5	3.0	3.0	3.4	2.3
-2.2%	-3.8	-	-4.1	-1.2	-2.5	-3.2	-6.1	-5.9	-3.4
3.4%	2.0	-	3.7	2.7	2.8	1.4	1.5	2.4	0.8
-3.4%	-4.9	-	-5.1	-0.6	-0.2	-1.0	-3.8	-4.5	-1.7
4.5%	4.4	-	6.3	4.4	4.2	3.5	1.2	2.4	3.2
-4.5%	-5.6	-	-5.7	-2.6	-1.8	-2.9	-3.0	-4.0	-2.4
5.7%	6.0	-	6.6	6.7	5.8	5.3	3.1	5.4	5.3
-5.7%	-5.6	-	-8.4	-5.2	-3.2	-5.3	-5.6	-6.4	-4.8

Table 26 Second storey ledger slip south side (mm)

Target	B2-S	B2-M	B2-Si	B2-Mi	B3-S	B3-M	B4-S	B4-M	B5-S
2.2%	4.3	3.8	6.7	1.8	0.5	3.0	0.2	0.1	0.8
-2.2%	-3.2	-4.0	-5.1	-2.0	-1.3	-0.2	-2.9	-2.1	-0.9
3.4%	5.8	6.0	7.8	3.3	2.8	5.5	0.1	0.2	2.3
-3.4%	-4.7	-3.4	-5.8	-3.5	-3.7	-3.1	-1.3	-1.4	-2.8
4.5%	6.7	-	10.3	4.8	3.6	7.1	2.6	3.6	4.0
-4.5%	-3.5	-	-6.7	-5.6	-6.6	-5.3	-6.3	-6.5	-5.0
5.7%	6.3	-	11.6	7.0	5.6	9.3	4.7	6.0	5.4
-5.7%	-4.9	-	-7.0	-8.1	-9.4	-7.9	-8.8	-9.1	-7.2

A.3.8 Wall displacements

Table 27 Wall displacement north side (mm)

Target	B2-S	B2-M	B2-Si	B2-Mi	B3-S	B3-M	B4-S	B4-M	B5-S
1.1%	45	66	43	51	52	49	52.6	51	50.6
-1.1%	-58	-44	-56.3	-51	-52	-48	-51.3	-46	-54.1
2.2%	35.4	100.9	111.3	110.2	114.5	105.2	110.8	106.1	114.7
-2.2%	-82.2	-100.9	-114.9	-104.3	-108.4	-105.5	-114.4	-113.7	-108.7
3.4%	79.0	167.2	157.8	163.0	177.2	163.5	165.3	166.8	178.4
-3.4%	97.6	-141.0	-170.6	-160.0	-166.3	-166.2	-167.4	-168.2	-166.3
4.5%	88.8	-	214.6	-214.4	238.5	229.8	230.4	234.7	242.1
-4.5%	-126.8	-	-219.5	-220.1	-225.7	-227.8	-227.7	-230.7	-230.3
5.7%	120.3	-	273.2	281.0	298.8	292.8	293.5	292.4	302.9
-5.7%	-161.0	-	-274.2	-279.0	-283.6	-285.8	-292.0	-294.0	-291.1

Table 28 Wall displacement south side (mm)

Target	B2-S	B2-M	B2-Si	B2-Mi	B3-S	B3-M	B4-S	B4-M	B5-S
1.1%	54.63	71.95	43.7	60.4	51.8	55	49	52	56
-1.1%	-63	-45	-58.2	-52.5	-53.6	-54	-47	-54	-50
2.2%	92.1	122.4	115.7	111.0	109.5	118.2	104.3	106.0	110.0
-2.2%	-122.2	-92.9	-110.6	-113.5	-107.1	-114.1	-105.1	-113.7	-114.3
3.4%	157.0	176.2	162.1	184.5	167.8	183.9	171.0	166.1	167.1
-3.4%	-163.1	-142.5	-172.6	-173.9	-170.2	-175.2	-176.8	-168.2	-177.1
4.5%	200.2	-	206.9	240.6	228.2	237.2	229.5	234.2	231.2
-4.5%	-235.2	-	-219.0	-237.0	-232.7	-232.4	-232.3	-230.7	-224.1
5.7%	235.0	-	273.8	296.1	286.2	290.2	280.8	291.8	295.0
-5.7%	-290.1	-	-273.3	-298.7	-296.2	-296.2	-296.8	-294.0	-277.9

A.3.9 Strength degradation

Table 29 Strength degradation at target drifts (%)

Test	Cycle	1.1%	-1.1%	2.2%	-2.2%	3.3%	-3.3%	4.4%	-4.4%	5.5%	-5.5%
B2-S	1st	86.9	-80.8	180.0	-176.6	264.9	-263.0	314.4	-302.0	316.4	-312.3
	2nd	84.2	-78.5	169.5	-168.8	247.3	-249.4	287.8	-284.5	317.9	-312.4
	3rd	82.9	-77.3	165.5	-164.7	239.6	-241.5	277.2	-274.1	315.0	-271.3
B2-M	1st	91.6	-114.7	195.4	-196.1	-	-	-	-	-	-
	2nd	86.7	-113.1	183.2	-173.9	-	-	-	-	-	-
	3rd	86.2	-112.0	178.1	-168.9	-	-	-	-	-	-
B2-Si	1st	26.9	-34.0	78.6	-98.2	193.6	-218.4	244.1	-260.5	255.1	-270.0
	2nd	26.3	-33.8	76.4	-96.7	182.7	-208.4	220.5	-240.0	218.3	-239.5
	3rd	26.1	-33.7	75.6	-96.1	177.6	-203.2	209.6	-230.1	203.4	-222.8
B2-Mi	1st	83.9	-104.1	181.7	-189.1	223.5	-219.5	227.7	-220.7	214.3	-210.2
	2nd	80.6	-102.1	167.6	-178.4	188.8	-191.2	196.9	-200.1	183.3	-180.4
	3rd	79.7	-101.1	163.0	-173.5	181.8	-177.8	180.7	-187.3	166.8	-164.1
B3-S	1st	131.3	-151.4	221.8	-251.0	290.8	-306.8	267.9	-287.0	277.9	-291.1
	2nd	123.6	-146.3	202.3	-237.0	232.5	-262.5	231.2	-262.2	240.1	-258.3
	3rd	120.6	-143.7	194.4	-229.7	213.0	-247.7	219.9	-250.9	225.0	-
B3-M	1st	161.5	-159.1	240.7	-252.1	263.3	-254.9	219.3	-228.9	219.3	-225.9
	2nd	153.5	-152.8	215.6	-232.2	189.4	-209.7	193.0	-210.4	188.8	-202.1
	3rd	150.4	-149.6	206.8	-223.7	173.6	-193.2	180.5	-198.2	174.7	-184.3
B4-S	1st	163.5	-183.1	283.1	-291.6	348.5	-345.0	292.1	-275.7	282.4	-277.8
	2nd	156.4	-176.7	258.3	-274.3	298.3	-291.8	236.5	-250.9	243.7	-246.2
	3rd	154.0	-173.5	248.6	-265.4	252.4	-249.1	225.1	-239.0	226.4	-230.8
B4-M	1st	181.3	-211.0	289.9	-275.9	320.3	-304.6	302.6	-240.6	208.2	-222.9
	2nd	173.0	-202.0	266.1	-234.2	262.5	-273.9	157.1	-193.6	178.9	-199.1
	3rd	169.8	-197.5	257.0	-227.4	250.0	-253.6	135.0	-182.3	165.9	-181.9
B5-S	1st	112.1	-134.8	194.2	-234.5	264.1	-285.2	262.6	-279.9	277.9	-283.5
	2nd	107.3	-130.3	177.1	-220.7	211.8	-247.8	230.6	-256.2	246.1	-258.4
	3rd	105.0	-128.0	170.1	-213.9	188.7	-233.3	216.6	-243.6	233.3	-245.9

A.3.10 Energy dissipation

Table 30 Energy dissipation at target drifts (%)

Test	Cycle	1.1%	-1.1%	2.3%	-2.3%	3.4%	-3.4%	4.6%	-4.6%	5.7%	-5.7%
	1st	773	-1002	10228	-13538	31589	-33642	57058	-62875	95744	-98843
B2-Si	2nd	1920	-5877	14778	-20144	35575	-42840	64713	-69560	104360	-108000
	3rd	6698	-7850	21122	-26437	48624	-49760	80292	-90867	115401	-123034
	1st	4150	-6936	21173	-29915	58903	-73922	115310	-131989	183694	-202890
B2-Mi	2nd	7862	-9718	33031	-37060	79617	-86497	140512	-150181	212754	-223979
	3rd	10426	-11758	40222	-43833	92206	-97974	157108	-165859	231778	-244848
	1st	7479	-12000	31960	-46223	85143	-108999	159508	-181954	240462	-266615
B3-S	2nd	13810	-16825	50230	-57356	115391	-126784	190172	-202941	276249	-291650
	3rd	17733	-20699	61940	-68203	130655	-140889	209047	-218365	298663	-306256
	1st	8059	-12885	37391	-50418	92997	-111562	154672	-172597	225465	-243836
B3-M	2nd	15775	-18084	56223	-62569	117829	-126273	181819	-190411	255347	-266781
	3rd	19803	-22980	67895	-72960	131334	-138126	198219	-205615	276353	-283805
	1st	7717	-12673	37482	-53588	105232	-130098	197371	-216647	281221	-304424
B4-S	2nd	15205	-17678	60915	-68487	143083	-154971	227470	-239557	317511	-329507
	3rd	20060	-22716	75019	-81900	164515	-173369	248353	-256809	340166	-352032
	1st	7844	-14684	41328	-58322	106864	-127687	193641	-215495	267437	-287489
B4-M	2nd	16964	-20610	65565	-71619	140040	-149588	225574	-235088	298047	-310136
	3rd	22440	-25736	78858	-82067	161098	-169671	242134	-251405	318425	-328437
	1st	7037	-9937	29589	-41650	81021	-101485	151228	-173007	233638	-258391
B5-S	2nd	12545	-13646	45733	-53344	107072	-118399	180861	-194167	270301	-284560
	3rd	16535	-18435	57047	-63889	124337	-133741	201537	-211703	292933	-306415

A3.11 Storey drift at target displacement

Table 31. Storey drifts at target displacements (%)

Target	Storey	B2-Si	B2-Mi	B3-S	B3-M	B4-S	B4-M	B5-S
1.1%	1st	14.2	23.5	23.3	19	25.8	25.8	24.5
-1.1%		-15.3	-25.8	-25.9	-30	-25	-24.2	-24
2.2%		32.3	49.8	49.7	40	53.4	53.4	49.8
-2.2%		-31.8	-51.8	-52.9	-61	-52.2	-51.2	-48.8
3.4%		46.7	76.8	76.7	65.3	78.7	81	74.8
-3.4%		-48.3	-78.9	-79.3	-86.7	-78.7	-80	-74.3
4.5%		62.8	105.2	103	100	105.1	108	99.7
-4.5%		-63.2	-107.9	-106	-112	-105.9	-105.9	-99.9
5.7%		79.9	132.8	131	121	133.2	134.9	125.9
-5.7%		-77.9	-136.4	-133	-140	-133	-134	-126.6
1.1%	2nd	36	57.6	54	55	54.5	55.8	56.7
-1.1%		-43	-55.1	-57	-56	-55.2	-55.6	-60
2.2%		66.2	114.1	112	114.5	113.8	114.7	115.2
-2.2%		-67.9	-113.6	-116	-112	-114.2	-114.2	-114.7
3.4%		97.4	175.7	171.6	172	173.5	174.2	174.1
-3.4%		-91.6	-170.1	-175.8	-173.1	-174.2	-174.4	-174.6
4.5%		127	235.7	232	234.4	233.3	235	233.6
-4.5%		-108	-227.2	-235.4	-230	-233.8	-232.8	-232.7
5.7%		156.8	295.3	288.4	294.1	293.1	293.5	293.4
-5.7%		-148.9	-291.8	-295.4	-292	-292.9	-292.1	-292.5

Appendix 4: Structures after testing

Figure 52 B1-S after test

Figure 53 B1-M after test

Figure 54 B2-S after test

Figure 55 B2-M after test

Figure 56 B2-Si after test

Figure 57 B2-Mi after test

Figure 58 B4-S after test

Figure 59 B4-M after test

Figure 60 B5-S after test